ÉCOLE POLYTECHNIQUE
FÉDÉRALE DE LAUSANNE

Master Project

Polymer spiral film gas-liquid heat exchanger for waste heat recovery in exhaust gases

Development and test analysis

Practical work report for master degree

Collaboration with
Industrial Energy Systems Laboratory (LENI)
EPFL, Lausanne, Switzerland

and
Makatec GmbH
Bondorf, Germany

makatec
Membrantechnologie zum Heizen und Kühlen

Supervisor EPFL:
Professor Daniel Favrat

Supervisor Makatec:
Doctor Thomas Weimer

Antoine Breton
September 2012

Executive summary

In this master thesis report the development of an innovative spiral heat exchanger based on polymer materials is described. Building prototypes, erection of a test bench and firsts tests of the heat exchanger are presented.

The heat exchanger prototype survived all tests especially several days in contact with aggressive gases.

A facility integrating a Diesel exhaust gases production has been developed to test this heat exchanger design. Performance results obtained during the tests are analysed. Measurement acquisition software developed with Labview was also used. Challenges have been overcome to run the facility in stable conditions in order to obtain reliable measurement.

Heat load recovery achieved with the presented heat exchanger is in the range of 1.5 kW thermic but potential heat recovery about 3.5kW might be achievable. Overall heat transfer coefficient is improved compared to other polymer based heat exchanger design. Pressure drop on gas channel is in the range of several mbar and must be further improved and fouling must be minimized.

Such a design based on polymer film technology provides better corrosion and chemical resistance compared to conventional metal heat exchangers. Due to the smooth surface of polymer film fouling is reduced. Series production and usage of such heat exchangers would allow operating low temperature waste heat recovery in gases at affordable costs. One promising application is heat recovery in soiled gases in combination with ORC power generation.

Table of contents

Chapter 1 Introduction

As energy is everywhere, as energy is costly, as energy is even more demanded, it becomes nowadays more and more necessary to optimise energy usage in industrial processes. Such methodology requires finding out wherever energy can be recovered. Even more interesting than energy recovery is waste heat recovery. It means converting and using wasted energy that would normally be thrown out without regards into the atmosphere. More often it concerns low temperature heat and such energy makes recovery even more complicated. However low heat recovery represents a huge potential and one can still imagine making it profitable by converting it in electricity for example. Pursuing these objectives it becomes necessary to develop special technology to operate such heat recovery. This is the aim targeted by the European research project called Low-Temperature heat valorisation towards electricity production or more easily LOVE.

As largely as energy can be used, energy can be recovered from a multitude of sources. Being part of the LOVE project, we'll pay here a special attention to gases and liquid mediums; the aim of this master work report is to explore new designs of heat exchanger, which are able to recover low temperature heat in wasted exhaust gases. The heat exchanger design explored in the frame of this project is completely innovator and is based on polymer film technology. The reason of using polymer is to achieve a better chemical resistance to corrosive substances. Usage of polymer allows reducing fouling as it would occur in conventional metal heat exchanger. The good chemical resistances of polymers allow potentially proceeding to a heat exchanger cleaning using chemical substances.

Makatec GmbH has designed a spiral polymer film liquid-liquid heat exchanger, which is especially dedicated for heat exchanges in low heat fluid mediums. This heat exchanger presents several advantages. One can mention the possibility to adapt the exchange surface to the required heat load by increasing spiral length or width. Furthermore materials cost is low and the production of such heat exchangers in series would lower it even more. Allowing proceeding heat recovery at low cost and even for small wasted energy sources, it would be an important step reducing human energy consumption by proceeding to heat recovery everywhere possible.

Taking advantage of those considerations a new design of Spiral Polymer Film Gas-Liquid Heat Exchanger (SPFGL HEX) has been developed adapting the design of Makatec liquid-liquid design. This report will present the work accomplished for this development. In Chapter 2 one can find the objectives and the accomplished work and set up of the present master thesis. Chapter 3 explains the design and a methodology followed for SPFGL HEX realisation. Chapter 4 presents the NASATEC (New Available Sustainable Air Conditioning Technology) facility developed to test SPFGL HEX performances using exhaust gases and water. Chapter 5 is dedicated to SPFGL HEX performance analysis obtained with the test facility. Chapter 6 will extract the main point of this report and make some conclusions and improvements to realise. Finally Chapter 7 contains the Appendix and all specific details will be found in this chapter.

Chapter 2 Project highlights

2.1 Objectives

In order to operate low-temperature heat recovery, the LOVE project aims to develop and test innovative designs of HEX capable of running with aggressive substances which are corrosive, moist and dusty such as cement powder gases or exhaust gases. In other words, the aim is to recover heat contained in such gases.

The main objective of this master project is to develop a gas-liquid heat exchanger able to operate with temperatures below 120°C and reaching a heat load of about 5kW.

Since gases are highly compressible and the energy that would be required to balance pressure drop is significant, the lowest pressure drop is targeted in the gas heat exchanger channel. The targeted range is about 10 to 20 mbar. Pressure drop is the pressure loss in the gas or liquid flow between input and output of the exchanger due to the obstacles and friction in the channel.

The innovative technology provided by Makatec is based on polymer film. Using high heat transfer polymers, an exchanger based on such technology can resist aggressive substances mentioned above. It also lowers channel fouling by avoiding corrosion that would occur in conventional metal HEX when becoming rusty.

The use of polymer in a serial production of these heat exchangers lowers the associated production costs.

Makatec design for polymer spiral film liquid-liquid heat exchangers has been modified in a Polymer Spiral Film Gas-Liquid Heat Exchanger (PSFGL HEX) and adapted to allow flowing gases through the exchanger. The design of these heat exchangers will be developed in Chapter 3 .

The second part of the project consists in building a test bench which is able to measure and test performances of this type of heat exchanger. It aims to provide a flow of exhaust gases with a known composition and at a suitable temperature. It is also required to measure pressure drop, flow and temperature on both gas and liquid channel of the PSFGL HEX.

The ultimate purpose is to provide a test bench and a PSFGL HEX casing that can easily allow testing a prototype in order to optimise its performance with respect to heat recovery, overall heat transfer, pressure drop and temperature range.

One objective was possibly injecting water in the exhaust gas flow to obtain a fluegas at the PSFGL HEX gas input. The fluegas condensation would then improve the potential recoverable heat.

2.2 Project course

As the project has been driven with 40 per cent of the time at the EPFL in Switzerland and 60 per cent by Makatec GmbH in Germany; we'll present shortly here the project management timeline.

The project was executed within a 6-month time frame which can be divided into 4 main parts numbered in red on the left of the project Gantt task plan presented in Figure 2.1 below.

The *first part* took place at the EPFL. In this period, the first objectives were fixed and rehabilitation of the main components such as the engine unit and gas preconditioning devices has been achieved. Jointly a major part of the time has been spent on the Labview measurements software taking in account the functional understanding of the various sensors and the integration with the developed software. This part has been supervised by Professor Daniel Favrat, professor of LENI laboratory at EPFL and Johannes Wegele working for the LENI laboratory.

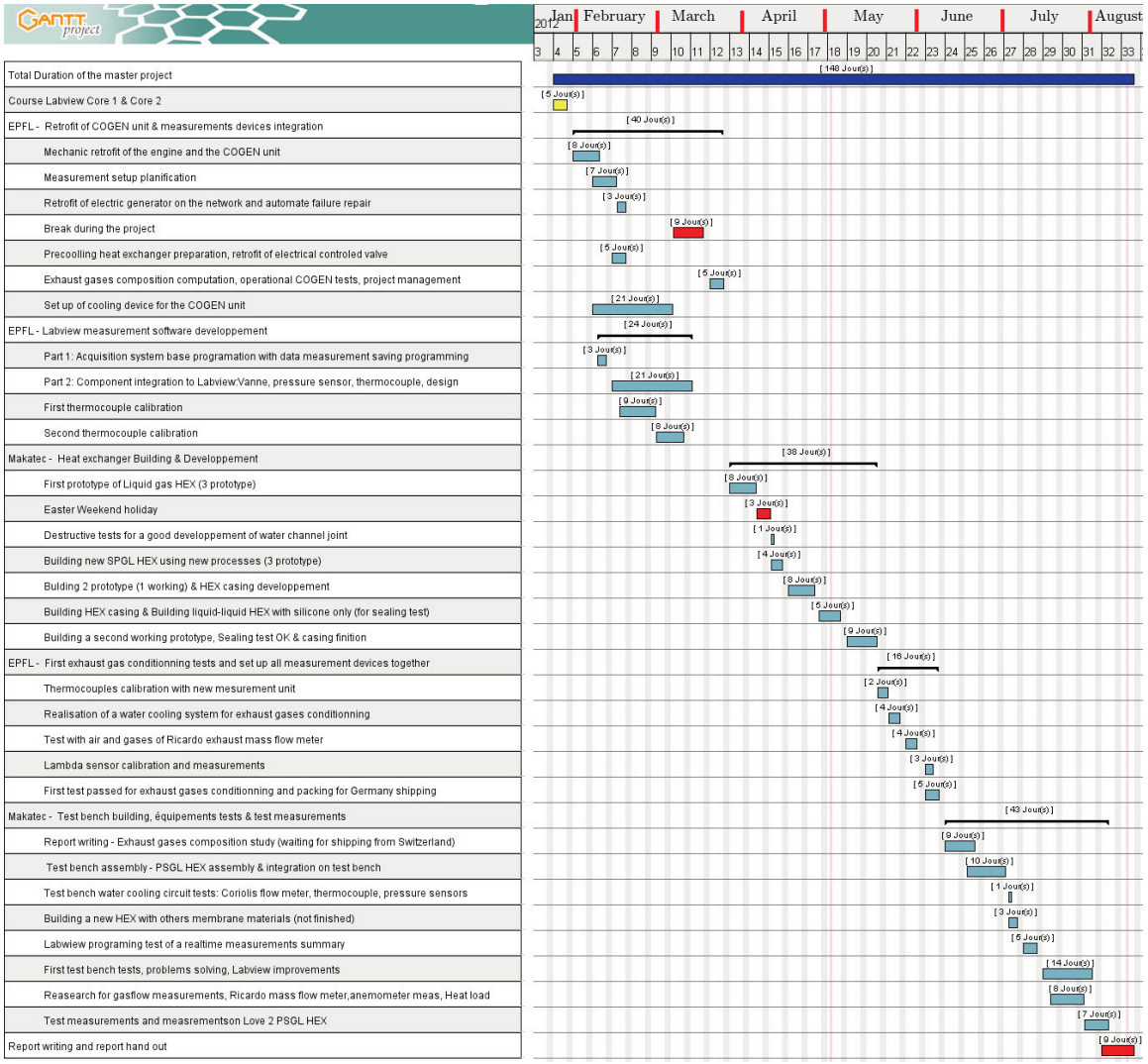

Figure 2.1: Gantt diagram of the complete 6-month master project, detailing the four main periods (red numbers on the left side of the table), achievement with duration of the realised tasks for each period of the project.

Part two of the project took place in Germany at Makatec GmbH, where polymer spiral gas liquid heat exchangers were developed. There, the best production processes were searched to insure a good sealing of the liquid channel of the exchanger. During this period, a special heat exchanger casing has been realised for the PSFGL HEX allowing exhaust gases to flow through the exchanger. This part has been supervised by Dr. Thomas Weimer, CEO at Makatec GmbH.

Part three was a short return to the EPFL. Once the specifications of the PSFGL were set, all efforts have been concentrated on the design of a complete facility or test bench integrating exhaust gases conditioning and measurements of the exchanger operating values. Feasibility tests have been done with various main components and future needs have been planned in order to take advantage of materials which were available at the LENI laboratory (EPFL) and therefore reducing future costs in Germany. Towards the end all equipements such as COGEN unit including a precooling, a gas heat exchanger, gas flow meter and the measurement devices were shipped to Germany by truck.

The *fourth* and last part of this project, all devices were put together in order to achieve a complete test bench capable of measuring PSFGL HEX performances when operating with exhaust gases and water. Labview software has been jointly improved for test requirements. After solving device failures, tests were successfully executed shortly before the end of the project.

2.3 Project learning and overcome challenges

In this part we wanted to highlight the multiple faces that took this project and which will be developed later in this report.

A large part of this project was devoted to understand, test and implement measurement devices. This part of the project was more oriented in the measurements technique. Thus it has been necessary to deal with pressure measurement in gas flow. Such flows are compressible and subjected to pressure oscillation which makes measuring it difficult.

There needed to find a way to deal with the electronic as it was necessary to understand how to operate with the differential pressure sensors available. It was necessary to understand electrical schemas; take measurements in the devices as ai properly had to understand how to make if functioning properly. It was also found that it was necessary to change the HP measurement unit as noise occurred on the thermocouple measurements, thermocouple calibration have been executed twice.

Gas mass flow measurements have been successfully accomplished. Measuring hot gas flow is a difficult task as gas in movement is unstable. Also devices for such measurements have to be temperature resistant. In spite of encountered problems, 4 methods have been explored providing for some of them successful results. It has

also been necessary to understand gas flow behaviour as it occurs in the laminar flow meter used or when analysing the pressure drop in the heat exchanger.

Also a good knowledge of the measurement devices has been acquired as I had to repair by myself failure on the automaton of the Cogeneration unit (COGEN unit) in Germany. It has been the same with the functioning of the Diesel engine.

Electricity challenges were accomplished as it was necessary to connect the COGEN unit to the 400V electricity network in order to release the electricity produced by its generator.

Building the test bench was necessary to find solutions as for removing sealing rings out of the second hand thermocouples without breaking them. Another innovative solution found was the use of some blind POP rivet to fix the PSFGL HEX casing insuring the gas is sealed properly.

It was necessary to understand and test how materials such as EPOXY resin, silicone and various polymers can be used in order to make the PSFGL HEX sealed and pressure resistant. Techniques have been developed to close liquid channel cross section of the PSFGL HEX.

Accident management has been required when a mercury column used for pressure sensor calibration overflowed, pulverising micro mercury balls all over the lab.

During this project management and planning resources were necessary because some devices were only available at one place. Welding, measurements devices were available in Lausanne and plumber fittings in Germany. For each part of the project it was necessary to plan in advance and bring the required materials and equipements.

It was necessary to reduce the costs as much as possible. High efforts have been dedicated using available devices.

It was also a time challenge as for each period of the project, it has been necessary to adapt the devices to the place. For instance I had to make the COGEN unit functioning in Switzerland and then later in Germany. And also to plan the transportation of all the required devices composing the developed facility.

Also a technical vocabulary has been acquired in the three languages as to know German, English and French.

To conclude with this part, this project has been fulfilled with everyday challenges and it has been an excellent way to use the theory acquired during my studies in developing a concrete and high innovative product as PSFGL is. Also facing and solving problems which for any knowledge have been previously acquired.

Even various topics have been treated during this project, as energy, polymer materials, programing, measurement technique, fluid mechanic, gluing technique, electronic, electricity, chemistry, management, and relational skills. We think this project is a good example of the various subjects that have to handle and mechanical engineer and that makes engineers life always challenging developing new technology.

Chapter 3 Polymer Spiral Film Gas-Liquid Heat Exchanger (PSFGL HEX) development

In this chapter, section 3.1 will present the design of a PSFGL HEX, in section 3.2 various materials used in a PSFGL HEX will be presented. Appendix F will provide gluing tests realised to develop a perfectly sealed liquid channel. In chapter 3.3 manufacturing processes will be described and chapter 3.4 will present the quality test driven at the end of the manufacture process.

3.1 Design of polymer spiral film gas-liquid heat exchanger

The developed polymer spiral film gas-liquid heat exchanger takes the form of a cylinder. Length is in the range of 700mm and outer diameter is 200mm. Width and length of the rewinding of PSFGL HEX can be adapted in function of the required heat load to be exchanged. Figure 3.1 shows such heat exchanger.

Figure 3.1: Polymer Spiral Film Gas Liquid heat exchanger designed for low heat recovery in soiled gases

The basic design of PSFGL HEX has been taken from the polymer spiral film liquid-liquid HEX already produced by Makatec. The main difference is concerning the gas side. The following Figure 3.2 presents the schematic of PSFGL HEX design; it will be described in detail below.

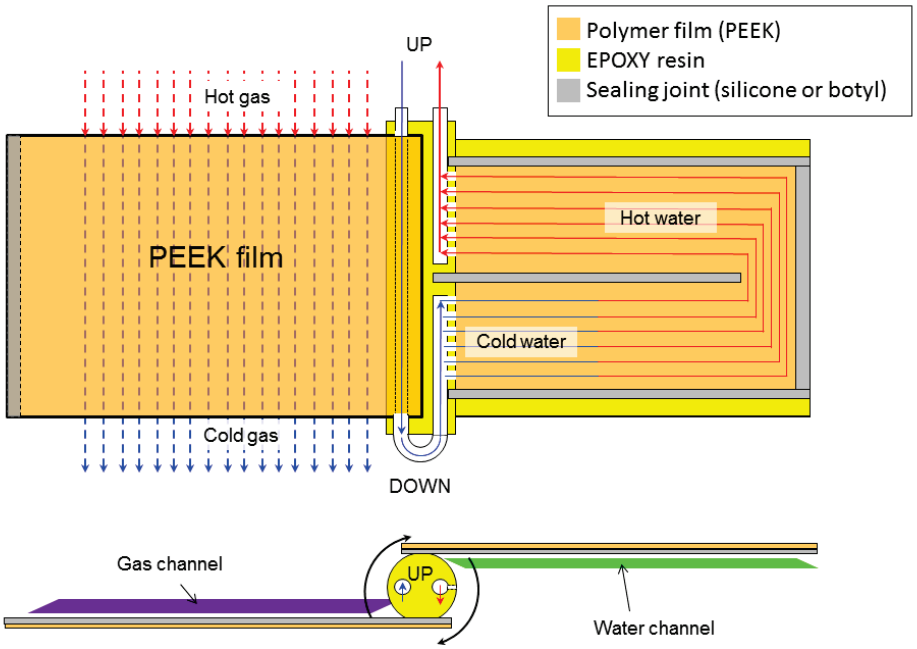

Figure 3.2: Schematic of a Polymer Spiral Film heat exchanger when unwinded. *Upper schema:* flat projection, when unwinded. *Bottom schema:* cross section of unwinded exchanger. View from UP.

Figure 3.3 below present the cross-section of PSFGL HEX and represent the flowing path of the gas and of the liquid as it will be explained below.

Fluid channel: The central body made of EPOXY resin insure both input and output of the liquid channel. Liquid spiral entrance is made through few holes made in the central body pipe. Such holes can be seen on Figure 3.4 number 1 below. Entrance is provided on the first half length of the cylinder and the flow runs from the spiral the central body to the outer spire. At the very end of the winding (outside) the joint located along the spiral at the half length of the cylinder stops and the flow passes from the first half length to the second half length of the HEX. Then the liquid flows through the spiral in the reverse sense, from the outer spire to the centre of the spiral and exit through holes made on the second half length of central body.

Gas channel: Gas flows through the whole spiral cross-section from one end of the cylinder cross-section to the other. Along the spiral winding gas channels and liquid channels are separated each other by a polymer film, meaning there are two films in the spiral, one for each side of a canal.

The interest of the gas channel design is to decrease the pressure drop on the gas side and to have a pseudo counter flow heat exchange between gas and liquid channel. Both criteria aim to improve the efficiency of PSFGL HEX.

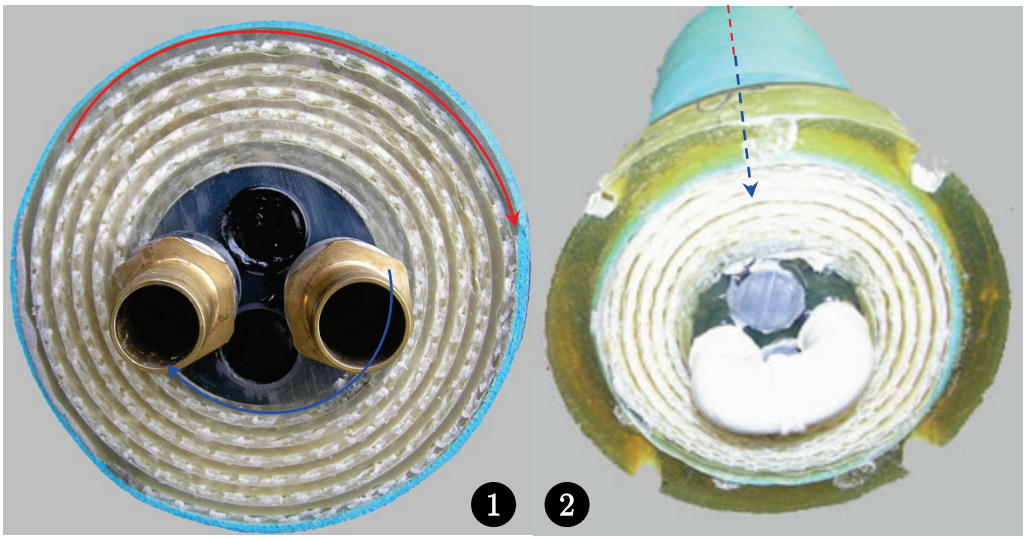

Figure 3.3: PSFLG HEX cross-section. *1)* Input gas cross-section. Full blue arrow is the cold water input in the spiral; full red arrow is the warm water at the outer spire of the spiral when going to the second half length of the exchanger. 2) Output gas cross-section. Dash line represents the direction of the gas flow when cooling through the exchanger.

The next section will present the materials used in PSFGL HEX.

3.2 Overview on materials used

PSFGL HEX is built with various materials and each material has its specific functionality. Selection of materials has been done with a special care according to technical and cost criteria.

Polymer film: Being the most important component the film is a key point in the PSFGL HEX. As it has the role to transfer the heat from the gas side to the water side of the heat exchanger, it requires the highest thermal conductivity and a temperature resistance over 100°C to reach high performances. In order to increase thermal conductivity the film has to be as thin as possible and at the same time resistant to the liquid pressure on the water channel. When pressed against the mesh it shouldn't be irreversibly bent. Thus it has to be a polymer to answer corrosion resistance constraint. Polymer also limits fouling on the heat exchanger walls.

Answering to these criteria Polyetheretherketone (PEEK) has been used. With the highest thermal conductivity of all polymers K=0.25 W/m K, PEEK is resistant up to 250°C. PEEK is an expensive material, with a film price of several tenth euros per square meter.

Mesh: The mesh allows creating a channel within an approximate 4mm thickness and a hard structure between both films of the heat exchanger. Mesh holes allow liquid and gas to flow inside the channels. The structure of the mesh is

important in order to create turbulent flow which is increasing the heat transfer between each side of the film.

Polypropylene (PP) mesh has been used as it was already used for polymer spiral liquid-liquid heat exchanger. The mesh is about 2mm thick. It means that two meshes have to be superposed for each gas and liquid channel. PP can resist to temperature up to 100°C, is a relatively cheap material and has a very good chemical resistance. Chemical resistance is an import issue. First to stand aggressive gases but to allow also chemical substances to clean a dirty heat exchanger.

Pipes: The input and output pipes have been designed in Polypropylene Holomer (PP-H). This material has a temperature resistance similar as PP of about 100°C, also relatively cheap it is easily available in pipe shape.

EPOXY resin: As we need to build a leak-proof liquid channel, Epoxy resin has been used. It can resist to very high temperature above 200°C and has a good chemical resistance too. As it is a viscous fluid after mixing the two components, it becomes later hard and sticks to the film. It provides to the spiral a rigid structure that is hardly to acquire in PSFGL HEX as only one side has to be closed on the cross-section of the cylinder. For polymer spiral film liquid-liquid HEX it is possible to close the complete cross section casting epoxy on both cross sections. As it requires quite long preparation and is also costly, EPOXY resin has been used during the project for all temperature resistant and custom designed shapes, including the components in the exchanger casing.

Botyl: This material looks like chewing gum and allows maintaining the spiral together during the production process. As it is sticky, it provides a provisory sticking of the mesh and film together before the liquid channel sides are closed with EPOXY resign.

Silicone: As silicon is able to stick well to the film, the sticking analysis in Appendix F has shown that one component silicone can well stick to the film and to the EPOXY once dried out, but not to the mesh.

Polyurethane: To provide a rigid outer matrix polyurethane strips have been used. As it hardens after a few tenths of a minute and has a good temperature resistance up to 200°C, polyurethane strips are commonly used as plaster bandage in medicine. Those strips can be obtained at low price and allow to build a rigid outer shell to PSFGL HEX.

3.3 Polymer spiral gas liquid heat exchanger manufacturing processes

Our first aim was to concentrate our efforts on mechanical resistance and sealing of the PSFGL HEX water channel. The next step after this project is to improve PSFGL HEX performances.

First steps in building a PSFGL HEX is the casting of the EPOXY central body. As shown in Figure 3.4 both input output pipes and winding pipes are casted in an EPOXY cylindrical matrix. Then two series of holes are made first on the first half length of the body and secondly on the second half length of the body allowing liquid enter/exit from the pipes in/to the spiral of the exchanger.

Then both films and meshes are cut to the appropriate dimensions. Botyl band is placed on mesh sides in order to glue temporarily sides of the spiral winding during fabrication. To improve sealing joints, both films have to be plasma treated wherever it is glued.

Figure 3.4: Central body made of EPOXY resin. 1) Two series of holes are designed for liquid spiral entrance and spiral exit. Liquid input and output are both located in the right bottom corner, clear grey pipes. 2) Section of a central body. Liquid input pipe cross the complete body, output pipe stops at body half length.

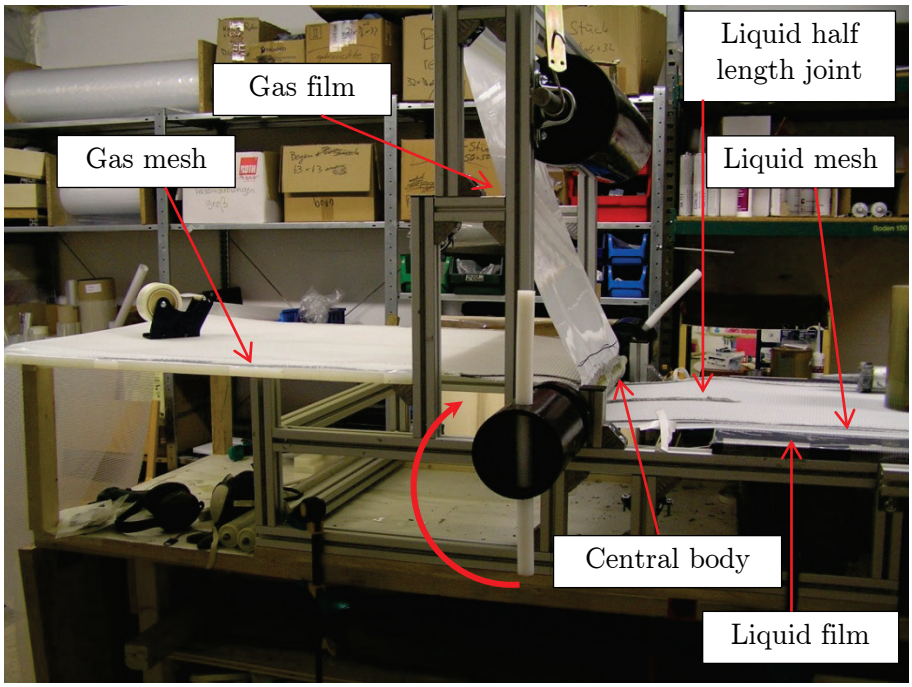

Figure 3.5: Configuration to wind of a Polymer Spiral Film Gas Liquid heat exchanger.

Figure 3.5 presents the machine used to wind a PSFGL HEX. The liquid film and mesh(above) are placed on the right hand flat surface. The separation joint is made in the middle of the mesh width.

The gas mesh is placed on the left flat surface in Figure 3.5. Gas film is unwinded from an upper cylinder insuring the film to be tightened when winded in the PSFGL HEX. The winding operation of an exchanger is made by turning the central body as the red arrow shows in Figure 3.5.

The next step is to inject EPOXY resin before it becomes hard on the both cross-sections of the liquid spiral. This operation is very critical; epoxy resin has to be at approximately 55°C to penetrate deeply into the liquid spiral reaching the Botyl joint. At this temperature the disadvantage is that EPOXY resin becomes quickly hard and doesn't have time to flow through the liquid mesh. One also has to keep in mind that no resin must penetrate in the gas mesh on the other side of the film. As gas mesh cross section must be left open. Figure 3.6 number 1 and number 2 present the cross section before and after this operation. Detail of a sealed liquid cross-section is presented at number 3.

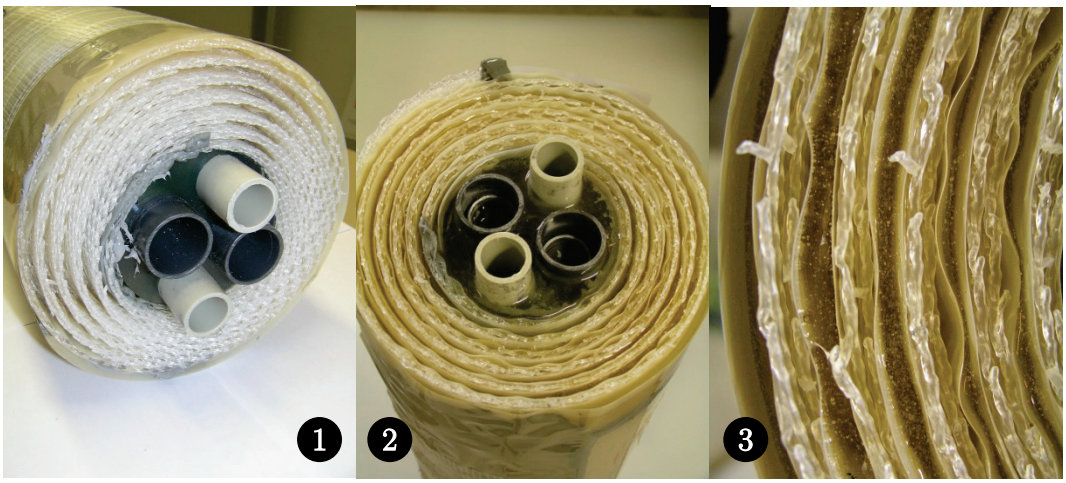

Figure 3.6: Cross-section of polymer film spiral gas liquid heat exchanger. 1) Just after the winding operation of the exchanger. The liquid channel is closed temporally with Botyl band. Liquid mesh is less wide as gas mesh and is a few centimetre far away from the exchanger cross section. It can be seen in the photo. 2) Exchanger lateral cross-section when liquid channel have been sealed with EPOXY resin 3) Detail of exchanger side cross section. Yellow lines are liquid channel closed with EPOXY. White lines are the gas mesh. Films are visible between EPOXY and mesh.

Once the operation is done, polyurethane bands are winded on the outer surface of the cylinder to give the heat exchanger a hard shell. This shell is required in order to increase the pressure resistance of the heat exchanger.

The last step is to cast an EPOXY binding on the gas output side. See Figure 3.7 number 1 as it is when finished. Its function is to fix the exchanger in its casing and seal gas input and output. Epoxy is casted in a pipe surrounding the exchanger as shown on Figure 3.7 number 2 and 3. The pipe is then removed when EPOXY is hard. This step is critical as EPOXY resin shouldn't flow on the bottom mould that has been closed before operating with foam.

When uncased, the binding has to be finished with an angle grinding machine. Surfaces have to be flat to provide a good sealing and notches (see Figure 3.7 number 1) have to be cut to allow screws to fix the exchanger on its casing base.

When finished a polypropylene elbow fitting is welded at the exit cross section as shown on Figure 3.7 number 1. This elbow allows liquid input to be made from the input gas cross-section where water output is done. It avoids to have water input on the output gas cross-section in the bottom of the PSFGL HEX.

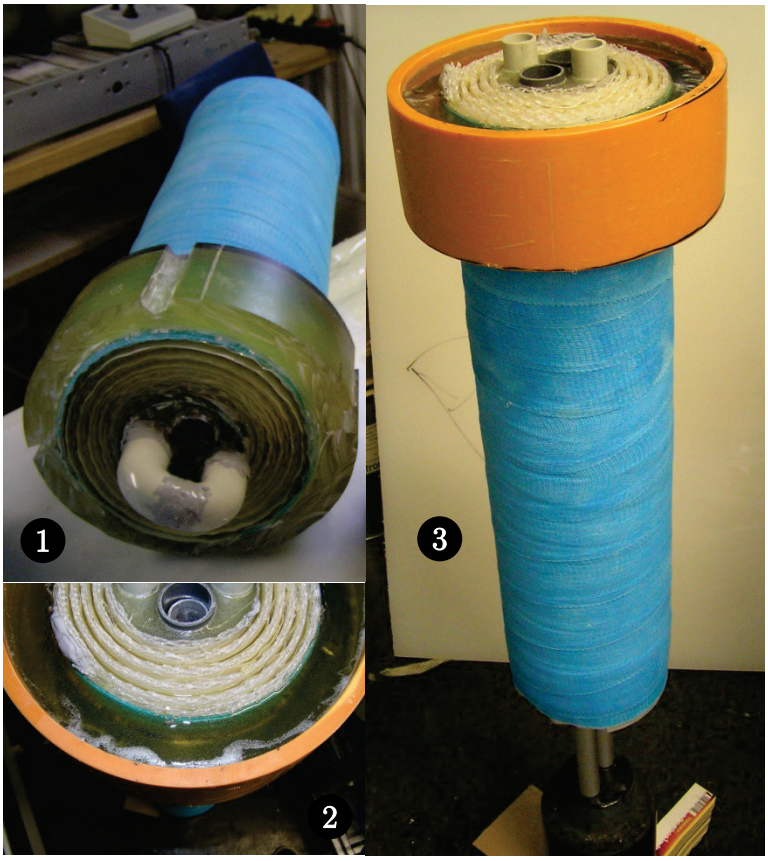

Figure 3.7: EPOXY binding is casted to make a sealing joint between gas input section and gas output section. 1) Epoxy binding when finished 2) Detail of the cross-section when epoxy is casted. 3) All exchanger when EPOXY is casted.

Once all those operations are realised, PSFGL HEX is finished and can be tested. Main test operations will be presented in the next section below.

3.4 First quality tests on water side

Here will be presented the sealing tests and water side functionality tests that are realised on PSFGL HEX.
Once the heat exchanger is finished and as soon as the silicon and the EPOXY on the inside of the heat exchanger have been completely dried out, the heat exchanger is placed under water in a tank. An air pressure of about 500mbar relative is exerted on the water channel. To proceed in this way, the input of the liquid channel is bound to an air pressure relief valve with a manometer, output is closed.

The presence of leakage is immediately detected if a regular bubble air flow is reaching the water surface as shown on Figure 3.8.

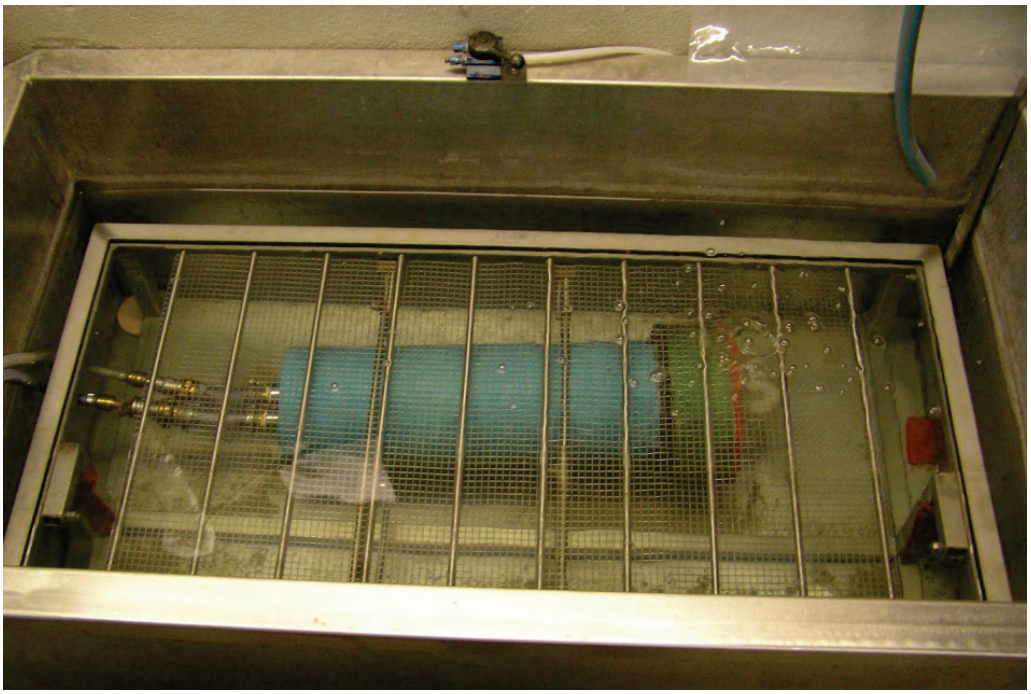

Figure 3.8: Static air pressure sealing test on liquid channel of PSFGL HEX. Air bubbles are reaching the water surface.

If no bubbles are detected after leaving the HEX under water for a period of an hour the HEX can be considered as static airproof and the liquid channel can be tested with water flow.

When the static air test is passed, the HEX is placed in the Makatec water flow test bench designed for testing polymer spiral film liquid-liquid heat exchangers. On this test bench the water channel of the PSFGL HEX is tested with hot water up to 60°C flowing up to 650 kg water/h as presented on Figure 3.9.

Figure 3.9: Makatec water flow test bench with a PSFGL HEX to be tested on the liquid side. The hover bind on the gas output sucks up air to cool the water.

Test procedure begins with a lower flow rate of about 100 l/h and with low temperature of 25°C. After 2 hours, if no leakage occurs with the maximum flow and maximum temperature the PSFGL HEX is assumed to be sealed. The PSFGL HEX is then ready to be tested using exhaust gases and water in the Nasatec test bench that will be presented in Chapter 4 , this is the next chapter.

In this chapter we have seen in detail how was designed, build and tested a PSFGL HEX. The next chapter will present the facility set up developed in order to test PSFGL HEX in its appropriate working condition with aggressive medium such as exhaust gases and with water.

Chapter 4 Measurement facility

In order to describe the efficiency and the possible heat recovery of a PSFGL HEX a Nasatec facility (New Available Sustainable Air Conditioning Technology) has been developed integrating a set up conditioning exhaust gases produced by a Diesel engine. Section 4.1 to 4.5 will shortly describe the facility units and theirs realisation. The following sections will concern the software developed using Labview in section 4.6, the exhaust gases analysis in section 4.7, the pressure drop and temperature measurement in section 4.8 and 4.9, lambda measurements in section 4.10, instrumentations for water and exhaust gas flow measurements in section 4.11 and Appendix D and finally the dynamic behaviour of the test bench in section 4.12. More information about the specific instrumentation will be found in the Appendix A , Appendix B , Appendix C ,Appendix D , Appendix E and Appendix G .

On the next page a diagram flow sheet of the test bench is presented.

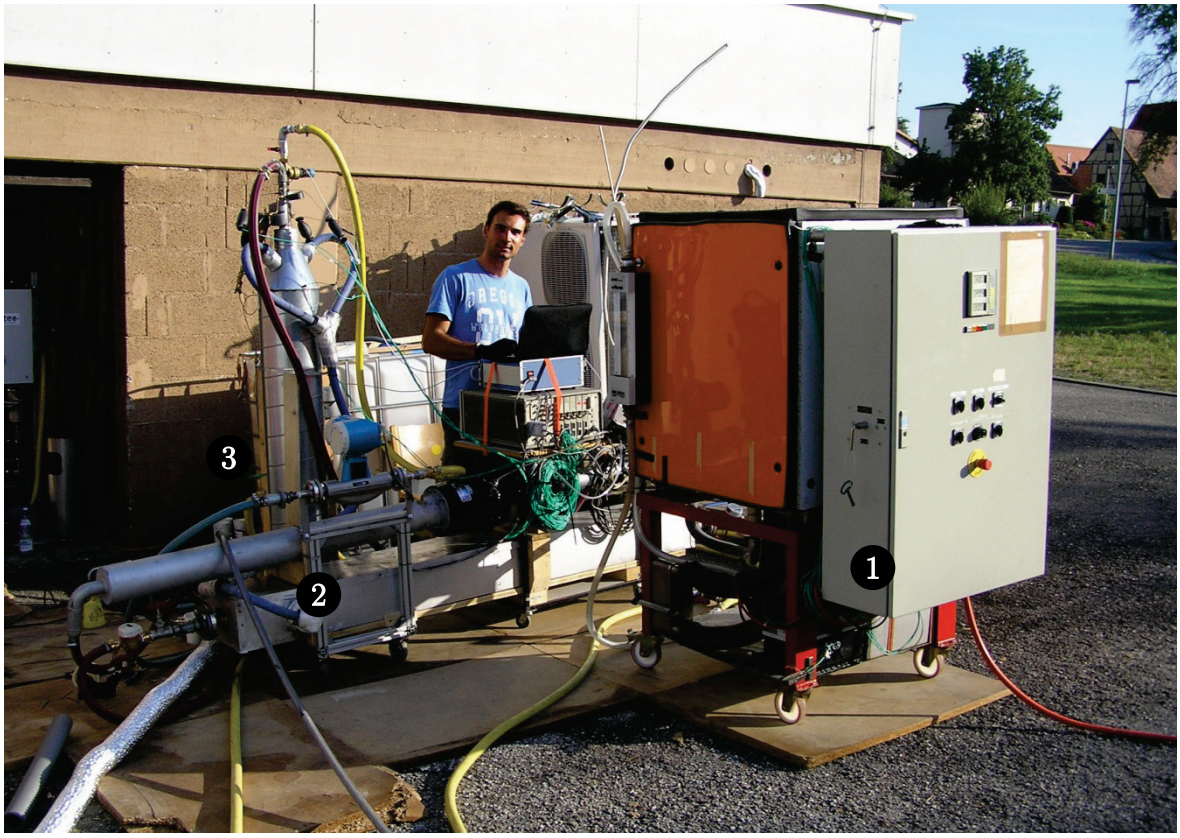

Figure 4.1: The Nasatec test bench and its operator during a test run at Makatec GmbH. 1) The COGEN unit with control panel. Inside orange cube is a Lombardini Diesel engine and an 11kW electrical generator. 2) Inside the rectangular steel casing is the pre -cooling heat exchanger conditioning exhaust gases. 3) Vertical cylindrical casing with a hat on the top is the spiral polymer film gas liquid heat exchanger (SPFGL HEX) casing. SPFGL HEX to be tested is placed inside.

Nasatec test bench flow sheet

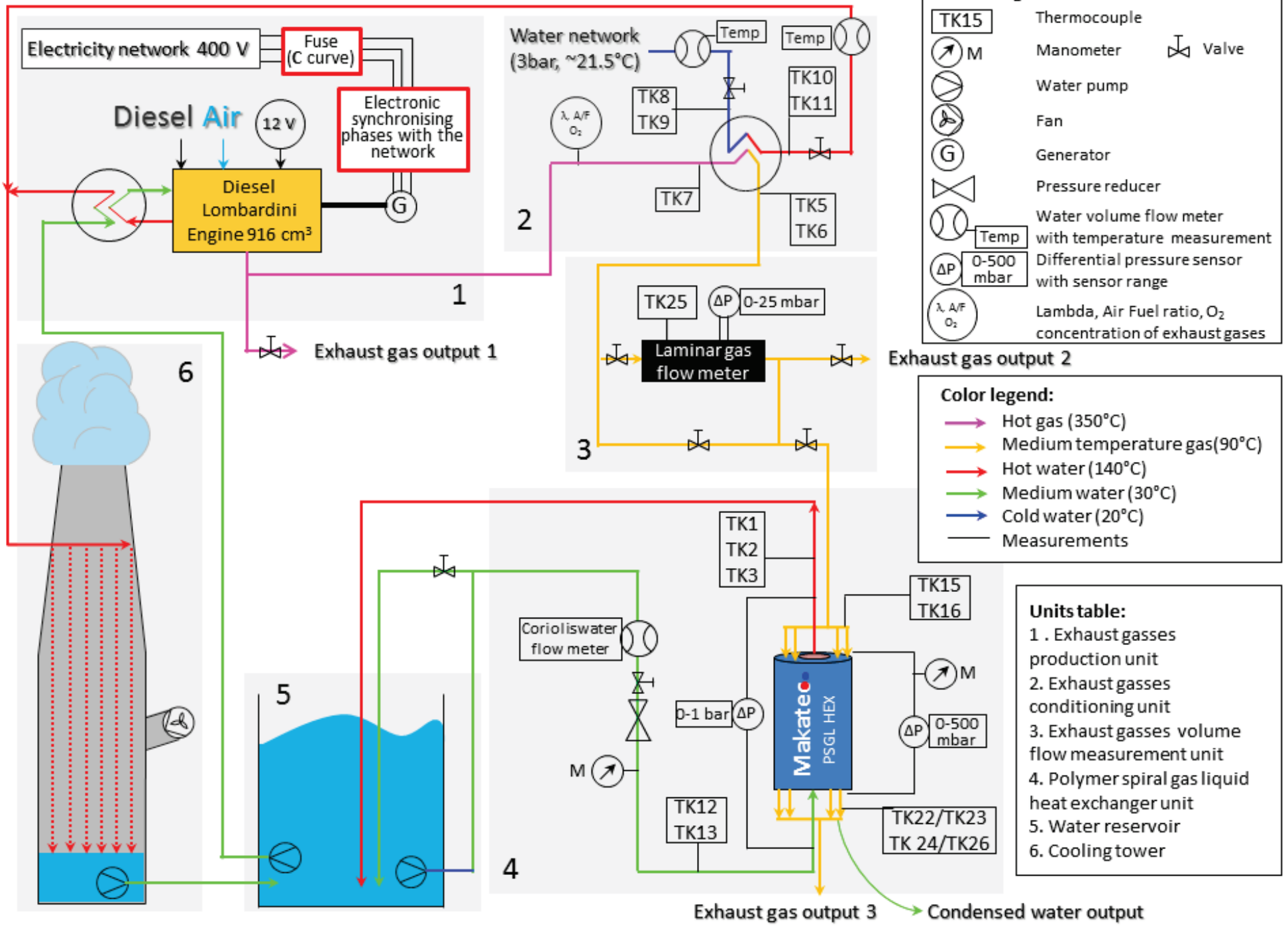

4.1 Polymer spiral gas liquid heat exchanger test bench setup and realisation

The test bench has been realised using mostly devices and materials which were already available at EPFL or at Makatec. It was necessary to realise this installation at minimum costs. The flow sheet of the Nasatec test bench is presented on the previous page. In the following paragraph, the main units of the facility will be identified and described.

Unit 1 (see flow sheet on page above) is the co-generation (COGEN) unit that contains a Lombardini 916cm3 Diesel engine coupled to a 11kW electric generator and electronics which allows to produce current phased with the network current. The goal of this unit is to produce electricity and heat from Diesel fuel. In our project this unit has been used mostly as a source of heated corrosive and soiled gases. The electrical generator is used to create a load on the engine which allows the engine to run at full speed. At full speed the engine produces an appropriate exhaust gas flow of about 20g/s. For detailed explanation about this unit one can refer to Appendix B .

Unit 2 is the gas conditioning facility. It consists of a steel tubular heat exchanger (called later steel HEX or steel tubular exchanger) from EPFL which has been rehabilitated to pre-cool the exhaust gas. As a reminder, the aim of PSFGL HEX is to recover low heat temperature from soiled gases. In order to provide similar operating conditions we need to cool down the exhaust gases from 350°C at the engine's exhaust pipe to about 100°C at the steel tubular exit. Cooling operation is done with fresh pressurized tap water in this steel tubular heat exchanger. Temperatures and water volume flows are measured at the heat exchanger's inputs and outputs. For more details about the gas conditioning facility see section 4.3 and Appendix C .

Unit 3 is the gas flow measuring unit. This unit can measure volume or mass of the exhaust gas flow. This unit is composed of a laminar gas flow meter coupled to a series of valves which allows the gas flow either flowing in the flow meter or by-pass it. There is also the possibility to release the preconditioned gas flow to the atmosphere. This would be necessary when the engine is running and no gases have to flow through the PSFGL HEX. More details about the laminar flow meter are given in the section 4.4 and Appendix D.1.

In Unit 4 the PSFGL HEX is placed in its steel casing. The water side of the HEX is cooled using water from the reservoir and the gas side is fed with temperature conditioned exhaust gases coming from unit 3.

Pressure losses on both HEX sides are measured with pressure differential sensors, input and output temperatures are measured with thermocouples. To obtain

accurate measurements several thermocouples have been placed at each measurements point. Thermocouple numbers that figure in the test bench flow sheet were attributed at the very beginning of the project, when thermocouples were calibrated. It has sadly happened that some thermocouples haven't been used yet or have been broken; thus thermocouples numbering is more linked to the slot on the measurement unit rather than to a logical numbering on the test bench.

Water flow in the HEX has been measured with an accurate coriolis mass flow meter. More details about water flow measurements are given in section 4.11.

Unit 5 is a cubic meter reservoir of water used to supply in cooling to the other units. Two garden water pumps have been placed in the reservoir in order to make the water flow through cooling circuits.

Unit 6 is the cooling tower. Hot water from the engine and the steel HEX flows through the tower to be cooled. In the cooling tower, an air flow is created by a fan, in order to cool efficiently the hot water.

In the following sections we'll enter deeper in the various units.

4.2 Unit 1 – Exhaust gas production unit

The gases are produced by a co-generation unit that has previously been used at the EPFL for a study on a small hybrid power plant for electricity production. The co-generation unit is composed of a 3 cylinder, 903 cm^3 Diesel Lombardini Engine coupled to an 11kW electricity generator able to be electronically synchronised with the network and to produce electricity. Appendix B details the complete work accomplished for the retro fit of this unit according to the purpose of this project and some recommendations concerning the functioning of the unit. A complete exhaust gas composition analysis can be found in Appendix A .

Figure 4.2: Cogeneration unit after the retro fit operations in the mechanical hall of LENI laboratory at the EPFL. Photo shows the setup of the first tests of the conditioning facility equipment as tubular heat exchanger, gas flow meter and lambda sensors with a buffer water reservoir.

4.3 Unit 2 – Exhaust gas conditioning

The temperature of exhaust gases at the exhaust pipe of the engine is around 500°C, their composition depends on the λ value measured at the exhaust exit. Lambda measurements and analysis are presented on chapter 4.10 and an exhaust gas composition analysis is proposed in Appendix A

For generating a gas flow in the PSFGL HEX, the gas has to be cooled down from about 600°C to a temperature below 120 °C. In order to achieve this, the gases are carried and cooled through a steel heat exchanger. The cooling water heat load is evacuated through the cooling tower of unit 6.

At the steel heat exchanger exit an arrangement of four valves drive the gases through the steel Ricardo gas flow meter. There remains the possibility to by-pass the gas flow meter. The flow meter is made of metal and insulating it properly is difficult. By by-passing it, it avoids important temperature losses in the gases. In chapter 4.4 and Appendix D page 75 all procedures and methods explored to measure exhaust gas flow are presented.

4.4 Unit 3 - Exhaust gas volume/mass flow measurement

The gas flow measurement unit has to fulfil the following requirements:

- Measurement device must support temperature up to 120°C.
- Presence of soot particles and steam in the flow must not be penalising.
- The volume flow measurement range has to be from 0 to 80m^3/h, it corresponds to the range of the maximal volume flow of the engine which would be measured for the tests.

First knowing the approximate max rotation speed of the engine specified by the manufacturer [1] is about 3600 t/min, and knowing that the cylinder capacity is 0.916 litres, we can compute the maximal volume flow of the engine. We have to use the assumption that the cylinders volume is completely empty at each two rotations of the engine (four-stroke engine).
The maximal volume is given by equation (4.1) as following:

$$\dot{V} = \frac{\omega_{engine}}{60} \cdot \frac{C_{cylinder\ capacity}}{2} = 27.48 \text{ l/s} = 98.9 \text{ m}^3\text{/h} \quad (4.1)$$

As it has been done in Appendix A.5 this volume flow at about 2 bars has to be corrected at the temperature of the gases when entering in the PSFGL HEX casing (120°C). The mass flow converted in volume flow through the ideal gas law gives a volume flow of about 81m^3/h. This value is close to the computed value at the same conditions through the Diesel consumption with the computed exhaust gases composition in Appendix A.5. (As reminder the value was 22.3 l/s = 80.28 m^3/h).

As it hasn't been possible to measure the real rotation speed of the engine, we can use the result of equation (7.15) to set a maximal limit for the exhaust gas volume flow. This limit would be 81m^3/h of exhaust gases at 120°C.

A laminar gas flow meter shown on Figure 4.3 has been finally used for the realisation of this measurement. This type of device is able to compute a volume flow while measuring the gas flow pressure drop and the temperature in the laminar flow meter. The volume flow can be converted in mass flow using formulas that are presented in Appendix D.1.

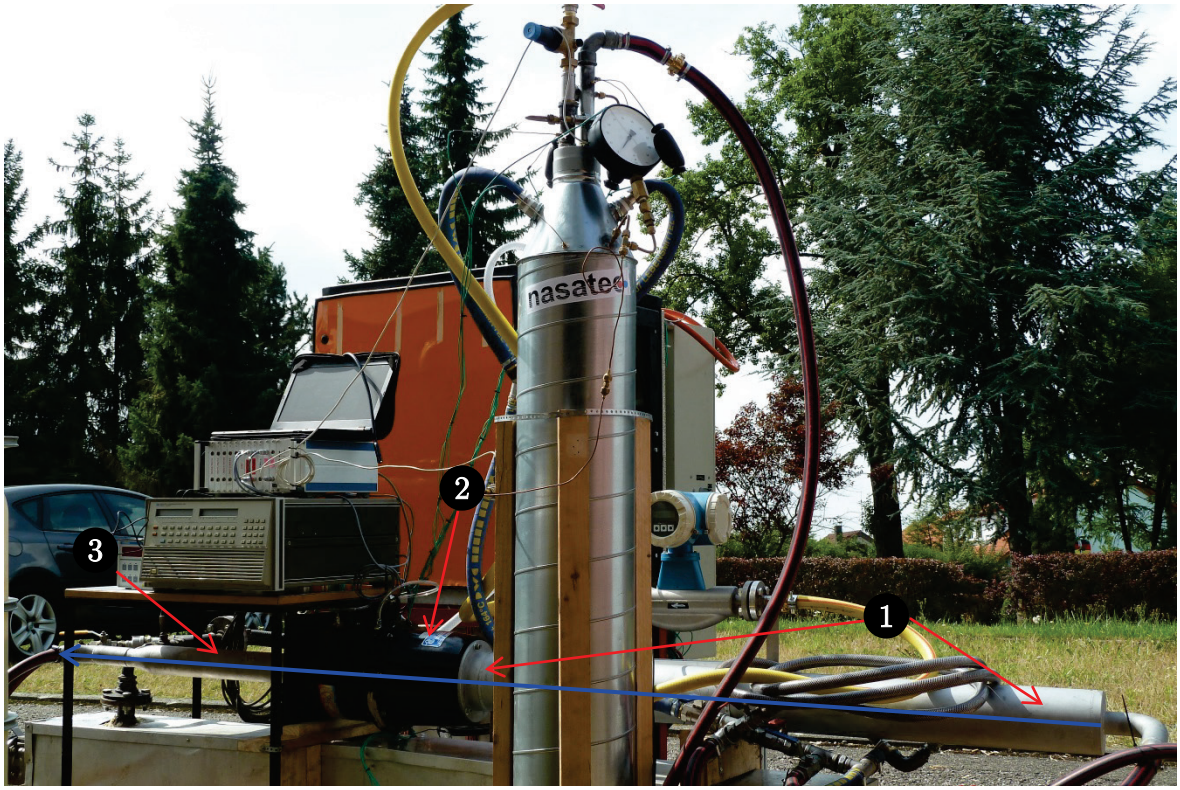

Figure 4.3: Nasatec test bench and its gas flow meter. 1) Straight input pipe of the flow meter measuring 1.3m to insure the flow to be fully developed and be laminar. Thermocouple is placed at the very end near the central part. 2) The black cylinder in the middle is the main element of the volume gas flow meter. Pressure drop is measured on this part. 3) Exit pipe. Blue arrow show how gases are flowing in the flow meter.

Considerable efforts were made to provide an appropriate volume and mass flow measurement. After some tests with the laminar flow meter, the mass flow was much higher than expected in the results given by the gas computations that are presented in Appendix A.5. Doubting the truth of the calibration equations of the flow meter, two others methods to measure the gas mass or volume flow were explored and are enumerated here.

The first method which also gave good results was implemented in the Labview software. It uses the heat load of the steel exchanger used to pre-cool gases. This method provided good mass flow measurements in the expected range, but it had to be carried out with special care. Deeper details about this method are given in Appendix D.2.

The second method consists in using a vacuum cleaner and an anemometer such as used in the air conditioning trade. By vacuuming air at the PSFGL HEX gas output, we were able to measure the gas pressure drop in the exchanger and the volume flow vacuumed with an anemometer. A function allowing computing the volume air flow as a function of the pressure drop in the gas side of PSFGL HEX has been established. Measuring the pressure drop in the gas side of the PSFGL HEX, the correlation in the measurements of volume flow and pressure drop in the gas channel of PSFGL has been compared with the volume flow measured with the laminar flow meter. Conclusion was that flow meter and the anemometer were

giving approximately the same volume flow measurements. More details about the results of this method are presented in appendix 0.

Going further, a third method using the volume flow measured by the anemometer and the corresponding pressure drop measured in the gas channel has been tested. The idea was to derive an equation which uses the pressure drop measured in the gas channel of the PSFGL HEX as a parameter to give the gas volume flow in the heat exchanger. This method did not provide accurate results at first. But with additional care it could become a good way to confirm the order of magnitude of the flow. The main disadvantage of this method is the increasing error in the measurements when exhaust gas fouling occurs. Pressure drop is hard to measure with accuracy, and measuring the volume flow through this value is a bit hazardous. Also the volume flow equation has to be derived for each heat exchanger. The methodology of this method is explained in appendix D.4.

Now returning to the solution developed by using the laminar gas flow meter of branded RICARDO INSTRUMENT and sold by G.Cussons Ltd, product number P7212. It is able to measure volume flow up to 400m^3/h and has been finally used to measure the gas flow. In this laminar flow meter, exhaust gas flow has to cross two wire-meshes. After a measurement time period the wire-mesh became full of combustion soot. The consequence was then an increase of the flow pressure drop meaning that the differential pressure measured in the mass flow meter gave an incorrect measured value.

The flow meter had to be the opened regularly and cleaned with compressed air flow and vaporized water as shown on Figure 4.4 numbers 1 and 2.

Figure 4.4: Laminar mass flow central element 1) Central element of the flow meter during cleaning with water and compressed air flow. 2) Exit and central elements of the laminar

mas flow meter once opened. 3) Entrance-wire mesh soot up after few hours of operation. 4) Entrance wire-mesh once cleaned.

To solve the gas flow soot up problem and obtain accurate measurements it has been necessary to make a duration soot up test in order to evaluate how long the measurement is accurate after a fresh cleaning service of the flow meter. Exhaust gases were allowed to flow through the flow meter during 3 hours. The results are presented in Figure 7.23.

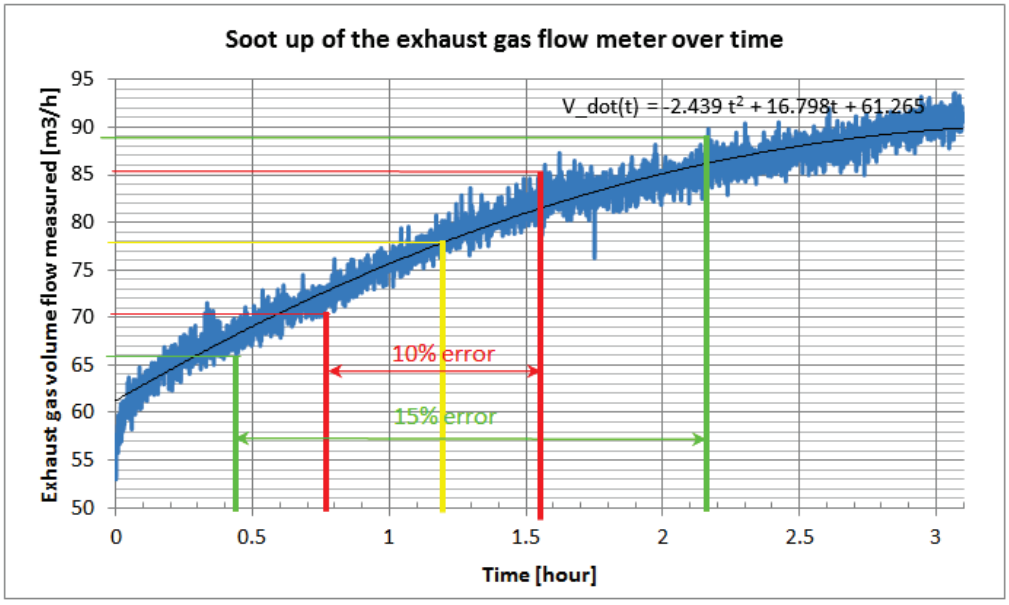

Figure 4.5: Changing of the measured value due to soot up of the exhaust gas flow meter over time when a constant 76.2 m3/h of exhaust gases flow through the flow meter during 3 hours. Cleaning service has been operated before test. Yellow line marked the aimed measured value at the specified flow. Red line indicates the operational interval of time when the error in the measurement is in 10% range. Green lines represent the same but for a 15% error of the right measured value.

Figure 4.5 shows that measured values are accurate in the range of 10% if flow measurements are operated within the 49 minutes between 45 and 94 minutes after cleaning the wire-mesh of the flow meter. If a measurement accuracy of 15% is required, the accurate measuring period is extended to 1 hour 44 minutes beginning 26 minutes after cleaning and ending 130 minutes after cleaning. The same graph is available in Appendix D when volume flow is converted into mass flow.

A gas temperature lower than 40°C in the flow meter results in water condensation. To deal with the condensation issue, the gas conditioning unit must be running in a stable state and must condition the gases to a temperature higher than 60°C before driving the flow through the flow meter in order to diminish water condensation in the flow meter.

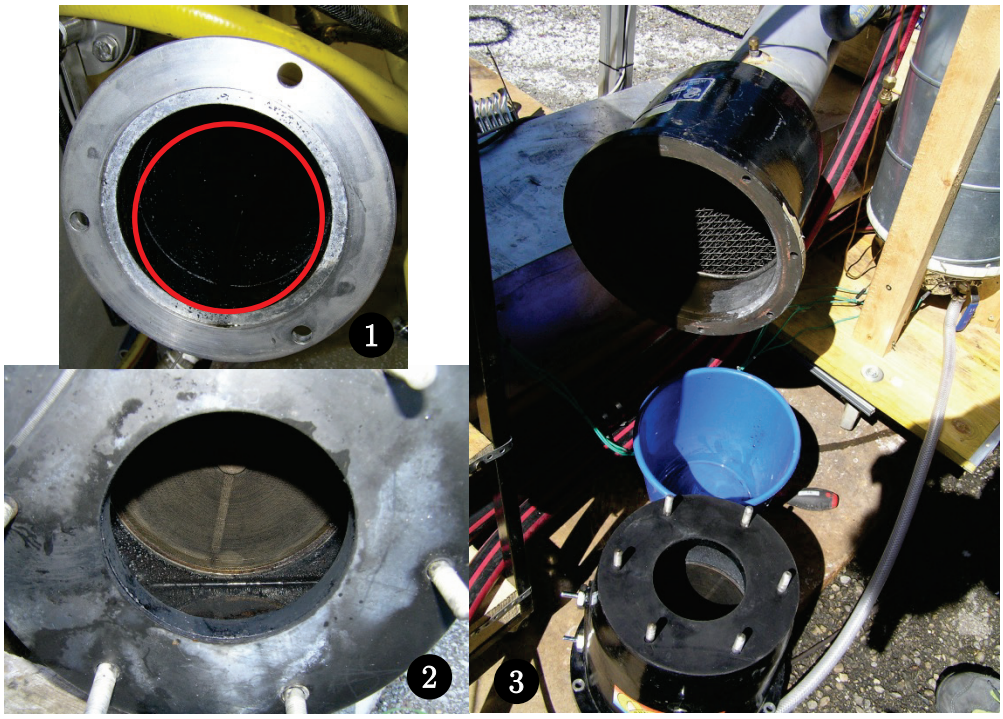

Figure 4.6: 1) Location of thermocouple in the input pipe of the flow meter view from the central element side. 2) Central element sight from the exit pipe of the flow meter when condensed water is accumulated after a test session. 3) Emptying of the input pipe element where condensed water is also accumulated.

4.5 Unit 4 - Polymer spiral gas liquid heat exchanger casing

In this section the specification of PSFGL HEX casing is presented. This casing was developed for providing exhaust gases and water to the PSFGL HEX. All connections for measurement devices have been integrated insuring the casing is completely gas sealed to a pressure up to 300mbar.

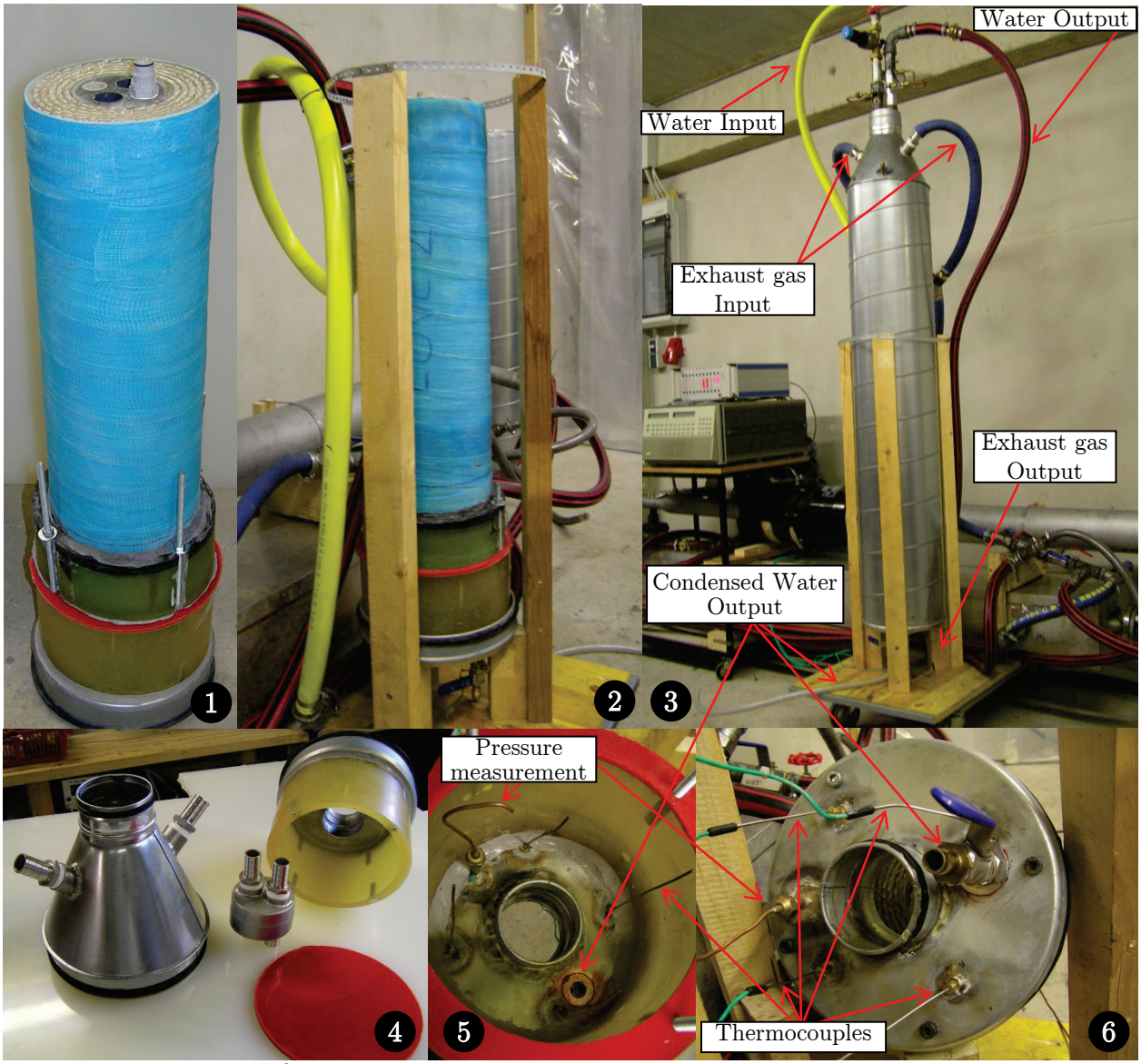

Figure 4.7: Pictures of the polymer heat exchanger casing. 1) PSFGL HEX screwed on the modified lid 2) PSFGL HEX mounted on the test bench without the outer steel pipe 3) Flow inputs and outputs on the casing once closed 4) Modified air conditioning fittings with the epoxy cylinder and red silicon joint 5) Inside of the lid and cylinder with thermocouple and intake for pressure measurement at gas output 6) Outside of the lid with the 4 thermocouples and output tap for the condensed water in the PSFGL HEX.

The heat exchanger casing has been developed according to the following criteria:

- Temperature resistance up to 120°C according to the maximal temperature supported by the PSFGL HEX
- Pressure proof and without gas leakage, the casing has to be able to resist to the input pressure gas flow
- Availability of components, all materials have to be easily replaceable and rapidly available.
- Cheap price, using common materials allows cost reduction.
- Simplicity & reliability, when tests are operated; the casing has to be easily and quickly opened. The possibility to change the tested exchanger is required.

The PSFGL HEX casing is mainly composed of a ∅250 mm steel pipe whose bottom end is closed with a modified lid, including a homemade epoxy cylinder. Allowing the PSFGL HEX to be bound to the casing provides a good sealing between both ends of the PSFGL HEX gas side. A flexible extensible aluminium pipe fixed at the very bottom allows releasing exhaust gases far away into the atmosphere (not shown on Figure 4.7).

The top end of the casing is composed of an air conditioning reduction from ∅80mm to ∅250mm (see the different parts manufactured on Figure 4.7a). With two inputs for exhaust gases welded on both sides, a cover which is fixed on the ∅80mm output of the reduction was designed for the input and output of the water side. As for the gas water inputs and outputs, they were welded to the cover to fix water hose to the casing.

The water side temperature flow is measured at both, input and output, by three thermocouples.

For the gas input/output, two/four thermocouples have been placed in the flow at the nearest point of the PSFGL HEX gas input/output.

When multiple thermocouples were placed at the same measurement point, the final temperature used for the measurement is the averaged value.

In addition to the joints fixed to the air conditioning fittings insure the gas sealing of the casing, blind POP rivet were also used to fix the upper and bottom lid to the outer cylinder. Blind POP rivet is strong enough to resist the gas pressure inside the casing and provide an effective binding between the parts of the casing.

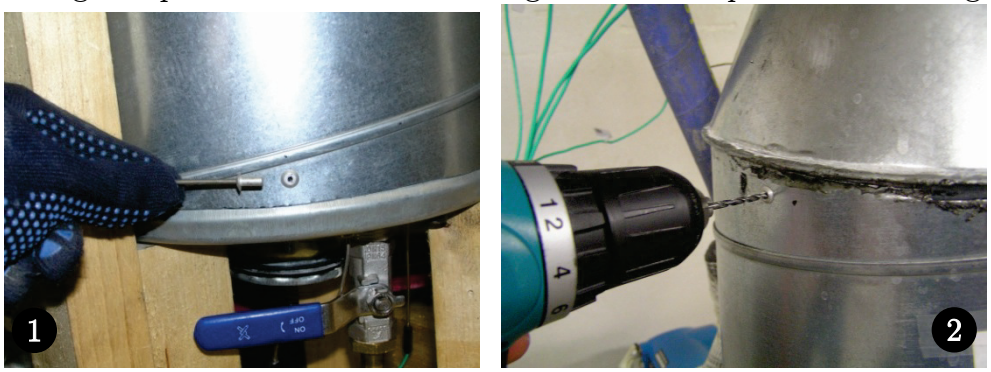

Figure 4.8: 1) Blind POP rivet used to insure gas sealing of the casing. 2) Way to open the casing, by making a hole in the rivet.

It must be mentioned that the first option was to develop a transparent heat exchanger casing. This would have allowed seeing the gas flow at the input and output during tests. For this application two transparent materials would have been used that could be temperature resistant up to 120°C.

Polycarbonate was considered for the first material since it is not fragile but limited to temperatures up to 140°C. The second material that would have been used is glass which could be washed and is able to resist very high temperatures. However, glass would require careful manipulation.

According to the criteria mentioned above, price and availability were difficult to satisfy. Thus it was decided to develop a steal casing using air conditioning components as presented here.

4.6 Data acquisition software with Labview

The data acquisition is made through an interface developed using Labview programming. Labview is a programming language developed by National Instruments. Appendix E page 83 will explain more deeply how it has been designed and how it must be used. Below, the main front summary panel when the test bench is operating is presented on Figure 4.9. It is the front panel of the measurement program. This panel summarizes in real time all measurements done on the installation. An explanation is given below.

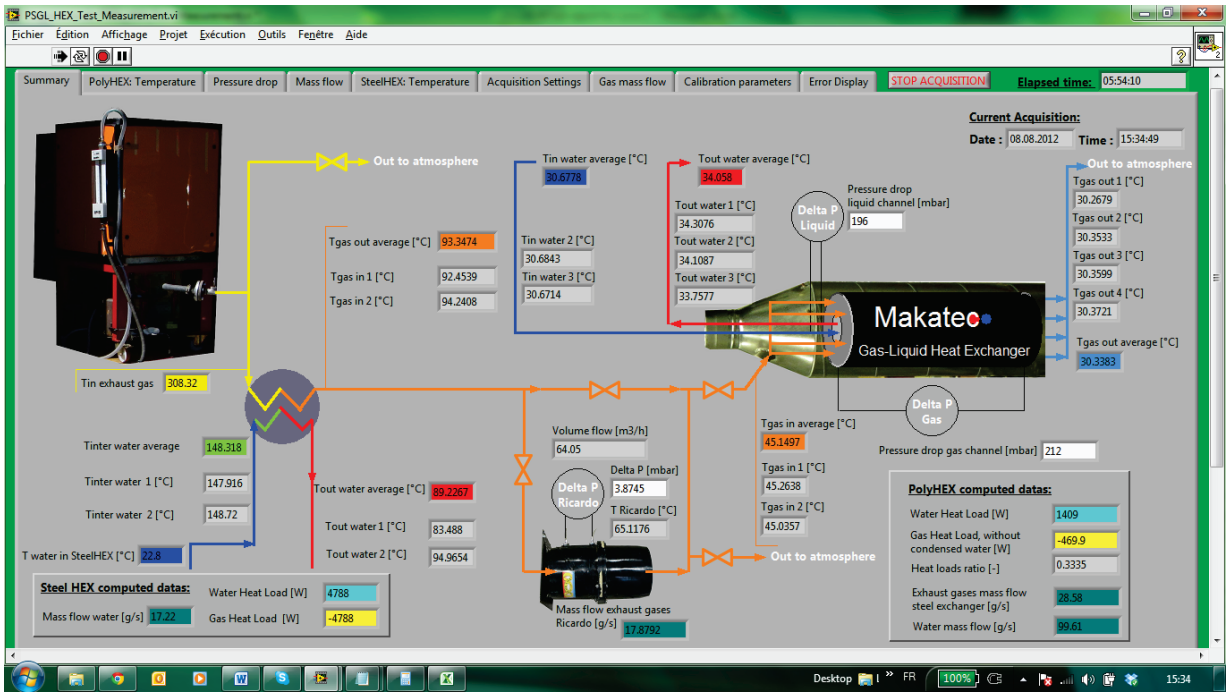

Figure 4.9: Labview front summary panel, when the test bench is operating.

Regarding Figure 4.9, yellow colour is used for very hot gas flow, orange for intermediate gas temperature, light blue for low gas temperature flow. Dark blue is dedicated for cold water and red is for hot water. Pressure drop on gas side and on liquid side of the PSFGL HEX are indicated in white displays. Actual and elapsed time is displayed in the right top corner. PSFGL HEX heat load and mass flow are displayed in the bottom right box.

As often few temperature measurements are realised at the same place, averaged values are displayed in coloured displays. All single measured temperature is displayed in a grey display.

A Data Acquisition Control Unit HP3852A allowing to do tension measurements related to the differential pressure sensors and thermocouples that have been used. An USP-GPIB adapter allows connecting the measurement unit to a laptop. The HP measurement unit can also provide a controlled signal. This would be used to control automated devices on the test bench like valves for example. It has been tested but hasn't been used in the test bench. Such commended devices were costly and wouldn't be helpful in our facility for a first try, but might be later implemented.

Lecturer can refer to Appendix E to have more information about software functioning.

4.7 Exhaust gases analysis

In the purpose of this project, the composition of exhaust gases has been analysed. All computations regarding this analysis are presented in Appendix A .

In this appendix, one will first find the composition of the exhaust gases at the engine output. Secondly it will shown how the molar mass of such gases can be computed. Thirdly, the specific heat capacity Cp of the gases in function of the temperature of the gases is computed, it shows the temperature dependence of the Cp of exhaust gases.

Lastly, the procedure to measure the engine consumption at full load will be presented in order to obtain an estimation of the exhaust gases mass flow at the engine operating point.

Note that all the results presented in section Appendix A have been computed with a $\lambda = 1.7$ (refer to section 4.10 for more details about the lambda).

4.8 Pressure losses measurements

Pressure losses have been measured using Keller PD-11 differential pressure sensors bought in 1990. As these sensors haven't been used for years, it was necessary to understand how the signal could be measured. After talking with the customer service at Keller, it was clear that the sensors unit which has been realised in the past by the LENI Laboratory doesn't provide a standard 0-10V output for the differential measurement.

Knowing it, four of these sensors for the following range 0-100/0-200/0-500/0-1000mbar have been calibrated. Calibration consisted in measuring the difference potential at the output of the sensor unit while measuring manually the high difference of mercury column created by the pressure at side + of the sensor. Side − have been released to atmospheric pressure. Atmospheric pressure has been measured at about 980mbar during sensor calibration.

Measuring the output tension at some few differential pressure points in the measurement range of the captor allows computing the slope a and the intercepts b of the captor conversion equation (4.2).

$$P(U) = a \cdot U[V] + b \qquad [\text{mbar}] \tag{4.2}$$

Pressure on the + side has been provided with azote. It was expanded to the suitable pressure using a pressure regulator bounded to a bottle of azote to 200bar. A manometer mounted on the + side of the calibration bench allows to indicate approximately the pressure on the side + of the sensor, as shown in Figure 4.10. A few differential pressure points, in the specific differential pressure range of each sensor have been set and the output voltage has been measured for each point.

Using both values, differential pressure $P(U)$ measured with the high mercury column and the output voltage U measured by the HP acquisition unit at this differential pressure point, coefficients of the linear equation (4.2) converting the output voltage in a differential pressure have been established for each sensor. Those equations have been reported in Table 4.1. Placement of each sensor has also been reported in the same table.

Table 4.1: Conversion equation for differential pressure sensors

Serial Number	Sensor correction	Sensor placement
2584 [0-100mbar]	Dp = 2001.1 U[V] + 64.117	Ricardo Gas mass flow
1477 [0-200mbar]	Dp = 1403.6 U[V] - 10.647	Reserve sensor
1483 [0-500mbar]	Dp = 1940.1 U[V] + 18.871	Gas channel pressure drop
1475[0-1000mbar]	Dp = 2730.8 U[V] + 94.219	Liquid channel pressure drop

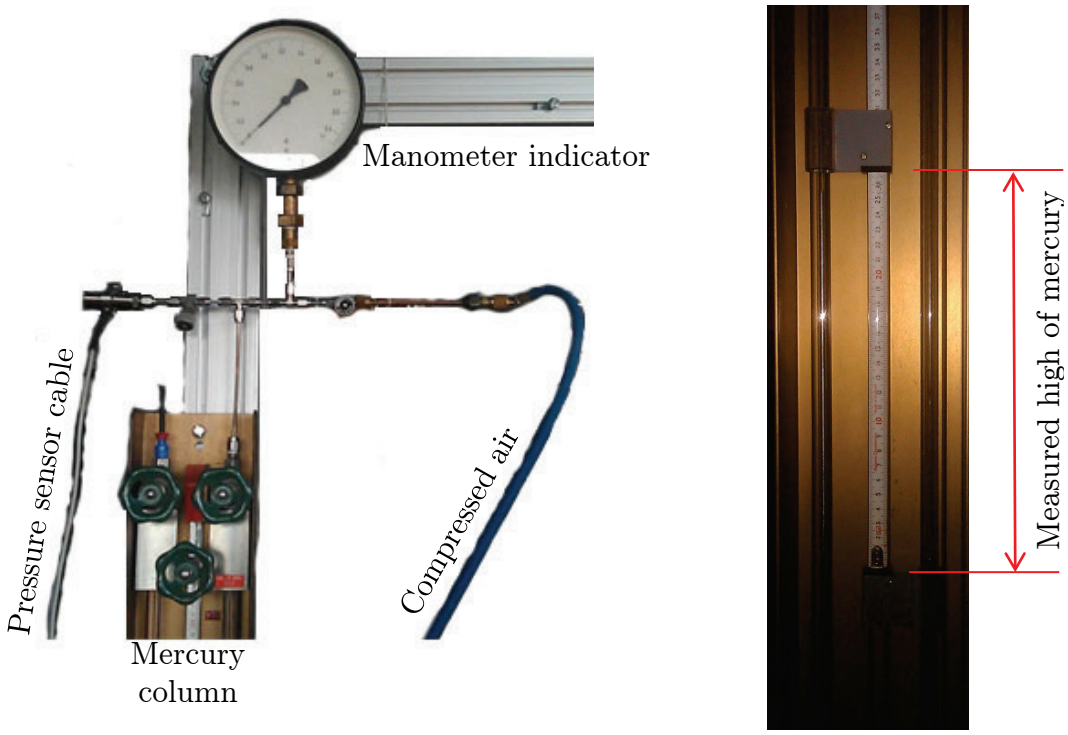

Figure 4.10: Set up of the calibration bench for the differential pressure sensor. On the right the pressure is measured as a height of mercury column with a sliding meter and converted in mbar.

Once the sensors have been calibrated, voltage output is measured by the HP acquisition unit during the tests. The Labview software converts the voltage into differential pressure through the linear conversion equation which was established before.

Pressure losses have been measured between input and output for both PSFGL HEX liquid and gas channel. Such differential pressure sensor has been used to measure the pressure drop in the Ricardo exhaust gas flow meter, for more information see Appendix D . Finally another digital differential pressure sensor in the range 0-25mbar has been used for measuring the differential pressure in the laminar flow meter.

For the pressure drop measurement on the water side of the PSFGL HEX, copper pipes connected to the sensor have been installed between input and output of the liquid channel.

Figure 4.11: Differential pressure sensor mounted on the installation. 1)Liquid differential pressure sensor mounted on the SPGL HEX casing. 2) Gas differential pressure sensor fixes onto the facility

As to finish this part on differential pressure sensors with a humour touch, one has to be careful when using mercury column and never let the pressure be higher as the high of the column. It happened precisely during the calibration that the whole lab with all of its installations was recovered of micro ball of mercury. Trying to collect this mercury with a sheet of paper was hopeless and a company specialised in treatment of special waste had to be hired to get rid of the mercury which was hovered. Thanks God!

4.9 Temperature measurements

A set of 26 thermocouples has been calibrated (20required, 6 as reserve). Measurements have been proceeded at 7 points in the range [0-90]°C using a 15°C steep. For calibration, all thermocouples have been inserted in a bloc of steel which was placed in a temperature regulated bath. The metal bloc insures that the thermocouples measure the average temperature of the bath during the calibration.

This bloc has been placed in a mixture of water and glycol (avoiding freezing at 0°C) of a Lauda PK20 temperature regulated bath. For each point a reference temperature has been measured with a Quartz thermocouple.

For each thermocouple a linear correction has been computed using the measurement points. The correction takes the following form:

$$T_{Quartz\ thermocouple} = T_{corrected} = a\,T_{measured} + b \quad [°C] \tag{4.3}$$

The calibration coefficient a (multiplicative component) and b (additive component) are given for all thermocouples in Table 7.5, in Appendix G.2.

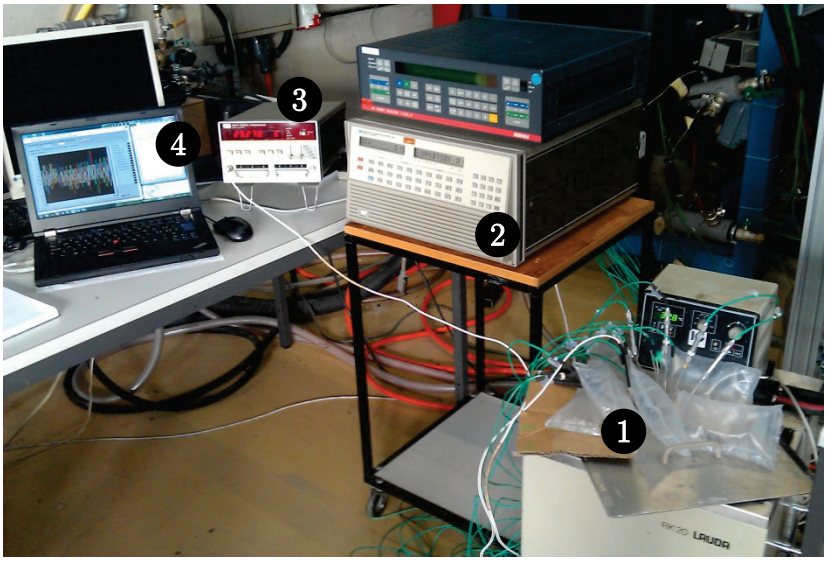

Figure 4.12: Setup prepared to determine the temperature correction of the thermocouples. 1) Regulated temperature bath where thermocouples are immersed all inserted in a steel bloc guarantying an homogenous temperature 2) Measurement HP unit, measuring the potential difference of each thermocouple 3) Quartz thermocouple unit for measuring the reference temperature. 4) Labview interface converting potential measured in a temperature and saving thermocouples measured values.

It is to mention that after the first thermocouple calibration, measurements were still not stable, temperature accuracy obtained was in the range [+0.8; -0.8]°C compared to the quartz thermocouple taken as reference. It has been found that noise in the HP measurement unit affected the measurements and was the cause of the poor accuracy. The solution has been to use another HP measurement unit and to proceed to a new calibration. It solved the problem and the temperature obtained for all thermocouples were in a range of [-0.2;+0.2] around the reference value of the quartz thermocouple.

Also tested, but finally not used some were some homemade thermocouples. Such thermocouples are made using special thermocouple wire. One wire is made of copper and the other one is made of constantan iron. By welding both wires at one end, and measuring the potential difference at the other, we obtained a thermocouple of type T for the temperature range [-100;350]°C (see source [2] for detailed measurement tables). It has been found that accuracy after calibration was even better than type K thermocouples which were used can operate in the range [-150;+1350] °C.

As all thermocouples used were not new, it has been necessary to find a way to remove the clinched sealing ring without breaking the thermocouples. This ring was used previously to fix the thermocouples to a defined depth. It insures sealing between the thermocouple and the hole where it's inserted. Figure 4.13 and its legend explain the process of remove the ring allowing using the thermocouple at the desire deepness.

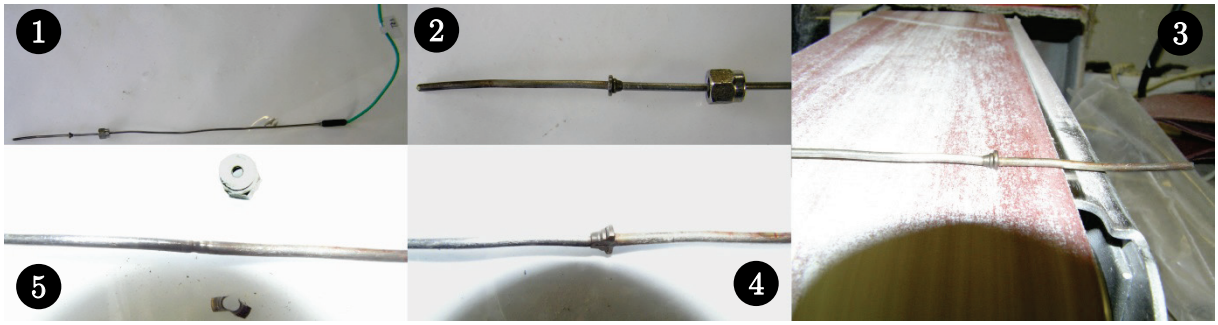

Figure 4.13: Process operation to remove clinching ring on thermocouple. 1) Thermocouple in the initial state sealing ring clinched 2) Zoom on the sealing ring and the nut to fix the thermocouple 3) The sealing ring is sanded with a sander tape 4) both faces are sanded to the thermocouple surface as much as possible but without damaging the surface. 5) Once sanded sealing ring can be broken with hands and the nut can be removed. A new sealing ring can be clinched to the required depth.

4.10 Lambda measurements

The Lambda measurement has been realised in order to be able to estimate by computation the composition of the combustion gases which has been already presented on section 4.7.

To confirm the lambda measurement accuracy, a brand new lambda sensor produced by *ECM,* model *NOx CANg* has been kindly lent by Mr Benoit Gay working at Liebherr Machines Bulle SA.

Proceeding jointly to measurements with the EPFL *Horiba Air/Fuel Ratio Analyser MEXA-110λ* [1] and comparing the value with the brand new calibrated Liebherr lambda sensor the following conclusions have been made.

The deviation between the two devices was in a maximal range of 0.06 sensor for λ measurement and of about 0.4 for the A/F Ratio. Usually the lambda value of the Horiba sensor was below the ECM sensor measured values taken as reference as it was freshly calibrated.

[1] Operating and troubleshooting information about the Horiba Analyser can be found in the manual instruction [15].

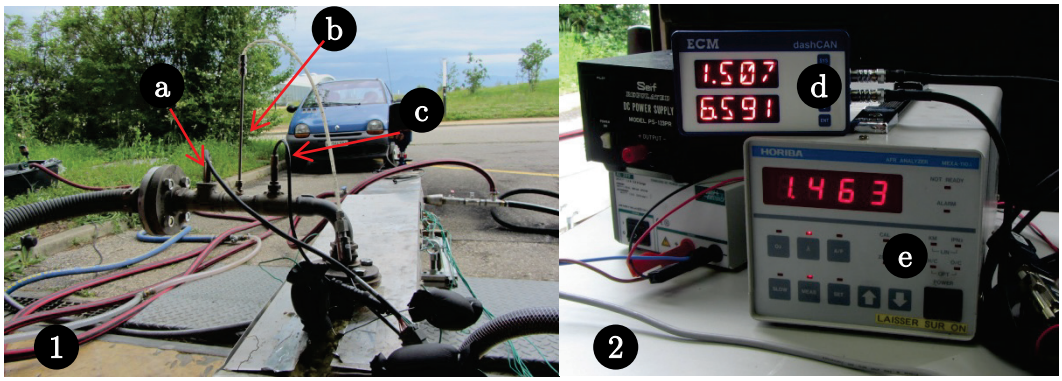

Figure 4.14: 1) set up for the lambda sensor calibration. At the exhaust exit was mounted on T tubes in this order: a) ECM lambda sensor, b) Pressure sensor for the ECM sensor c) Horiba Lambda sensor. 2) Display of the lambda sensors during measurement, when engine is cold. d) ECM display, with the measure lambda on the top display, bottom display is the O_2 concentration

For information, some conclusion concerning lambda measurements will be presented. First when the engine is cold the lambda is about 1.5. After about 8 to 10 minutes at full load, the lambda value tends to be stabilized around 1.8-1.9.

The air fuel ration measured is varying from 21 to 22 and the O_2 concentration is between 6.5 and 7.2% at full load. Concerning differences in the measurements between both lambda sensors, Horiba sensor air fuel ratio value was 0.1 higher as the ECM measured value. For the O_2 concentration measured value, the Horiba vas about 0.05 below the ECM value.

One important point is the setup of calibration that has been done driving the full exhaust gas flow through the steel HEX and through both HEX and Ricardo mass flow meter. When measuring the absolute pressure with the ECM pressure sensor very close to the exhaust exit (next to lambda sensor, see Figure 4.14 number 1a) an absolute pressure of 780mbar has been measured at full gas flow. Measuring absolute pressure of 720mbar, at the same time, the counter pressure of the tubular steel exchanger at full gas flow is 60mbar.

When gases are flowing through the tubular steel exchanger and the Ricardo mass flow meter the counter pressure in the pipe increases of 180mbar, measuring 900mbar with the pressure sensor.

4.11 Water flow Measurements

Water flow measurements have been realised using a coriolis Promass 80 branded Endress+Hauser. Such devices have been used for the water flow in the PSFGL HEX. In addition two heat-payers have been used to measure the water flow in the conditioning tubular steel heat exchanger. A photo of these devices is presented on Figure 4.15.

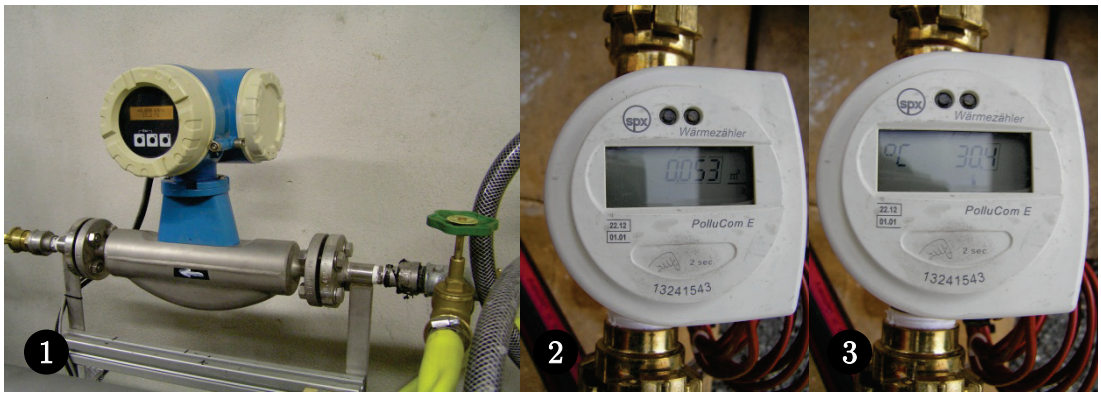

Figure 4.15: Water mass flow meter used on the test bench.

1) Coriolis mass flow meter used to measure water flow in the PSFGL HEX. 2) Heat payers used to measure the water mass flow and temperature flow in the steel exchanger. 3) Heat-payers indicating water temperature. Measurements are manually entered in the Labview interface.

4.11.1 Coriolis mass flow meter

Coriolis mass flow meter is a very accurate device. It allows to measure mass flow and accuracy reached is of one gram. As the HP measurement unit is only able to make tension measurements, two resistances of 240Ω each (total accurate resistance is 475.1 Ω) have been placed converting the output current signal of the coriolis flow meter in a tension measured by the acquisition unit as shown in Figure 4.16.

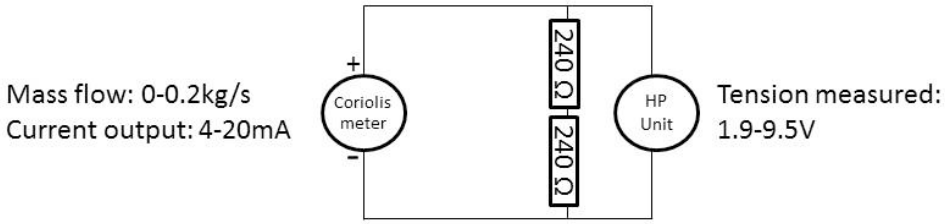

Figure 4.16: Electrical schema to convert current output signal of the coriolis mass flow in a measured tension and compute the mass flow through the Labview software.

Equation (4.4) is converting the tension measured by the HP measurement unit in a water mass flow in gram per second. The measurement is quite stable and the zero have some time to be set from one gram unit but normally no more than this. Accuracy of this measurement is in the range of 1 gram per second.

$$\dot{m}_{water} = 26.3\, U[V] - 50.07 \text{ [g/s]} \tag{4.4}$$

Using Equation (4.4), the Labview software converts the tension into mass flow unit and uses the value to do later computation in the software. The values are also saved for a postponed data analysis.

4.11.2 Heat-payers

Heat-prayers as shown on Figure 4.15 have been used because they are a cheap solution, such device costs 20 euro on ebay, second hand. Heat-payers are able to measure water mass flow and temperature as they are normally used for power heating purpose mainly for house heating installation.

As they are cheap, they require do to manually enter the measured value in the Labview interface. Measurement actualisation is done only when the mass flow changes in a large proportion of the previous measured value. Meaning flow variation should be in a range of 10 litres per hour to keep the measurement updated and displayed.

These devices are designed for water mass flow in the range of few cubic meters per hour; measuring mass flow of $0.05m^3/h$ is not easy but still feasible and accurate. This has been concluded through good accuracy of gas mass flow measurement made by using the steel heat exchanger heat load. This gas measurement technique needs the water mass flow measured with the heat-payers. It is presented in Appendix D.2.

It happened that, due to the very low mass flow, the heat-payer didn't actualise the flow measurement. To conclude with those devices one can say that heat-payers accuracy is of $0.005m^3/h$.

4.12 Test bench dynamic behaviour and measurement reproducibility

This section presents some comments about the behaviour of the test bench during tests.

The preheating period of the exhaust gas conditioning unit is about 20 minutes. It includes heating of the engine to reach a lambda of about 1.8, and then let gas flow in tubular steel exchanger reaching a stable exit gas temperature of 90°C.

Figure 4.17 presents the evolution of all temperatures in the tubular heat exchanger during the preheating phase.

The bottom right curve shows the input gas temperature reaching 320°C; the curve on the bottom left side shows the water temperature near the gas input at 140°C, higher temperature should not be reached because the pressure would become too high and the pipes binding connections would not resist. On top right curve the exit gas temperature is reaching 90°C and top left curve the water output temperature is reaching 85°C. During the first 4 minutes the temperatures of all graphic in the Figure 4.17 are close to the ambient temperature. It means that the COGEN unit is turned on but the gases do not flow into the tubular heat exchanger.

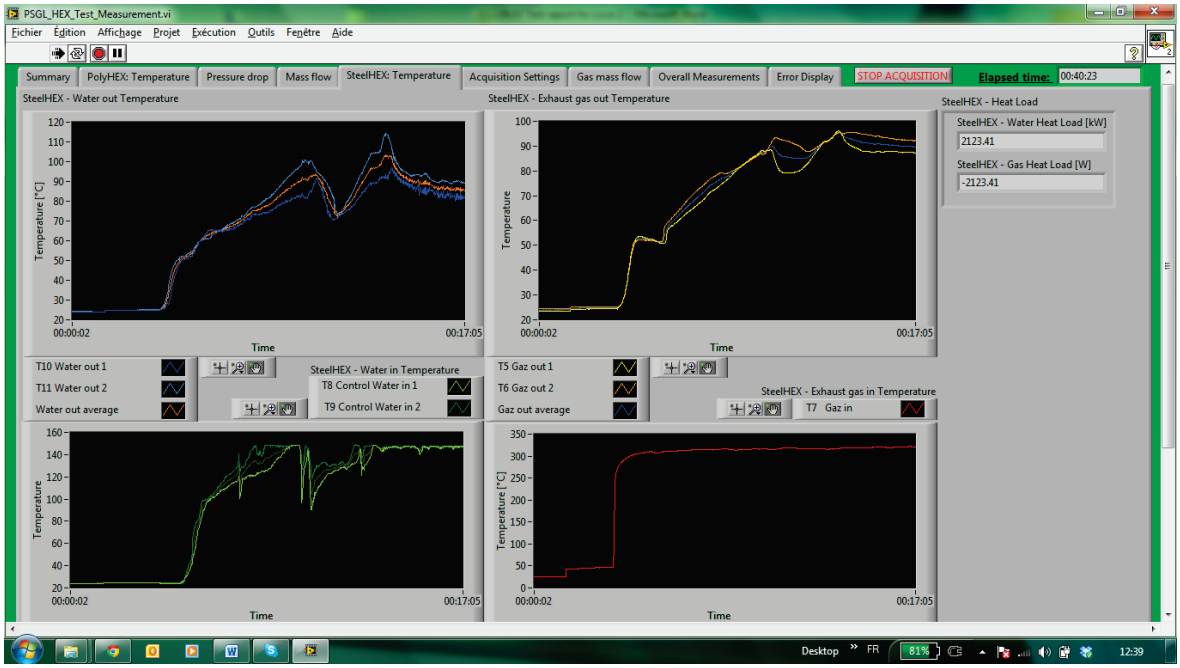

Figure 4.17: Screen shot of the Labview interface showing preheating of the engine and exhaust gases conditioning unit. 20 minutes duration is required to reach a stable gas exit temperature in tubular heat exchanger.

Water mass flow in the tubular steel heat exchanger is difficult to adjust when water flow is around 50l/h. Water flow has been set to cool exhaust gases at 90°C however the gas entrance temperature in the PSFGL HEX casing is decreasing to 65°C due to the pipes heat losses.

Table 4.2 below gives the estimate accuracy of all measurements on the test bench.

Table 4.2: Accuracy in the measurement observed by operating the test bench.

Measurement	Accuracy
Pressure drop on gas channel	+/-10mbar
Pressure drop on liquid channel	+/- 5mbar
Exhaust gas volume flow, 0-65m^3/h	+/- 7m3/h
Exhaust gas mass flow, 0-20g/s	+/- 2.7g/s
Water mass flow on PSFGL HEX	+/- 1g/s
Water mass flow on tubular HEX	+/- 10m^3/h (+/-2.7g/s)
PSFGL gas input temperature	+/- 5°C (between both measured values)
PSFGL gas output temperature	+/- 7°C (between 4 measured values)
PSFGL input and output water	+/- 0.6°C (between 3 measured values)
T tubular HEX input water, heat-payers	+/- 1°C
T tubular HEX input water thermocouple	+/- 5°C (between both measured values)
T tubular HEX output water	+/- 4°C (between both measured values)
T tubular HEX input gas	+/- 5°C
T tubular HEX output gas	+/-7°C (between both measured values)

To let the reader appreciate the difficulty to measure pressure drop in gaseous flow, Figure 4.18 shows fluctuations in the measured values for the liquid pressure drop on the top graphic (on the figure about +/- 2mbar) and for gas pressure drop on the bottom (on the figure about +/- 4mbar). Gas pressure drop oscillate very slowly and it requires waiting for a stabilised value for each measurement point.

When environmental temperature in the surroundings of pressure differential sensors is stable, differential pressure measurements can be reproduce with accuracy. The procedure is first to interrupt the gas flow. And after waiting for the sensor to be stabilized, the measured value should be around 0mbar. When gas flow valve is opened again, and reaching the same gas volume flow as before, the pressure drop measured should be the same as done on Figure 4.19 for the pressure drop (white curve). This operation tests the reproducibility of the pressure drop measurement.

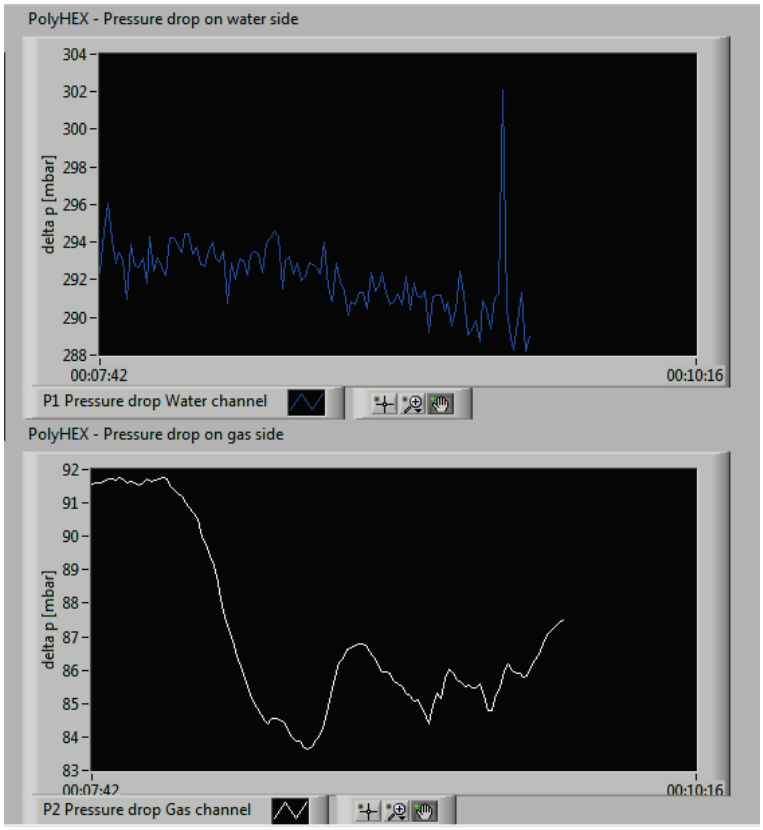

Figure 4.18: Fluctuation in the measured value when measuring liquid (top) and gas(bottom) pressure drop.

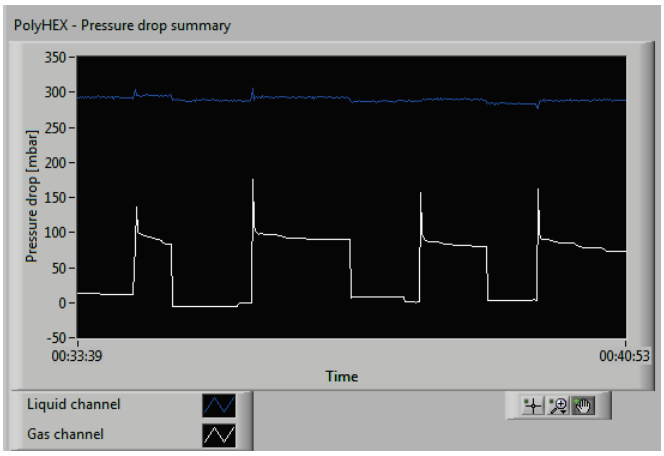

Figure 4.19: Water (blue) and gas(white) pressure drop. Water pressure drop is stable over time with a good accuracy. Gas pressure drop can be measured at the same value after stopping gas flow.

Figure 4.20 justifies the accuracy (see Table 4.2) for the tubular heat exchanger used for conditioning exhaust gases. One can evaluate the accuracy between the multiple temperatures, each measured at the same point of the steel tubular heat exchanger. On Figure 4.20 all the lines in the middle show an average temperature. Top left graphic: Water input tubular hex +/-3°C, Top right graphic: Gas output tubular hex +/-7°C, Bottom left graphic: Water input tubular hex +/-5°C, Bottom right graphic: Gas input tubular hex +/-5°C. Note that the steel tubular exchanger heat load is in the range from 3 to 5kW when the exhaust gas flow is at maximum (66m3/h).

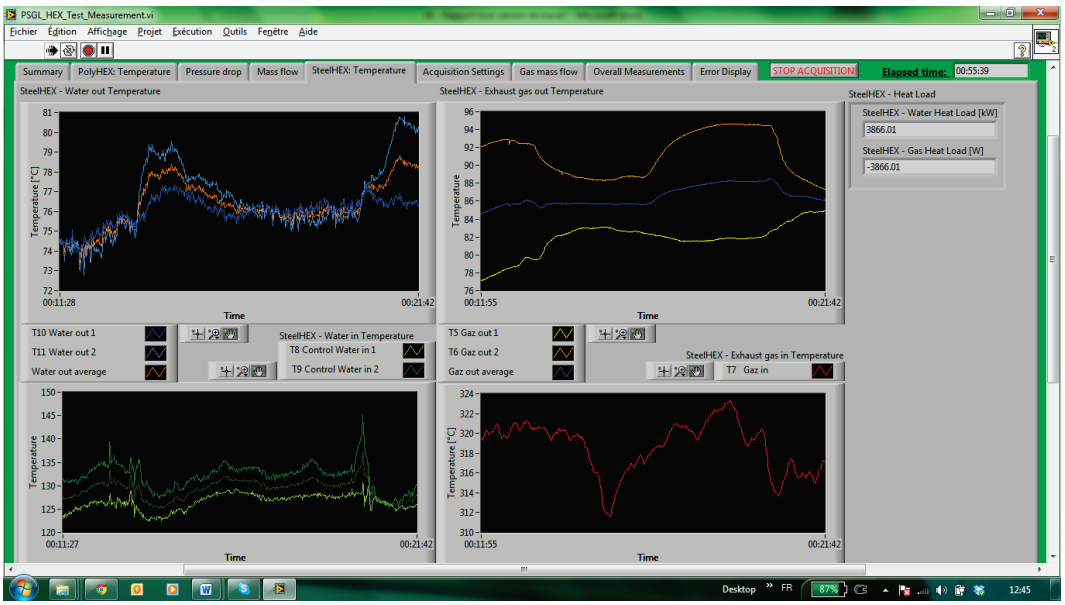

Figure 4.20: Fluctuation between the various measured temperatures in the heat exchanger. Few measurements are done at the same place. Middle line is the average value

In this chapter the test bench and its operability was presented. It is important to keep in mind that many challenges have been achieved to allow measurement reproducibility. Chapter 5 will be dedicated in analysing the PSFGL HEX performances measured with the facility during the tests sessions.

Chapter 5 Heat exchanger measurement results

This chapter presents and analyse results obtained using the NASATEC (New Available Sustainable Air Conditioning Technology) test bench that was developed. A PSFGL HEX prototype numbered LOVE 2 was tested.

Section 5.1 and 5.2 are dedicated to pressure drop on gas and liquid channels, section 5.3 to the heat load transferred between both heat exchanger channels. We'll then discuss the overall heat transfer coefficient of PSFGL HEX in section 5.4. Section 5.5 will present the state and the fouling of the exchanger after the tests. The feasibility to regenerate the exchanger will be discussed. Finally futures heat exchanger and the test bench improvements will be summarized in Chapter 6 .

5.1 Pressure drop on gas side

As pressure drop has always been a crucial subject in heat exchanger, PSFGL HEX pressure drop is also a critical topic and our target is to decrease it as much as possible. Indeed gases are compressible and it requires a non-negligible quantity of energy - about 400W for 65m3/h gas flow with a 200mbar pressure drop using a fan efficiency of 0.8 – to balance the pressure drop using by example a fan. At the same time we want to improve the heat exchange in the exchanger. Improving heat exchange requires making the flow to be turbulent when more mixing occurs. We can here mention that both needs are going against each other. The aim is to reach a pressure drop on the gas channel in the range of 5 to 15 mbar with a flow up to $65m^3/h$.

Pressure drop on the gas channel of PSFGL HEX was measured during the tests using differential pressure sensors integrated to the NASATEC test bench.

Measurements were realised after the PSFGL HEX prototype had already been working for about 20 hours meaning the gas channel was then partially fouled with exhaust gases particles. Pressure drop measured and here presented is then higher as the one we can expect when the PSFGL HEX is clean. As pressure drop measurements were achieved nearly at the end of the tests, reader can refer to section 5.5 for a state representation of the exchanger at this point.

Few possibilities are then offered to solve this problem. First would be to increase the thickness of the gas spiral channel by adding few more mesh layers. Also one can consider decreasing the PSFGL HEX length or increasing spiral rewinding length but these last options will jointly increase the pressure drop on the

liquid channel. For future gas pressure drop improvement we recommend to double Gas channel thickness to 8 mm and to measure pressure drop and influence on the exchanged heat load.

Interpretation of the pressure losses in gas channel of PSFGL HEX as a depending function of the gas volume flow and is presented on Figure 5.1. It appears straight away that gas pressure drop reaches 180mbar when exhaust gas volume flow is 65m^3/h. It must be mentioned that we are then far higher from the targeted range as to know 15 mbar at the same volume flow rate.

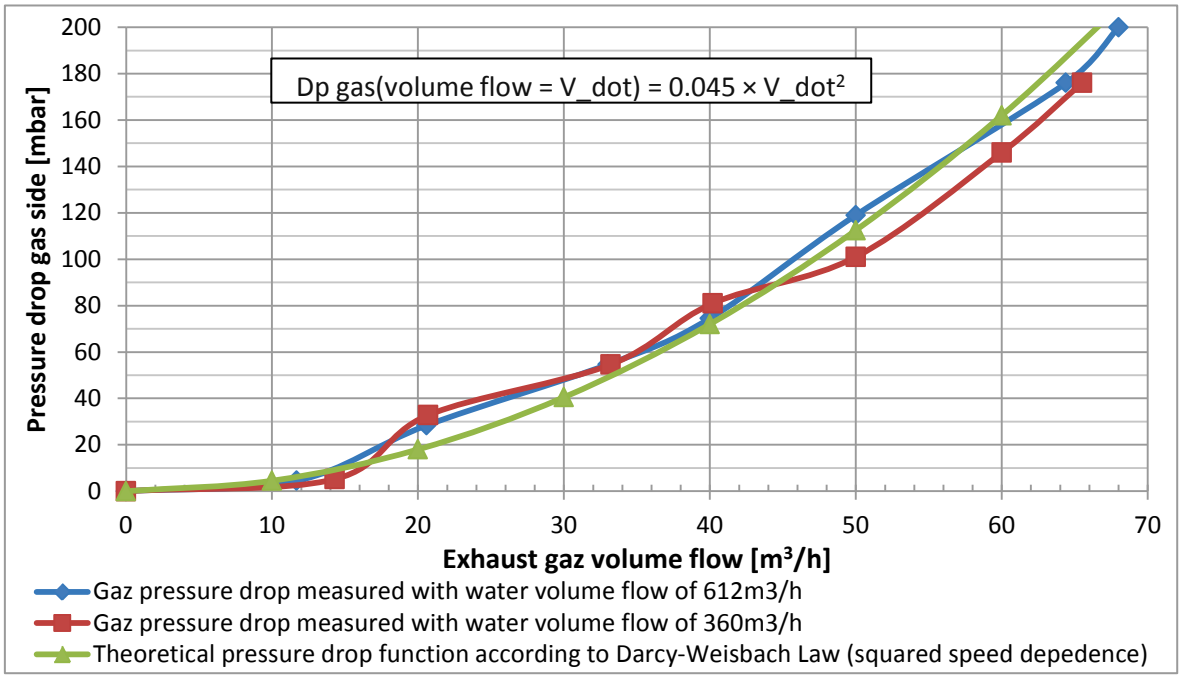

Figure 5.1: Pressure drop in the gas channel measured in a PSFGL HEX as function of the exhaust volume flow.

Driving an analysis about the pressure drop depending on the speed, we can identify in Darcy-Weisbach equation [3] presented below and numbered as (5.1), that the theoretical pressure drop as it has to be in a pipe, should vary with the square of the flow speed.

$$\Delta P = f_D \frac{L}{D} \frac{\rho}{2} V^2 = K \cdot V^2 = \frac{K}{A^2} \dot{V}^2 = K' \cdot \dot{V} \qquad \text{[Pa]} \qquad (5.1)$$

Using the measured values, and taking in account that Pascal and milibar changes a factor 10^2 we can find in the equation (5.1) a value for K'. It is quite straight forward that the value of K' remains constants in a range of K'= 0.0025 to 0.007, but is more often stable at K'= 0.004.

As it appears in Figure 5.1, the green function with the triangles using Darcy-Weisbach law with K'= 0.0045 fits very well with pressure drop measurements. The derived function using the volume flow of the gas becomes equation (5.2).

$$\Delta P = 0.045 \cdot V^2 \quad \text{[mbar]} \qquad (5.2)$$

It must be mentioned that pressure drop measurements on the gas side have succeeded. As we were able to approximate with the Darcy-Weisbach law the measurements we are able to confirm the veracity of those results.

We can make another conclusion paying attention to both square and lozenges measurement curves of Figure 5.1. For the gas volume flow range of 0 to 70m^3/h, pressure drop on the gas channel doesn't vary significantly with a variation of flow in the liquid channel. This affirmation can be justified as the following; the pressure in the water channel is relatively low and water flow doesn't bend the film when water flow increases in such proportion. Also, gases are compressible and water here considered as incompressible, gases are compressed whenever gas channel thickness would become thinner. In that sense gas channel pressure drop is not modified by such water volume flow variation.

Indeed red curve with the squared and blue curve with the lozenges of Figure 5.1 are quite close together. Slight differences in between both curves can be justified by the accuracy in the measurement that is in the range of 10 to 20 mbar. As gases are compressible, pressure in gas flow always oscillates and measurements become difficult. We have to stress the good performances accomplished in the measurements we were able to fit results with the theory prediction.

Finally the similarity between the two curves confirms the reproducibility of the measurement when preceded correctly.

As we have presented here the pressure drop in the heat exchanger that reaches 200mbar when exhaust gases flowing at 68m^3/h, the next section will present the results of the pressure drop on the water side.

5.2 Pressure drop on liquid side

As already mentioned above, measuring pressure in a fluid flow is less complicated than in a gas flow. This has for consequences that measurements of the pressure drop on the water side of the PSFGL HEX reported on Figure 5.2 are more accurate in the range of 10 to 15 mbar.

Figure 5.2 illustrates the pressure drop on the liquid channel of PSFGL HEX as a function of the water volume flow for three various gas flows. In PSFGL HEX water volume flow shouldn't be much higher than 650m^3/h, and the pressure drop measures of nearly 300mbar for such maximal water flow is going along expectations. Pressure drop on water channel here measured are in the same range than pressure drop in Polymer Spiral Film Liquid-Liquid Heat Exchanger already developed by Makatec GmbH. We don't have any particular comment concerning these measurements rather than the pressure drop will be increased when the length of the spiral of SPFGL HEX is increased.

We would like to point out that when the gas flow varies Figure 5.2, pressure drop on water side is not significantly influenced. It can be justified as gases are compressible and can't significantly compress the liquid channel. This is true for a gas flow in the range of 0 to 65m^3/h and an increase in the volume gas flow range from 0 to 70 m^3/h.

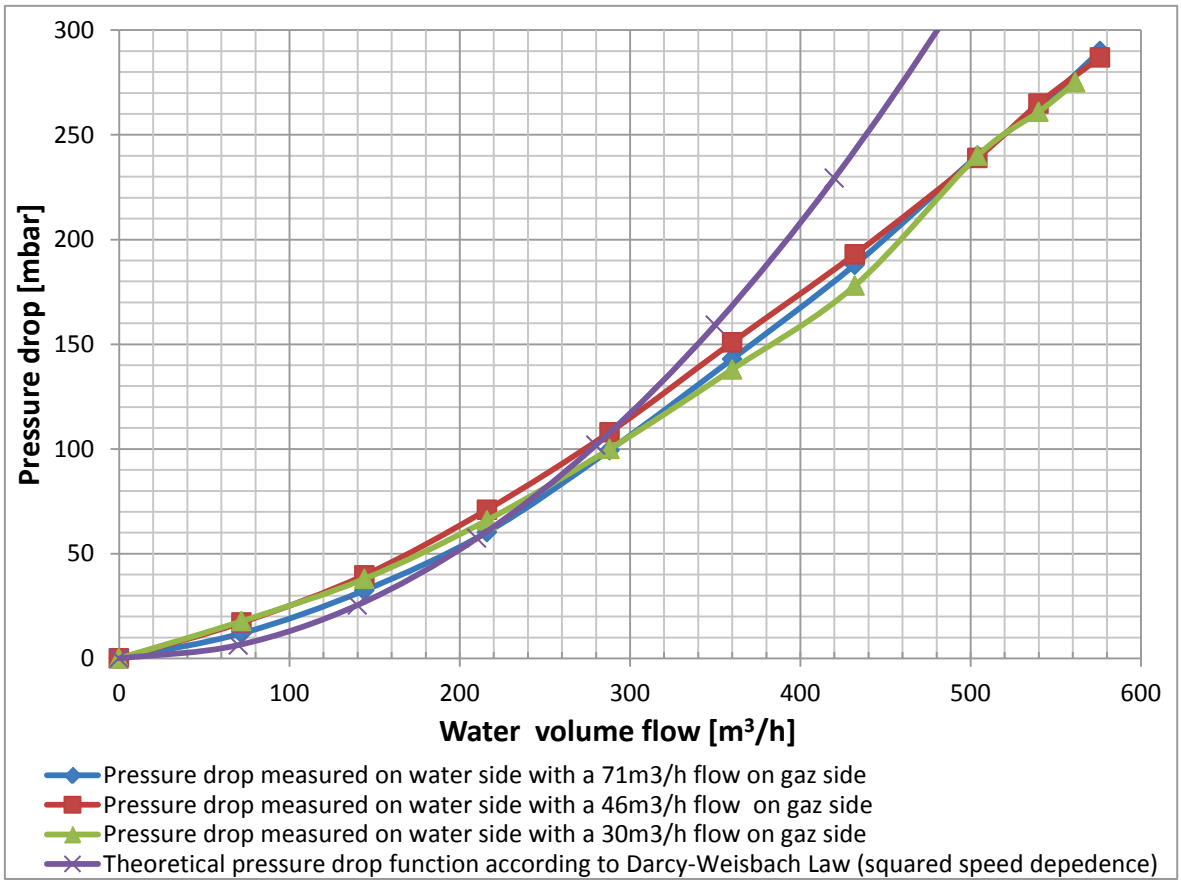

Figure 5.2: Pressure drop measurements on water side of Polymer Spiral Film Gas Liquid heat exchanger as function of the water volume flow.

Proceeding as we have done above in section 5.1 and trying to find a K' constant for the equation (5.1), we find that the value of K' is not constant and varies from 0.0009 to 0.003 on the range 0 to 600m^3/h. Choosing K' = 0.0013 in equation (5.3), which corresponds to the value that has been more often computed using measurements, the approximate Darcy-Weisbach law of equation (5.1) was plotted using purple cross in Figure 5.2.

We observe that for water flow from 0 to 300 m3/h measurements fit well to the Darcy Weisbach predictions. Above 300m3/h pressure drop on liquid channel is below the Darcy-Weisbach law. It is justified as follow; assuming the film is in a certain measure deformable and water is not compressible, when water flow grows it deforms the water channel and makes it wider. Thus as water channel cross-section

is increased, water pressure drop decreases. Gas channel thickness then might become thinner, but as gas is compressible, pressure in the gas is locally increased.

$$\Delta P = 0.0013 \cdot V^2 \quad \text{[mbar] V} \in \text{[0-300m3/h]} \tag{5.3}$$

The reproducibility of pressure drop on water side can be assumed considering that the three measurement curves on Figure 5.2 gave the same pressure drop profile.

5.3 Polymer spiral film gas liquid heat exchanger (PSFGL HEX) heat load

As we have been limited by the time duration of this master project, we are only able to present here one heat load point of 1.2 kW that is really meaningful. Measured values for a 1.2kW heat load are presented in Table 5.1 below. All values will be commented below.

We can shortly mention that during the test a 2 kW heat load was reached but the output temperature of the gases measured was below water input temperature. This occurred when water flow was at highest flow rate of 612m^3/h and the temperature difference between input and output on the water side was less than a few tenth of Celsius degree.

This scenario couldn't be justified as when temperature difference between input and output is very small, measurement accuracy as uniform temperature of the water flow becomes critical. Then we decided to present only the operating state with a 1.2kW heat load that is more representative for real SPFGL HEX performances when temperatures differences at each side of the exchanger are suitable.

It has to be point out that the results presented use the condensation of the water contained in the exhaust gases. Condensation of the water occurs as it has been presented in Appendix A.6 when exhaust gases exit SPFGL HEX at a temperature lower than the dew point temperature of 40°C. As input temperature of the gases was not as high as initially targeted the output temperature was under exhaust gases dew point. In these conditions the heat load recovered is much higher. It is also a way to justify the good results obtained.

Table 5.1: Data for the presented operating state of PSFGL HEX with a heat load of 1.2kW

Data	Measured value
T input gas[°C]	65,3
T output gas [°C]	36.1
T input water [°C]	31.0
T output water [°C]	47.5
Gas mass flow [g/s]	18.5
Water mass flow [g/s]	17.8
Cp gas [kJ/(kg K)]	1.035
Cp water [kJ/(kg K)]	4.183
Heat load water [kW]	1.235
Heat load gas [kW]	-0.569
Heat load condensed water [kW]	-0.466
Total heat load gas side [kW]	-1.026
Heat load ratio (gas/liq) [-]	0.83

As cooling water input temperature was of 31°C, we couldn't obtain a better temperature as tests were operated outside during summer and cooling tower became less efficient. The corresponding overall heat transfer coefficient of the heat exchanger will be computed in section 5.4. There is the need to have a temperature difference of about 10 to 15°C between input and output of the water side to compute a meaningful Logarithm Mean Temperature Difference (LMTD) in the exchanger.

In order to obtain such temperature difference water flow was drastically decreased to 64m^3/h (17.8g/s) to obtain a quite homogenous temperature in the output flow. Water output temperature to consider is of 47.5°C.

Reducing water volume flow means also to decrease the heat load of the exchanger as water become warmer inside the exchanger and heat exchange between gas and water decreases.

Heat load limiting factors was gas input temperature that was only 66°C. This value is quite below the 100 to 120°C that we initially targeted. The targeted gas input temperatures haven't been possible as the tubular steel exchanger in charge to condition the exhaust gases temperature in PAFGL HEX is to sensitive. Encountered problems are explained in section 4.12 and in Appendix C .

Exhaust gas volume flow of 66m3/h (18.5g/s) was the maximum volume flow produces by the COGEN unit.

Temperature gas output was of 36°C, this temperature would have been lower, going in an increase of the heat load of the exchanger, if water input temperature could have been reduced to 21°C by using tap water.

One way to increase the heat load of the exchanger is to make exhaust gases become a flue gas. This means deceasing exhaust gases temperature below the dew point temperature. This will condense water contained in the gas and water condensation energy will be transferred to the water flowing on the water channel, thus increasing the heat load recovered on the water side of the exchanger.

The exchanger heat load considered is the water heat load of 1.2kW. Indeed, as gas output temperature is below the exhaust gases dew point temperature of 40°C (as reminder it has been computed in section A.6 page 69) condensed water at 36°C was collected at the exchanger gas output. The cooling power of this condensed water represents -0.466kW. The heat load on the gas side is then the sum of heat load computed with the temperature of the gases and the heat load of condensed water and is -1.026kW.

One can ask why the heat load ratio gas under liquid is of below 1 at 0.83. It is probably justified by the fact that all the condensed water hasn't been collected. A part of condensed water still remains in the exhaust gas flow. Some quick computations gave that collected condensed water mass flow is of 0.2g/s and to obtain a heat load ration of 1 it would have necessary to collect 0.3g/s of condensed water. It means we can expect that we were able to collect about one third of the condensed water with our exchanger casing.

Computing from the exhaust gases composition analysis it was found that if all water contained in the exhaust gases flow of 66m3/h (18.5g/s) have been condensed, 1g/s of water would be condensed in the exchanger. When all this water would have condensed, it would represent an increase of 2,2kW in gas heat load.

We can conclude that making exhaust gases condensing represent for PSFGL HEX a huge improvement potential that hadn't been here completely exploited.

As we hadn't been able to optimise the test bench to obtain an input gases temperature of 100°C and water at about 20°C as input cooling water had been used for the tests. We can expect doing some quick computation that providing to PSFGL hex such higher condition values as the one targeted and presented above are going in a sense of a huge potential heat load increase in the range of 3.5kW.Table 5.2 present the expected operating values when heat load is about 3.6kW. It would also require a complete condensation of water contained in the exhaust gases that would probably not possible.

Table 5.2: Expected operating values for an approximated heat load of 3.6kW

Data	Measured value
T input gas[°C]	100
T output gas [°C]	26
T input water [°C]	21
T output water [°C]	69.5
Gas mass flow [g/s]	18.5
Water mass flow [g/s]	17.8
Cp gas [kJ/(kg K)]	1.035
Cp water [kJ/(kg K)]	4.183
Heat load water [kW]	3.618
Heat load gas [kW]	-1.418
Heat load condensed water [kW]	-2.200
Total heat load gas side [kW]	-3.618
Heat load ratio (gas/liq) [-]	1

Injection of water in gases before the exchanger input would increase the dew point temperature and would provide a better water condensation. Such a device could figure in the test bench improvement task.

5.4 Overall heat transfer of the heat exchanger

As overall heat transfer coefficient is able to describe how much energy can be transferred by a surface unit of an exchanger. The product of the overall heat transfer coefficient by the exchanger surface U*A coefficient allows to compare the efficiency of various heat exchangers independently of theirs size or exchange surface.

Using equation (5.4) [4] below we can compute the overall heat transfer coefficient.

$$Q = U\ A\ \Delta T_{LMTD} \tag{5.4}$$

Where A is the surface of the heat exchanger and U is the overall heat coefficient of the exchanger, Q the exchanger heat load and ΔT_{LMTD} the Logarithm Mean Temperature Difference computed using formula (5.5) below.

$$\Delta T_{LMTD} = \frac{\left(T_{gas\ in} - T_{water\ out}\right) - \left(T_{gas\ out} - T_{water\ in}\right)}{ln\left(\frac{T_{Gas\ in} - T_{Water\ out}}{T_{gas\ out} - T_{water\ in}}\right)} \tag{5.5}$$

Values used to compute the overall heat coefficient are presented in Table 5.3 on the next page.

Table 5.3: Data used to compute the overall heat transfer coefficient.

Data	Value
Heat load Q [kW]	1.2
Exchanger surface [m^2]	2.4
LMTD Counter flow	10.16
Overall heat transfer coefficient [W/(m^2 K)]	49.21
$U \cdot A$ [W/K]	118.1

As our SPFGL HEX design is very innovative, it is difficult to find in the literature other prototypes to make a comparison of the obtained results. However we will compare our results with another polymer spiral design used for gas-gas heat recovery.

The overall heat transfer coefficient with a spiral polymer film gas-gas heat exchanger that was tested in [5] is of 6 to 7 W/(m^2 K) without condensation and of 11 to 18 W/(m^2 K) with flue gas condensation. Their heat exchange surface is 1.95m^2 and is comparable to ours. However one has to consider that theirs gas input temperature is of 130°C and output temperature is below 60°C. Vapour fraction was about 15 to 17% whereas ours should be around 5%. Comparing our overall heat transfer coefficient, we can conclude that our PSFGL HEX provides a good overall heat exchange coefficient as it is 3 times higher. We have to consider that the heat exchanger to be compared to our PSFGL HEX is a gas-gas exchanger. Gas-gas exchange makes their overall heat transfer coefficient drastically decreasing.

Now regarding the targeted operating temperature presented in Table 5.2, a Logarithm Mean Temperature Difference ΔT_{LMTD} =14.1 would be computed. The overall heat transfer coefficient would be of 106 [W/(m^2 K)] in such operating conditions and $U \cdot A$ factor would be 255.3 [W/K]. Such operating condition would double the heat transfer in our PSFGL. Increasing the temperature would represent a huge potential for our PSFGL HEX.

We can conclude that our PSFGL HEX design can provide a very good heat exchange for gas and liquid mediums. However other tests have to be proceeded in the future to evaluate correctly PSFGL HEX potential and performances.

5.5 Heat exchanger fouling

This section aims to give a state of the PSFGL HEX tested after the tests have been realised. The goal is to evaluate the fouling of the heat exchanger. The fouling is the deposit of particles on the heat exchange surface inside the heat exchanger. Metal heat exchanger fouling also happens when rust is formed in the inside surface. During test, the heat exchanger has received an exhaust gas flow for about 25 hours. It was exposed during several days to corrosive substance. However after the tests our prototype is still in good operating condition and completely sealed.

Figure 5.3 present the casing when opened after the tests. It has been observe that pipes are in good state and the inside surface is fouled with soot but it doesn't prevent the casing to operate correctly. Presence of soot on the bottom of the casing means that exhaust gases have been circulating between the SPFGL HEX and the casing. Such a circulation would have decreased gases entrance temperature in PSFGL HEX, reducing performances.

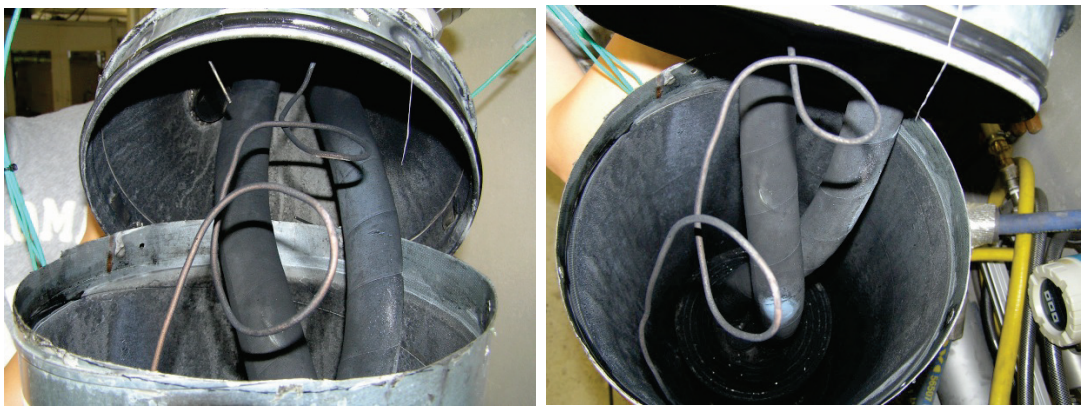

Figure 5.3: State of PSFGL HEX casing when opened after being tested for 25 hours.

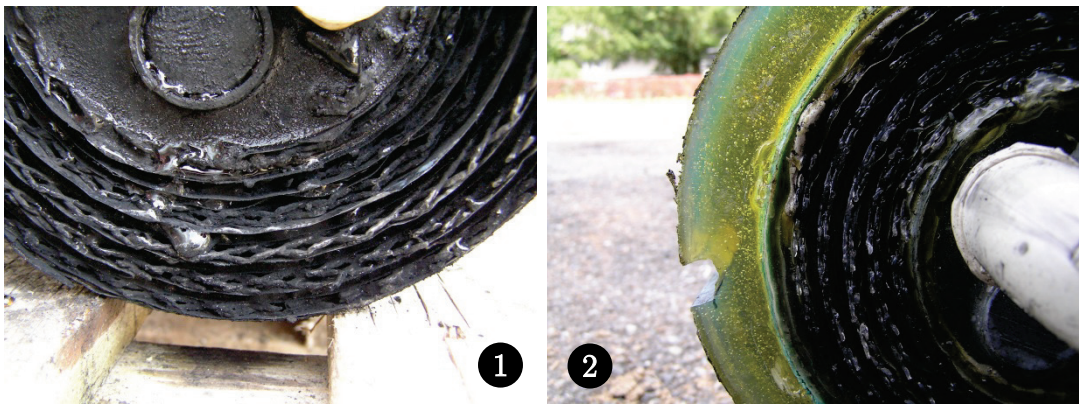

Figure 5.4: State of PSFGL HEX cross sections after being tested for 25 hours. 1) State of the gas input cross-section 2) state of the gas output cross-section

Figure 5.4 present the state of the gas channel of PSFGL HEX after the tests. Gas Input cross section is fulfilled of soot. Soot seems to remain on polymer surfaces

and the mesh and the film do not seem to be deteriorated in theirs structure. On this exchanger side mesh and film look black dark as a thick layer of soot covers polymer surfaces. Concerning the EPOXY resin that sealed the liquid channel, it is still in good state and has not at all been deteriorated. Gas channel output seems cleaner as the mesh is still transparent. The film is covered by a very tin soot layer cover the film making looks clear grey, but it still has its original colour.

Figure 5.5 present outside state looking of PSFGL HEX after 25 hours of tests. The polyurethane outside shell (blue) is now quite dark telling us that exhaust gas flow have flown between the casing and the exchanger during the test. The solution to avoid these losses could be to use expansive foam or an inner tube in rubber that could resist to tested temperature. This would avoid the gas to circulate along the heat exchanger and will decrease heat losses through the PSFGL HEX casing.

Figure 5.5: Outside state of the PSFGL HEX after the tests

Figure 5.6: Attempt of washing of PSFGL HEX with tap water under pressure.

Trying to clean the PSFGL HEX with tap water under pressure as shown on Figure 5.6, we have concluded that soot cannot be really removed perfectly but a

high soot thickness can be removed. The usage of chemical products to wash under pressure the gas channel would allow better results.
However this washing was able to give its nearly original colour to the film and to the gas mesh as shown on Figure 5.7.

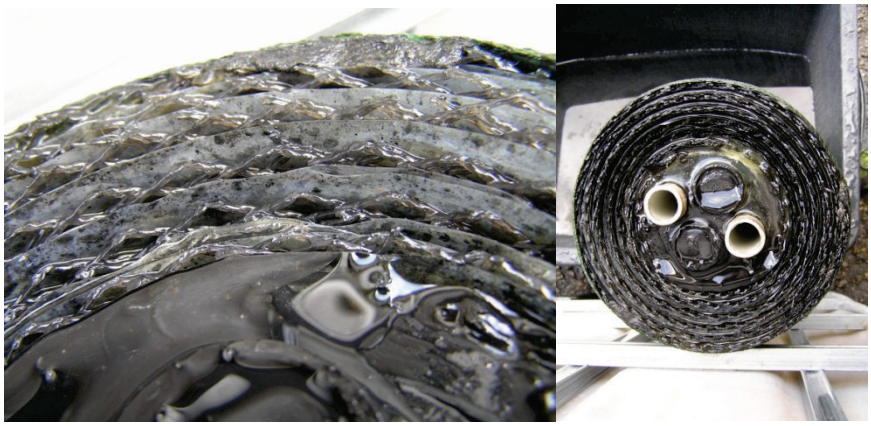

Figure 5.7: State of the gas channel input after the cleaning. Film and mesh is already clear.

Before finishing this section on fouling, we want to introduce quick pressure drop comparison between two state of the exchanger between the test and after the tests. The measurements were done using the anemometer volume flow measurement method presented in Appendix D.3 page 80. Figure 5.8 present these results.

Before showing the announced results we have to underline that the pressure drop measured using the test facility and the one measured with the vacuum cleaner and the anemometer method of Appendix D.3 (where air is vacuumed), did not provide the same maximum pressure drop.

In numbers at $55m^3/h$ we can compare that it would be 130mbar measured on the facility as shown previously on Figure 5.1 and it would be 80mbar as it will be presented below on Figure 5.8. As presented in Figure 7.14 page 82, the volume flow measured by the laminar flow meter and the anemometer are quite similar. As the sensor measuring the pressure drop is the same for both measurements, there remains two options.

Either making flowing gases or air through the exchanger changes the pressure drop. And this explanation should not be probable since temperature shouldn't influence the pressure drop and both molar masses are quite similar.

Either the pressure drop is changed when the gas is compressed or sucked in the exchanger. As the two pressure drop compared few lines above have been measured at the end of the test when the exchanger was fouled. We can conclude that the fouling has an effect on the pressure drop when one compresses or suck the gas into the exchanger.

The justification can be the following, when the gases have flown through the exchanger a more important thickness of soot is created on the input cross-section of the exchanger. But on the output gas cross-section the fouling is significantly lower. It can obviously be compared between Figure 5.4 for the input cross-section and Figure 5.5 for the output cross-section. In this sense the pressure drop could be changed if the gas is compressed or sucked, making the pressure drop higher when

compressed into the heat exchanger due to the soot thickness at the gas entry that obstruct the gas channel.

As we have not been able to present a comparison of the pressure drop before and after the tests to reflect the influence of fouling we present on Figure 5.8 the pressure drop before and after in the heat exchanger using the vacuum cleaner setup and the anemometer.

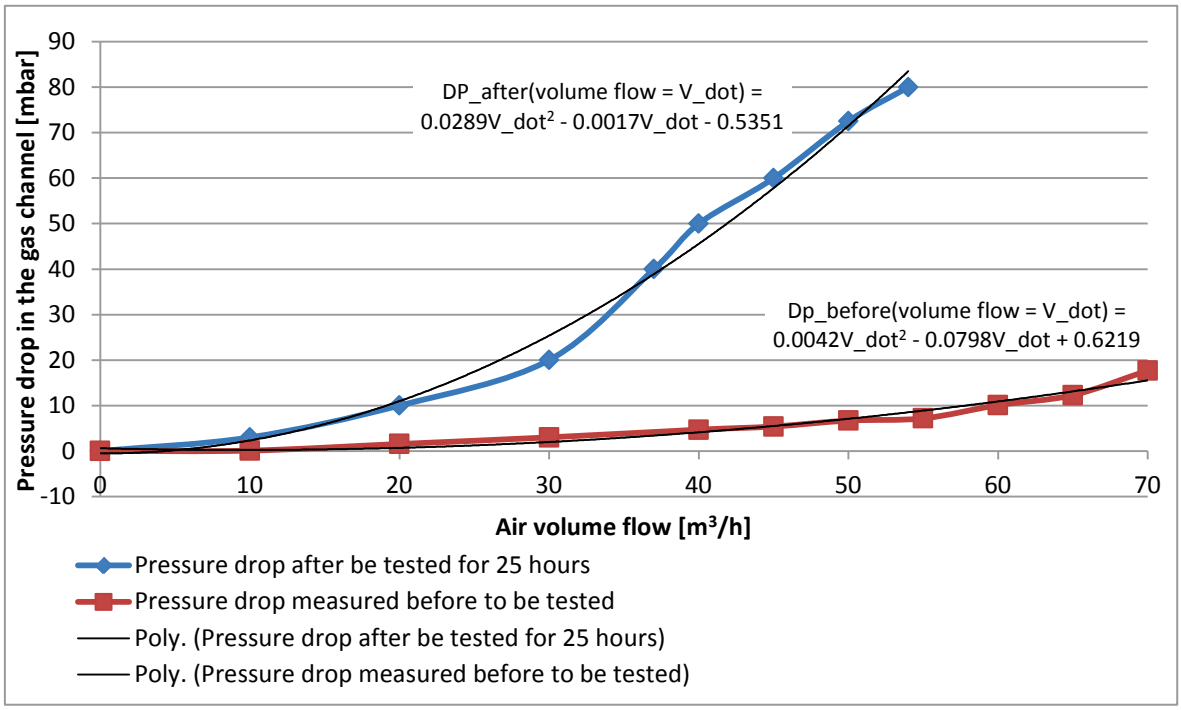

Figure 5.8: Comparison of the pressure drop of the gas channel in PSFGL HEX before the tests and after 25hours of operation with exhaust gases.

Analysing Figure 5.8 it appears that the pressure drop has largely increased after 25 hours of operation. It is justified by the exhaust gas fouling of the gas channel of PSFGL HEX. The lecturer can keep in mind that with an air flow of 55m^3/h the pressure drop has increased of 35mbar, increasing from 7mbar to 42 mbar.
For a 30 m^3/h air volume flow, the pressure drop on gas channel increases of 17 mbar, increasing from 3 to 20mbar. For both considered values, it represents an increase of 6 times the initial pressure drop on the gas channel.

The following conclusion is justified by values presented above; as to know a regular regeneration or cleaning of the PSFGL HEX becomes necessary when it operates with soiled gases.

Concluding on this section we can say that our casing as well resits to the test, it was easy to close and to open. It is a good and cheap solution for testing PSFGL

HEX during the first development phase of the product and will still be used for further development.

Concerning the state of the PSFGL HEX, we can say it was quite dirty and the use of chemical liquid substances flowing under pressure in the gas channel is probably the best way to be able to regenerate it cyclically.

Chapter 6 Conclusions

In Chapter 1 the frame of this project was described: the development of a new technology in order to recover low heat temperature from gases.

Chapter 2 explains the course of the project including objectives and the main encountered challenges.

Chapter 3 has been dedicated to the design and building process of the Polymer Spiral Gas-Liquid Heat Exchanger (PSFGL HEX), a strong and resistant product completely developed by ourselves.

Chapter 4 contains a large presentation of the complete facility which was developed. It includes a cogeneration unit with a Diesel motor, an exhaust gas conditioning unit and a test casing for the exchanger. The Labview developed measurement software has also been presented.

Finally Chapter 5 , presented the performances of this innovative heat exchanger which was tested on the facility. A 1.2kW heat transfer unit with partial water condensation has been a very good result, as well as an overall heat transfer coefficient of 50W/(m^2 K) using flue gas. A corresponding UA factor higher than 100W/K has been reached. A gas pressure drop of 200mbar for a 70m^3/h exhaust gas flow and liquid pressure drop of 300mbar at 600m^3/h have been measured. Remaining to tell that pressure drop in a liquid medium it is not as critical as it is for gases.

Comparing these results with other polymer heat exchangers, the PSFGL HEX is very good, they are even better considering the tested conditions. The development of this innovative heat exchanger has been very substantial, as it has been able to resist to several intensive days in contact with corrosive substances. Damages have not been detected after the tests and the heat exchanger can still operate properly.

However the main goals for a PSFGL HEX would now be targeted with a heat transferred of 25kW and a pressure drop on the gas channel in the range of 1mbar considering a gas flow of 100m^3/h. An overall heat transfer coefficient of 100W/(m^2 K) would also be necessary to reach a profitable heat recovery limit.

In order to reach better specifications and to proceed to further improvements, there should be made some modifications to improve the developed heat exchanger and the test bench.

At the present time, the pressure drop on the gas channel is still a strong issue and it has to be improved in the near future. To remedy this problem it would be meaningful to increase the thickness of the gas channel of the PSFGL HEX. Using

three mesh layers, one mesh with a small pattern on each side of the gas channel to stabilize the film and a large pattern mesh in the middle to increase gas channel thickness would decrease largely the pressure drop.

While this report is written a new PSFGL HEX prototype with a thicker gas channel has been produced showing a pressure drop under 4mbar with an $80m^3/h$ air flow. The mesh geometry has to be studied and optimized. Mesh geometry is a critical point and can lead to a significant pressure drop reduction on the gas channel. Using a high thermal conductivity mesh as carbon mesh would be recommended. It would also lead to a heat transfer improvement.

Now it would be very interesting to compare the efficiency of new films based on other materials like PE, PP, PET; those films will are less temperature resistant as PEEK but results could be of great importance regarding the performances of a PSFGL HEX.

The PSGFL HEX must be optimised in a way described above; the facility must jointly be improved to fulfil the new requirements of the PSFGL HEX. As the facility has shown good performances, a pressure drop optimisation on the gas channel of the PSFGL HEX would require improving the accuracy of the pressure drop measurements on the facility.

Concerning the facility attention should be focus on the following points: as the tubular heat exchanger used to condition the exhaust gases is over-sized and the exhaust gas output temperature is very sensible to a tiny variation of cooling water flow, it would be better to use a tubular heat exchanger mono-tube designed for the heat load range of 3 to 5kW. A water injection device could also be developed to increase the dew point temperature of the gases and increasing then the exergy or temperature high of the energy recovered.

The developed Labview software has shown good performances during the tests through a friendly user interface. However adding more time would allow improving it and making its code more modular.

Heat-payers used to measure water flow in the exchanger are not always reliable; finding another way to measure the water flow in the exhaust gases conditioning unit could bring improvement to this issue.

Concerning the gas flow meter there should be bought a new flow meter. A gas flow meter produced by KSPG Automotive seems to be a good solution. Documentation can be found in source [6]. This device will allow to decrease temperature losses in the flow meter and to have a better accuracy measuring the exhaust gas volume flow.

In order to reach higher gas temperatures in the PSFGL HEX, a proper insulation of the PSFGL HEX casing would be required. Using tap water at about 21°C to cool the PSFGL HEX would improve the heat transferred in the PSFGL HEX.

By changing the differential pressure sensors with sensors that have a temperature correction will lead to a better accuracy in the pressure drop measurements and to operate pressure drop measurement independently to the atmospheric temperature. Also the differential pressure sensor unit output voltage is not normalized to 0-10V. Adding a device scaling the output voltage in the range of 0-20mV or 0-500mV depending on the selected sensor to an output voltage of 0-10V would improve the accuracy of the pressure drop measurements.

For improving the accuracy of the temperature which was measured in the output pipe of the PSFGL HEX liquid channel, water mixers should be placed in the pipes to guarantee a homogenous temperature.

For an initial first try the tests have provided good results. Nevertheless the PSFGL HEX has to fulfil some more requirements to be profitable and therefore be used in combination with ORC power generation for heat recovery in soiled gases.

6.1 Acknowledgments

Here I would like to express my sincere gratefulness to all who helped me and guided during this six month of project. Especially for them who suggested me solution for various realisation and helping me solving daily challenges. Without the help of anyone the realisation of the test bench would have been much more demanding.

My first thanks go directly both equal to Prof. Daniel Favrat and Dr. Thomas Weimer for the trust they placed in me allowing me realising such setup using high valuable devices. I have appreciated theirs helpful comments and advices they shared with me along the project through direct discussions or Skype conferences.

My particular thanks and gratitude are also addressed to the ones who guided me during this project: all colleagues at Makatec, they all contributed to the nice mood during the months spend with them, particularly to Frank Moser, for his advices, his availability, Daniel Boee for the heps developing PSFGL HEX and for trying speaking French, Sven Kittelberger for opening his stocks for all types of various unexpected needed things to build the facility and for his humour sense, Thomas Hasenoehrl for the discussion on the way to Bondorf by bike or car, Sabine Wellerdiek for all administrative task as transports between Switzerland and Germany.

At the EPFL I want to thank you Gaia Piazzesi for the coordination of the project with the various partners and for organising the truck transport between of the devices between Switzerland and Germany, Johannes Wegele for helping me with the measurement devices, Labview, learning me to weld and showing me unexpected treasures hidden in a corner of LENI lab, Christophe Zurmuehle for helping me for the retrofit of the COGEN unit and for under measure mechanical work, Ahmed Yezli for his availability for fixing automation problems with the COGEN unit, Angel Iglesias for helping me with the Ricardo mass flow meter, Olivier Hodder for understanding how should work the COGEN generator Irwin Gafner for his advices for lambda measurements and advices repairing the engine.

At Liebherr I would like to thank you Benoit Gay for lending a brand new Lambda sensor, Michel Dupont for the advices for lambda measurements and the visit of Liebherr workshop.

At Keller France, Gilles Dubaret for long calls, helping me to understand how differential sensors function.

Finally, I would thank all friends and people that could have missed to thank personally here and that allow me to have a huge pleasure working on this project and spending a marvellous time in Germany.

Chapter 7 Appendix

Appendix A Exhaust gases analysis

A.1 Composition of exhaust gases

First task has been to estimate the composition of the Diesel. Using some contacts at Leibherr, we have obtained the measured composition of various lots of Diesel fuel oil. These values have been compared with a composition table realised by the LENI laboratory at EPFL.

Table 7.1: Diesel fuel oil property from various sources.

Fuel propriety	Liebherr, lot december 2011	Liebherr, lot march 2012	Composition Table LENI	Value Used
C mass %	86.61	86.94	86.0	86.6
H mass %	13.79	13.36	13.2	13.3
O mass %	0	0	0.2	0
S mass %	10.3	7.6	0	0.05
N mass %	0.05	0.05	0.6	0.05
LHV	43210	43050	42700	-
HHV	46140	45890	45400	-
ρ [Kg/dm3]	0.8169	0.8264	0.84	0.81
Cp [kJ/kgK]	2.2	2.2	-	Cf. §A.3

Note : Composition percentages for Liebherr are over 100% due to the error of measurements devices. A measurement of the Rho gave the value $\rho = 0.8094$ [kg/dm3].

First some assumptions have to be made for the computation:

1) The air in the combustion chamber is assumed to be dry
2) The combustion process is assumed to be complete
3) Air and combustion gases are assumed to be ideal gases
4) Standard condition of pressure and temperature have been taken as $P_n = 1$ atm, $T_n = 25°C$

Table 7.2: Molar mass of substances used for exhaust gases computation

Substance	Molar mass [kg/kmol]
O	16.0000
O2	32.0000
C	12.0100
H	1.0079
H2	2.0158
N	14.0100
N2	28.0200
S	32.0600
CO2	44.0100
H2O	18.0158
SO2	64.0600

Using the molar mass in the Table 7.2, the molar percentage in the Diesel of each substance can be computed as following:

$$\tilde{c}_i = \frac{c_i}{\widetilde{m}_i} \tag{7.1}$$

$$\begin{aligned} \frac{N_F}{M_F} C_u H_v O_w S_x \mathrm{N}_z + \frac{N_{Air}}{M_F} \lambda \, (0.21\, O_2 + 0.79\, N_2) \\ \rightarrow \frac{N_{CO_2}^{Gc}}{M_F}\, CO_2 + \frac{N_{H_2O}^{Gc}}{M_F}\, H_2O + \frac{N_{O_2}^{Gc}}{M_F}\, O_2 + \frac{N_{N_2}^{Gc}}{M_F}\, N_2 \\ + \frac{N_{SO_2}^{Gc}}{M_F}\, SO_2 \end{aligned} \tag{7.2}$$

Where *u, v, w, x* and *z* subscript are an average atoms numbers for an approached synthetic formula of Diesel. Those coefficients haven't been computed in this analysis as it haven't been relevant.

Using the table 11.3 of [7] and considering hypothesis mentioned above, we can obtain the following quantities.

The amount of air per kilo of fuel is given by:

$$\frac{N_{Air}}{M_F} = \frac{\lambda}{0.21} \left(\frac{c_C^F}{\widetilde{m}_C} + 0.5\, \frac{c_{H_2}^F}{\widetilde{m}_{H_2}} \right) = 0.8576 \text{ kmol Air/kmol Fuel} \tag{7.3}$$

The number of kilomoles of combustion gases per kilogramme of Diesel consumed is given by

$$\frac{N_{Gc}}{M_F} = 0.5\, \frac{N_{H_2}}{M_F} + \frac{N_{N_2}}{M_F} + \frac{N_{Air}}{M_F} = 0.8907 \text{ kmol Gc/kg Fuel} \tag{7.4}$$

Then the number of kiomoles of carbone dioxyde per kilogramme of fuel is:

$$\frac{N_{CO_2}^{Gc}}{M_F} = \frac{N_C}{M_F} = 0.0729 \text{ kmol } CO_2\text{/kg Fuel} \tag{7.5}$$

The number of kilomoles of water per kilogramme of Fuel is:

$$\frac{N_{H_2O}^{Gc}}{M_F} = \frac{N_{H_2}}{M_F} = 0.0660 \text{ kmol } H_2O/\text{kg Fuel} \tag{7.6}$$

The number of kilomoles of dioxygen per kilogramme of fuel is:

$$\frac{N_{O_2}^{Gc}}{M_F} = 0.21 \frac{N_{Air}}{M_F}\left(1 - \frac{1}{\lambda}\right) = 0.0742 \text{ kmol } O_2/\text{kmol Fuel} \tag{7.7}$$

The number of kilomoles of dinitrogen per kilogramme of fuel is:

$$\frac{N_{N_2}^{Gc}}{M_F} = 0.79 \frac{N_{Air}}{M_F} + \frac{N_{N_2}}{M_F} = 0.6776 \text{ kmol } N_2/\text{kg Fuel} \tag{7.8}$$

The number of kilomoles of sulfure dioxyde per kilogramme of fuel is :

$$\frac{N_{SO_2}^{Gc}}{M_F} = \frac{N_S}{M_F} = 1.5596\ 10^{-5} \text{ kmol } SO_2/\text{kg Fuel} \tag{7.9}$$

A.2 Molar mass of exhaust gases

The molar mass of the combustion gases is given by the summing of the mass of each substances present in one kilomole of exhaust gases.

For each component of the combustion gases as it has to be CO_2, H_2O, O_2, N_2, SO_2, the molar concentration per kilomole of combustion gases and is given by:

$$\tilde{c}_i^{Gc} = \frac{\frac{N_i^{Gc}}{M_F}}{\frac{N_{Gc}}{M_F}} \qquad \text{[kilomol i/kilomol Gc]} \tag{7.10}$$

All computed concentrations figure in Table 7.3.

Table 7.3: Molar concentration of exhaust gases components

$\tilde{c}_{CO2}^{Gc}$	0.08189	[kilomol CO2/kmol de Gc]
$\tilde{c}_{H2O}^{Gc}$	0.07407	[kilomol H2O/kmol de Gc]
$\tilde{c}_{O2}^{Gc}$	0.08326	[kilomol O2/kmol de Gc]
$\tilde{c}_{N2}^{Gc}$	0.76074	[kilomol N2/kmol de Gc]
$\tilde{c}_{SO2}^{Gc}$	1.75105E-05	[kilomol SO2/kmol de Gc]

Converting each component's molar concentration per kilomole of combustion gases in a mass quantity per kilomole of combustion gases and summing all the mass of each component i (CO_2, H_2O, O_2, N_2, SO_2) by kilomole of combustion gases, gives the molar mass of the combustion gases as shown below:

$$\tilde{m}_{Gc} = \sum_i \tilde{m}_i^{Gc} = \sum_i \tilde{c}_i^{Gc} \cdot \tilde{m}_i = 28.92 \text{ kg of Gc/kilomol Gc} \tag{7.11}$$

A.3 Specific heat load of combustion gases

To compute the specific heat load of the combustion gases, we can take as reference the method used in [8] pages 331 and followings pages. We can compute a Cp of a mixture of gases on the temperature range of 0 to 1200°C.
However having problems in a first time with the Cp computations, Cp values have been taken from an Internet Diesel exhaust gases properties calculator [9] that would give a quite similar Cp as the method used. Other properties are given foe exhaust gases as density, cinematic and dynamic viscosity and more…
One needs to first compute the Cp of each component of the mixture separately to the targeted temperature using the aij of Table 7.4 using the following formula:

$$c_{p\,i} = \sum_{i=1}^{6} a_{ji}(10^{-3} \cdot T)^{j-1} \quad [\mathrm{J/(kg\ K)}] \tag{7.12}$$

Then the Cp of the exhaust gas mixture is given by summing for each component i:

$$C_{p\,Gc} = \frac{\sum_i (\tilde{c}_i^{Gc} \cdot \tilde{m}_i \cdot c_{p\,i})}{\tilde{m}_{Gc}} \qquad [\mathrm{J/(kg\ K)}] \tag{7.13}$$

Table 7.4: Coefficients table for computing the specific heat load of the substances

Coefficient Cp/Cp substances	j=1	j=2	j=3	j=4	j=5	j=6
CO2, i=1	432.54	1785.41	-1602.3	766.71	-152.33	0
H2O (vap), i=2	1920.74	-835.7	2896.83	-2805.54	1412.17	-296.05
O2, i=3	999.56	-955.05	3269.24	-3871.85	2065.51	-417.59
N2, i=4	1115.35	-562.52	1257.13	-829.38	186.38	0
SO2, i=5	447.58	480.77	789.81	-1863.1	1293.31	-307.01
Air	1057.69	-462.92	1182.59	-835.11	198.8	0
CO	1114.66	-597.47	1439.48	-1011.87	240.23	0

Plotting over the temperature range 0-600°C the specific heat load of the combustion gases, we have obtained the graphic on the Figure 7.1.

From this analysis we can conclude that the Cp can be approximate with accuracy on the operating HEX temperature range, from 10°C to 150°C with a linear approximation as presented on (7.14).

$$C_{p\,Gc} = 0.1872\,T[°C] + 1036.1, T \in [10 - 150°C],\ [\mathrm{J/(kg\ K)}] \tag{7.14}$$

When needed to take the whole temperature range from the very exit of the engine to a relatively low temperature, the other linear approximation on the range 0-600°C can be used. Equation (7.15) will be less accurate on low temperature.

$$C_{p\,Gc} = 0.2631\,T[°C] + 1027.9, T \in [10 - 600°C]\,,\ [\mathrm{J/(kg\ K)}] \qquad (7.15)$$

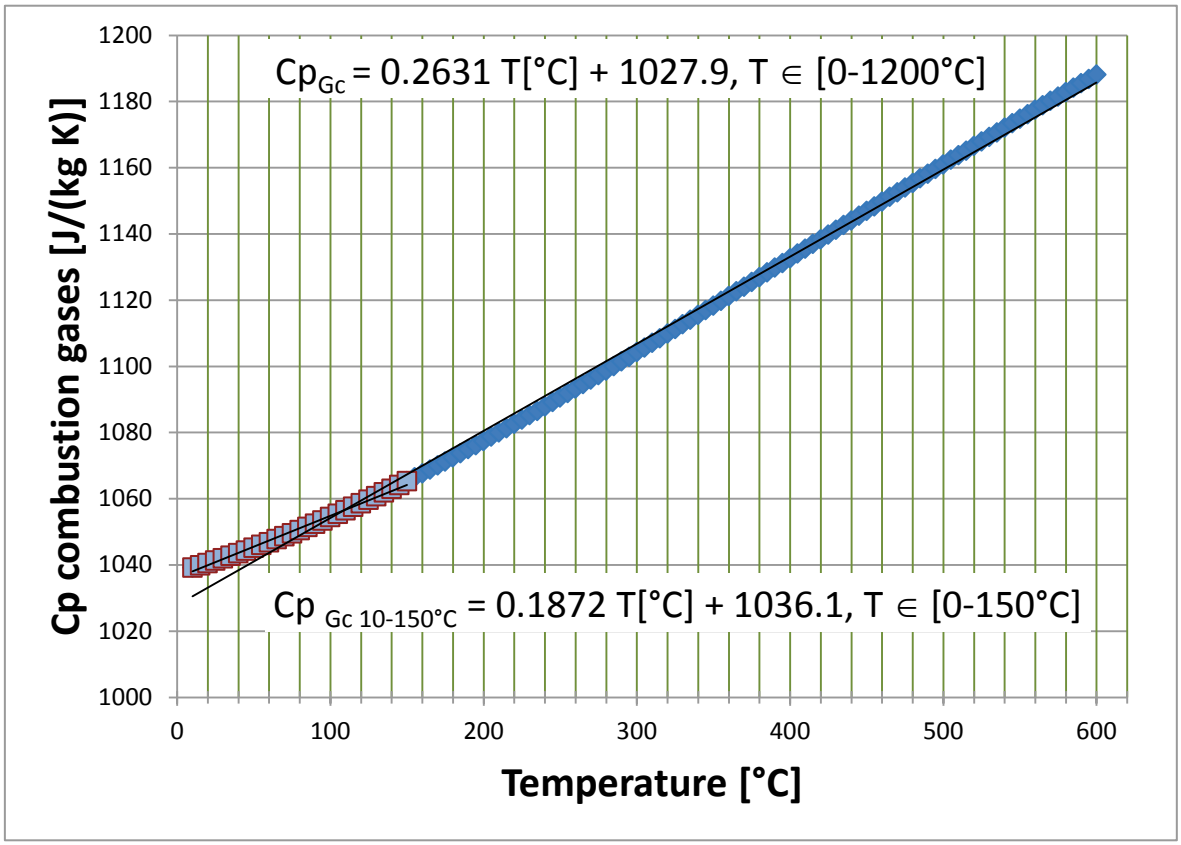

Figure 7.1: Specific heat load of the combustion gases plotted over the temperature. Two linear approximations of the Cp have been computed and are written on the graphic. One computation approximates the Cp on the temperature range from 0-600°C, the other is more accurate on the temperature range used in the PSFGL HEX(10-150°C).

A.4 Engine's consumption measurement at full load

In order to estimate the mass flow of exhaust gases when the engine is at full load, we have it has been necessary to measure the Diesel consumption of the engine.

A bottle filled with Diesel was setup to serve as a tank. Three runs have given the same results, and for each run the bottle filled with Diesel has been weighted before a 11 minutes operating run at full load with a weight of 690 gram and after

the run with a weight of 140.6 gram as shown on Figure 7.2. During the operation the exhaust gases went through the steel HEX and were driven through the exhaust pipe without flowing through the PSFGL HEX.

The Diesel consumption measured is in the range 0.81 to 0.84 gram of diesel per second in the condition mentioned above.

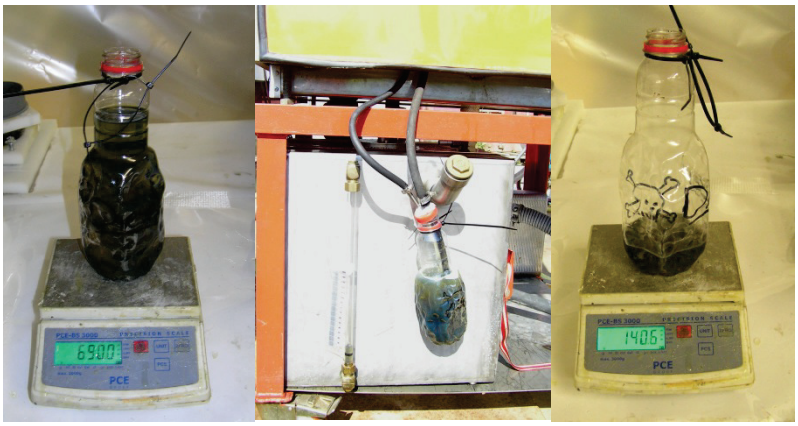

Figure 7.2: A bottle have been realised to supply the usual Tank to measure the Diesel consumption at full load. The bottle has been weighted before and after 11 minutes run at full load.

A.5 Exhaust gases mass flow at engine full load

After determining the Diesel consumption of the engine at full load to be beteween 0.81-0.84 g of diesel per second, it is relatively straight forward to find the exhaust gas mass flow leveraging equation (7.16). Using equation (7.4) page 64 which provides the amount of kilomole of exhaust gases per kilogramme of fuel consumed the exhaust gases mass flow is given as follows:

$$\dot{m}_{Gc} = \frac{N_{Gc}}{M_F} \cdot \widetilde{m}_F \cdot \dot{m}_F = [21.0\text{-}21.7] \text{ g of Gc/s} \tag{7.16}$$

Assuming the pressure at the exit of the cylinder is about 2bar (source [10], slide 36) and the temperature is 600°C, with a molar mass of the exhaust gases of 28.92 g/mol the ideal gas law gives straight forward a volume flow of 27.2 litres per second at the output of the cylinder chamber. Once cooled at the entrance of the PSFGL HEX, this volume flow is decreasing due to the decrease of temperature to 120°C. Thus the pressure is about 1.1 bars. The ideal gas law gives a volume flow of 22.3 litres per second at the PSFGL HEX casing input.

Through the different sections of this chapter we have estimate the important property of the exhaust gas flow produced by our COGEN unit. The following is a short overview of the values discovered in this section.

First in Appendix A.1 an average composition of the Diesel fuel was defined. With the combustion equation, the amount of each substance in the exhaust gases per kilogram of fuel burned was calculated.

In Appendix A.2 the molar mass of the combustion gases was computed. We found a molar mass in the order of 28.92 kilogram per kilomol which is very close to the molar mass of the air which is 28.85 kilogram per kilomol following reference [7] pages 514 and 521.

In Appendix A.3 the specific isobaric heat load has been computed and approximated for the two temperature ranges, 10-150°C and 10-600°C, depending on the operating temperature of the exhaust gases. The range of the Cp was from about 1039 J/(kg K) at 10°C to 1188 J/(kg K) at 600°C. We mention that the Cp of exhaust gases are more varying with temperature as the air Cp which is following source [11] from 1005 to 1068 J/(kg K) on the temperature range from 20°C to 400°C.

Finally in Appendix A.4 Diesel consumption of the engine at full load have been measured the and in Appendix A.5 we the maximum mass flow of exhaust gases of the engine have been estimated to 21-22 gram per second.

Knowing that gas flow measurement are always difficult to realise with accuracy we have now an approximate target reference of the value that has to be measured and also a maximal value for the gas mass flow. The next step is to implement an effective and reliable way to measure such exhaust gas mass flow in the range of 20 gram per second. Few ways have been explored and are developed in Appendix D .

A.6 Condensing temperature of the gases

The condensing temperature of the exhaust gases or also called dew point temperature is corresponding to the temperature for which the saturation pressure of the gases is corresponding to the partial pressure of water contained in the exhaust gases. Using relation 6.18 of the following source [7], the partial pressure of water in the exhaust gases is defines as follow using the computed values obtained by equations (7.4) and (7.6).

$$P_{water} = P_{atm} \cdot \tilde{c}_{water}^{Gc} = P_{atm} \cdot \frac{\frac{N_{H_2O}^{Gc}}{M_F}}{\frac{N_{Gc}}{M_F}} = 0.0711 \text{ [bar]} \tag{7.17}$$

Using the Clausius-Clapeyron law, that can be found in reference [7] equation number 5.161, we obtain the dew point temperature of the exhaust gases that is approximately 40°C when lambda of the engine is 1.7. If we wanted do increase this temperature, water has to be vaporized in the combustion gases. By example to

increase the dew point temperature to 60°C, molar concentration in the exhaust gases would have to be 0.2 mole of water per mole of combustion gases, meaning an increase of 13% of the water molar concentration in exhaust gases.

Appendix B Retrofit of the COGEN unit

After many years not been used there was the need to operate a retrofit of the cogeneration unit. By proceeding to the COGEN unit retrofit, few modification and maintenance operation that have been executed. Here is presented a state of the engine with mention of some failure that happened.

First of all an oil and filter change have been proceed at the beginning of the project. Be aware that after an oil change if the pressure is too low after a while then a failure can be triggered. There have been needed to reset the failure forcing error with a PC connected to the automaton. Thanks to the help of Mr. Ahmed Yezli at the EPFL that helped to reset the alarm. The pressure cylinder head contactor wires were previously not recorded to the automaton. We have added a plastic extension to insulate both connection of the contactor. See Figure 7.3.

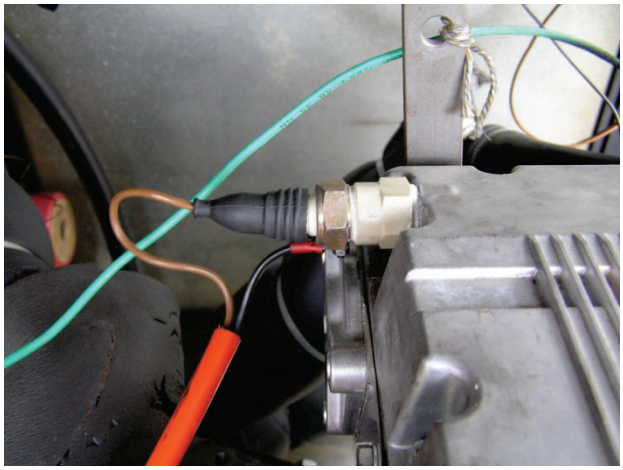

Figure 7.3: Insulation in polymer realised, in white to insulate the pressure contactor of the cylinder head.

A small plate heat exchanger placed on the bottom platform of the unit as shown on Figure 7.5 number 2, has been installed on the cooling circuit of the engine. It allows evacuating the heat produced by the Diesel engine.

A flexible steel pipe has been mounted on the exhaust exit, allowing connecting the COGEN unit to the steel heat exchanger flange. We can see it the end with the flinch connected to the Steel heat exchanger on Figure 4.14 picture 1.

Concerning the usage of the engine, to start it one have to turn both “selecteur de mode” on 1 and “arret demarage” on 1. Also selector “pompe circulation“ has always be on manual. The position of all front panel selectors when the unit is operating is shown on Figure 7.5 3).

One needs to pay attention to make the engine running upper 3000rpm before it is automatically synchronised on the electricity network after few seconds running. It means to pull quickly the gas lever when the engine has started, but not to fast to do no damage the engine when cold. As reminder Figure 7.4 present the characteristic torque speed of a standard generator. It tells that if not the generator will then operate as an electrical engine and will make the Diesel engine stall making the engine consuming rather to produce electricity.

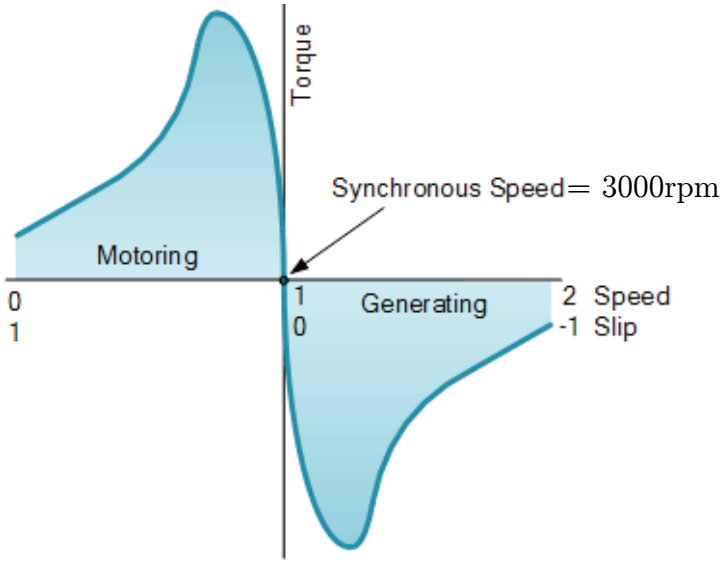

Figure 7.4: Operational curve of a standard generator. If the speed of the generator is not higher than the synchronous speed (3000rpm for 50Hz network) when linked to the network it will work in the motoring mode rather than in generating mode. In motoring mode electricity is consumed, in generating mode electricity is produced.[2]

Note that if the generator is running in the opposite sense there is a phase inversion between phases of the network and those of the generator. Solution is to invert two phases in the 32A plug.

In good operating condition the current produced at starting by generator may be few time the maximum current at nominal operating point. To this reason there is the need that the plug is secured with a delayed fuse or HPC with a C or D curve allowing at starting much higher current as 32A on a very short time.

A rotameter measuring of engine cooling water volume flow has been installed as shown on Figure 7.5 number 1. We would recommend insuring the engine cooled by more than 8 to 10 litres per minutes when running at full load. This flow meter is more to insure the cooling water flow is enough to cool the engine properly. Note that an engine a water temperature security stops the engine if temperature of the cooling water is to high. Mentioning that the cooling water thermostat was initially rusty blocked in a closed position. Launching a failure after 10 minutes, the engine has been automatically turned off when cooling water temperature was to high.

[2] Figure taken from: http://www.alternative-energy-tutorials.com/wind-energy/induction-generator.html, consulted on the 14th of june 2012.

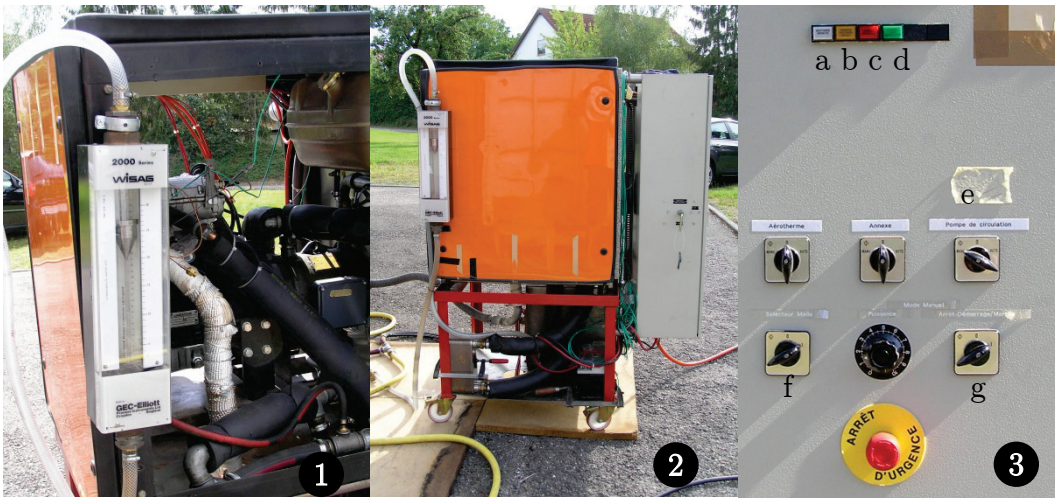

Figure 7.5: 1) The COGEN unit opened with the rotameter installed in operating state. 2) The unit with the plat heat exchanger installed to provide a sufficient cooling and the electrical cupboard fixed on the back of the unit. 3) Electrical cupboard front panel with position of selectors when operating. On the lateral face of the cupboard is a selector that has to be turned to connect the 12V battery used for starting the engine and regulation.

When the electrical generator is connected to the network and produce electricity, the green light see Figure 7.5, picture 3) button (d) is light up.

When a failure occur or when the engine stops light (b) and/or (c) will be lighted (see Figure 7.5 number 3), there is the need to press the "Quittance defauts", see Figure 7.5 picture 3) (a) button on the control panel. If the failure remains, then one needs to check automaton state panel inside the electrical cupboard. Figure 7.6 show this panel, signification of the red numbers that have been encountered will be here explained. Note that others error could happen.

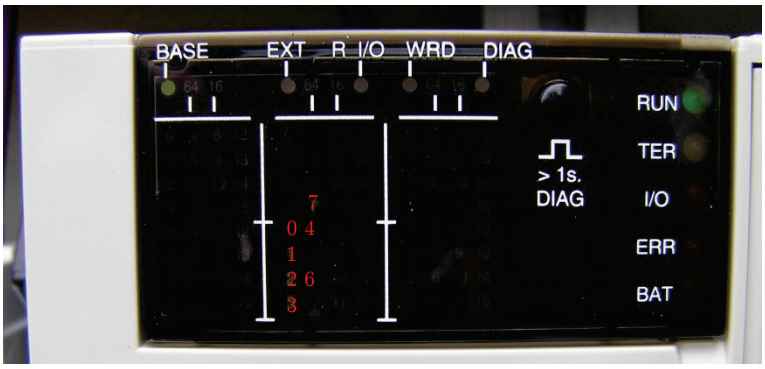

Figure 7.6: Panel of the automaton that is placed in the electrical cupboard of the COGEN unit. Explanation of number in red is given in the text.

0: light up when the "quittance defauts" button is pressed (see Figure 7.5, picture 3) button (d))

1: is light up when air pressure at the entrance of the engine is to low. To make the engine start it must be turned off. If it happens, there is the need to clean or change the air filter. Step to solve the failure is presented on Figure 7.7 and is

explained in the legend of the figure. This failure could happen if the engine is stopped by closing the air entrance pipe (on the side of the air filter cover).

Figure 7.7: Operation to clean or change the air filter. 1) Open the air filter cover 2) remove the filter and hover the soot and remount the filter 3) Press the red button on the pressure contactor located in the red cycle between the two wires to reset the failure.

2: is light when the oil pressure is sufficient. This light has to be turned on to allow the engine start.

3: is light when the current with the electricity network is working properly. This light has to be turned on to allow the engine start. (Figure 7.5, picture 3) button (d))

4: is light when the "Mode" selector button on the front panel is turned. This button starts the unit (Figure 7.5, picture 3) button (f))

6: is light when the "Demarage-Arret" selector on the front panel is turned. Figure 7.5, picture 3) button (g)) To turn on the unit both selector "Demarage-Arret" and "Mode" have to be turned on.

7: is light when the red light on the front panel "Alarme generale" is lighted. (Figure 7.5, picture 3) button (c))There is a failure or there need to do a "Quittance defauts", pressing the corresponding button on the front panel.

One can refer to the following report [1, 12, 13] for more information about the maintenance and operation of the Co-generation unit (COGEN).

Appendix C Steel heat exchanger conditioning exhaust gases temperature

Here we'll present the setup of the steel tubular heat exchanger that has been used to precool exhaust gases before entering into the PSFGL HEX with a suitable temperature. Encountered problems will be mentioned in this Appendix.

Figure 7.8 present the flow sheet of the steel tubular heat exchanger with measurement devices placement.

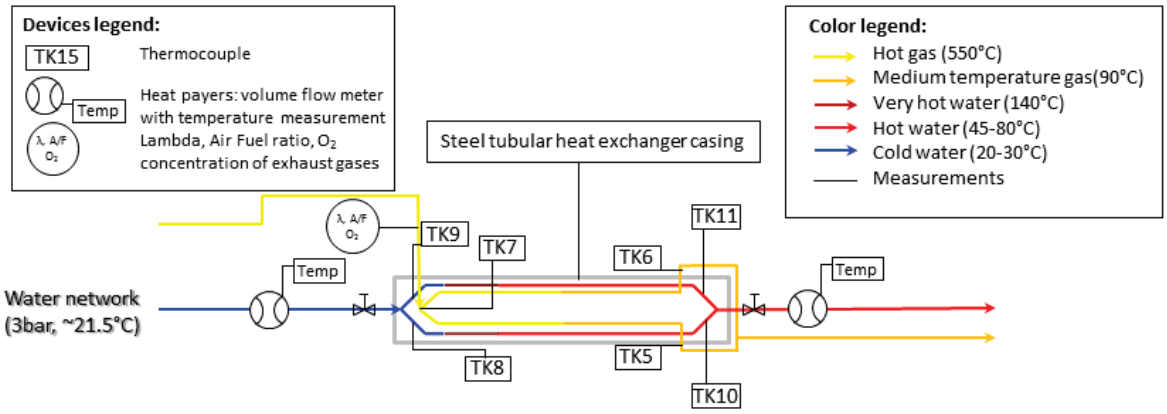

Figure 7.8: Flow sheet for steel tubular heat exchanger conditioning exhaust gases temperature.

This tubular heat exchanger has been previously built to recover heat produced by the COGEN unit. In our project it has been used as it was already prepared. Thermocouples were already placed and the exchanger was placed in an isolated casing that would be necessary to be able to control properly exhaust gases cooling.

However few problems can be enumerated with this steel exchanger. First it appears that cooling heat load would be about 3 to 5kW for a full exhaust gases volume flow. As this exchanger is over sized for an exhaust gases precooling and specific heat coefficient Cp of the gases are about 4 times smaller than specific heat coefficient of water, cooling water flow must be very low with 55l/h.

As it has been tested first in counter flow, it appeared that the water temperature at the water exit would be higher as 100°C as gas input is placed near water output in counter flow configuration. Steam creation makes the exhaust gases temperature conditioning very difficult to operate.

Secondly the exchanger setup has been changed as presented on Figure 7.8 to a co-current configuration and using a water tap cooling. It allows making water be under pressure in the exchanger increasing to 140°C water vaporisation temperature. The remaining problem with this configuration is the temperature profile that is not constant as water flow and gas flow speed are quite different.

As shown on Figure 7.8 the water input was 21°C and as gas flow input temperature is very high about 550°C, water near the gas input is heated to 140°C. At the water output, temperature is about 70 to 90°C depending on the water flow set. At gas output, temperature is still higher than water output and depends on the cooling water flow.

Thus cooling water flow is very low and phenomena of heat conduction occurred in the exchanger meaning that thermocouple TK8 and TK9 shown in Figure 7.8 haven't been placed well (when the exchanger have been built in the purpose of an old project) because measured temperature is 140°C and water input temperature is 21.°C.

Then those thermocouples have been used as an indicator to estimate the highest water point temperature in the exchanger. This allows avoiding steam creation in the exchanger. For computation water input temperature has been measured using the heat payers placed at the water input of the heat exchanger or using the temperature measured by thermocouples TK8 and TK9 before turning on the engine. Water input temperature must then be entered manually in the Labview software in the "Gas mass flow" tab.

One other problem of this exchanger is that the exhaust gas flow is separated in two tubes and make mixing problems as temperature and flow are not the same in each exchanger tube. Then at the output, the average temperature has been used. It would be much better to have one single tube with a suitable diameter for the entire exhaust gas flow.

In order to improve the facility developed during this project, we would recommend replacing this heat exchanger with another tubular heat exchanger in the range of 5kW, with one single tube. This heat exchanger must allow water and gases flowing approximately at the same speed in order to reach a better accuracy in the temperature conditioning of the gases by avoiding steam creation.

Appendix D Gas mass flow measurement

In this Appendix details for the 3 exhaust gas flow measurement methods that have been explored in this project are presented.

D.1 Laminar gas mass/volume flow meter measurements

As it has already presented on section 4.4, page 25, the chosen method to measure exhaust gas volume and mass flow has been the laminar Ricardo volume flow meter. As we have already explained how it has to be cleaned and how the measurements have to be proceeded, here will be given measurement equations of the flow meter and a quick explanation of the setup realised at the EPFL to compare the measured value with the value measured by others mass flow meter already calibrated for others experiments.

Concerning the calibration equations, the volume flow is measured using a differential pressure measured and the temperature of the gas flow that is measures in the flow meter with thermocouple TK25.
Once the volume flow has been computed, the mass flow can be computed.

Using the temperature measured in the flow meter, a temperature correction factor is computed as presented on equation (7.18):

$$T_{corr} = 81.2406\ (T_{flow} + 273.15)^{-0.77365} \tag{7.18}$$

On has to mention that T_{flow} is the temperature measured in the flow meter with thermocouple TK25, temperature is in degree Celsius.

Then the volume flow in litres per second can be computed using the pressure difference Dp in milibar through the flow meter as shows equation (7.19):

$$\dot{V} = 4.12135 \cdot \frac{Dp}{T_{corr}} \text{ [l/s], Dp in [mbar]} \tag{7.19}$$

Using various set up a Keller PD-11 in the range 0-100mbar has been first used to measure the differential pressure in the flow meter. Later is has been found that a numerical differential pressure sensor branded Rikenda previously used in the LENI laboratory for the range 0-25 mbar was more suitable and accurate. Knowing the differential pressure to be measured is about maximum 4 mbar maximal.
Once the volume flow has been computed the normal volume flow has to be computed to compute thereafter the mass flow in the flow meter.

The normal volume flow, which is the volume flow of the gas at 20°C and 1 atm is computed as following:

$$N\dot{V} = \frac{P_{atm}}{1{,}01325} \cdot \frac{273.15}{\left(\hat{T}_{flow} + 273.15\right)} \cdot \dot{V} \text{ [NL/s], } P_{atm} \text{ in [bar]} \tag{7.20}$$

Then the mass flow is computed using the molar mass of the exhaust gases:

$$\dot{m}_{gas} = N\dot{V} \cdot \frac{\tilde{m}_{gas}}{22.414} \text{ [g/s], } \tilde{m}_{gas} \text{ in [kg/kmol]} \tag{7.21}$$

Knowing how to compute the exhaust mass flow Figure 7.9 gives the time period when measurement is 10% (red lines) and 15% (green lines) accurate from the targeted value. Targeted value is the maximum exhaust mass flow computed in Appendix A.5.

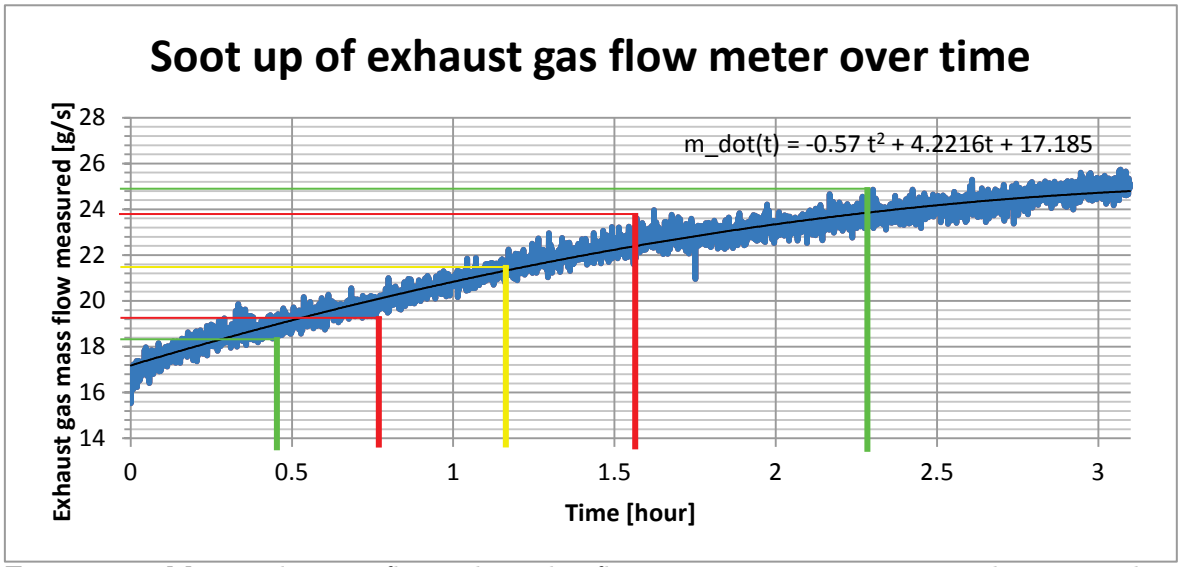

Figure 7.9: Measured mass flow when the flow meter is soot up over the time when operating. Red marks shows the 10% accuracy time period where measurements are 10% accurate around the targeted value. Green marks show the 15% accuracy time period where measurements are 15% accurate around the targeted value.

When 10% accuracy in the mass flow measurement is required, mass flow measurements have to be proceeded in the period of time when flow meter is operating from 45minutes to 1 hour 35 minutes after the mass flow has been cleaned. It lets 50 minutes of accurate measurements for each flow meter cleaning.

When 15% accuracy in the mass flow measurement is required, mass flow measurements have to be proceeded in the period of time when flow meter is operating from 25minutes to 2 hour 20 minutes after the mass flow has been cleaned. It lets 1 hour 55 minutes of accurate measurements for each flow meter cleaning.

In order to evaluate the accuracy of measurement equation presented above and used for measurement in the Ricardo flow meter, the setup presented on Figure 7.10. Compressed from the compressed air network of the lab have been blown through two other flow meter. The air flow was then driven in the Ricardo flow meter that was connecter to the PSFGL HEX casing with a PSFGL HEX places inside.

Flow meter 1 was more accurate for low mass flow up to 10g/s, flow meter 2 was more accurate in the range 10 to 30g/s. During this operation we have concluded that the measurement using the Ricardo flow meter were always in a range of 3 to 5g/s in the surroundings of the measured flow of the others flow meters.

Taking in account that the air flow was hardly stable, and that pipes were not surely sealed in the test setup this accuracy was taken as enough and calibration equations of the Ricardo flow meter were validated. As gas flow measurement was already known to be very difficult, it was thought that it would be enough for our gas flow measurements.

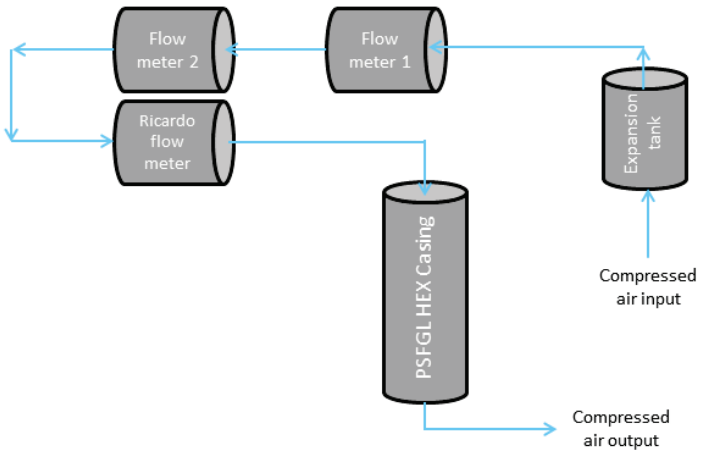

Figure 7.10: Setup realised at the EPFL to compare measured values of the Ricardo flow meter to values measured with other flow meter calibrated for other experiments.

Later at Makatec, it has been found that the Ricardo flow meter has to be cleaned more often and theses test to know how the flow meter would be soot up and how the flow measured would be influenced we were able to improve the accuracy of the Ricardo flow meter to 10% by proceeding to regular cleaning of the device. A measurement point using the laminar gas flow meter is presented below in Figure 7.11.

D.2 Mass flow measurement using the gas pre cooling heat load

This appendix describes a method explored that gave good results in measuring the exhaust mass flow using the heat load exchanged in the tubular heat exchanger used for exhaust gas conditioning.

The specific heat load Cp of the exhaust gases is known as it has been computed in Appendix A.3 page 66 or found using the Internet calculator [9]. The main assumption done is that the steel tubular heat exchanger is well isolated in its casing. Assuming that, it becomes possible to measure the mass flow of the gases using the heat load equation of the steel heat exchanger (7.22) as following:

$$\begin{aligned} \dot{Q}_{SHX} &= \dot{m}_{Cooling\ water} \cdot Cp_{Water} \cdot \Delta T_{Water\ SHX} \\ &= \dot{m}_{Gas} \cdot Cp_{Gas} \cdot \Delta T_{Gas\ SHX} \end{aligned} \tag{7.22}$$

The gas mass flow can be directly determined modifying the equation (7.22) and we obtain the mass flow of the gases by equation (7.23) as following:

$$\dot{m}_{Gas} = \frac{\dot{m}_{Cooling\ water} \cdot Cp_{Water} \cdot \Delta T_{Water\ SHX}}{Cp_{Gas} \cdot \Delta T_{Gas\ SHX}} \quad [g/s] \tag{7.23}$$

Figure 7.11 below shows a screen capture of the Labview software were thie presented flow measurements methods have been implemented. It stand for a comparison of the flow measurement computed with the steel tubular heat exchanger heat load and with the laminar flow meter.

Knowing that the Ricardo flow meter had been freshly cleaned at this point, we can compare both values measured when a maximal exhaust gas flow flows is measured. The value measured by the Ricardo is 17.1 g/s, this value is under the right value and should be higher when flow meter meshes have been soot up (not completely) at the point where measured value is accurate. Comparing it with the value measured with the heat load method, we see that the heat load method is quite accurate for the mass flow knowing the targeted value is 21.4g/s.

But now comparing the volume flow measured, we can conclude that the heat load method is completely inaccurate. This is justified to the fact that the mass flow has to be converted in volume flow and it becomes very complicated to guess an average temperature of the gas flow in the heat exchanger.

Computing volume flow, the Ricardo laminar flow meter is the only method that can give good results.

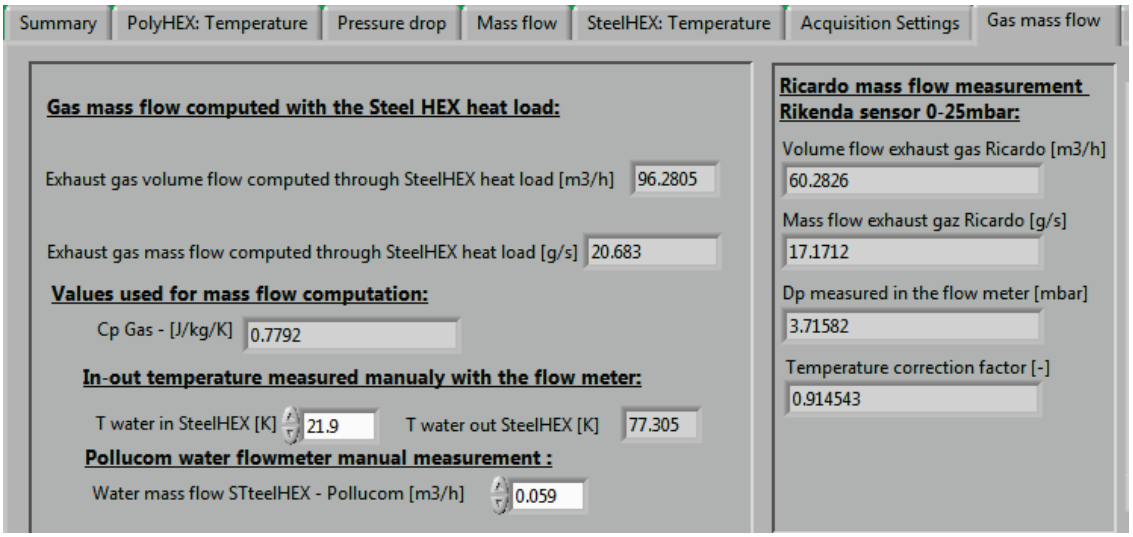

Figure 7.11 Comparison of the flow measured values between the Heat load method and the laminar flow meter.

To measure mass flow using the heat load method, one need to enter manually the water input temperature and the cooling water flow of the exchanger in the white commands bracket shown in Figure 7.11. Furthermore an average Cp of the gases inside the steel heat exchanger has to be entered on the “Acquisition settings” tab of the Labwiew software.

D.3 Volume flow measurement with a vacuum cleaner and an anemometer

In this appendix volume flow measurements between an anemometer used for air conditioning facility and the Laminar Ricardo flow meter will be compared. Proceeding to this comparison the setup presented on Figure 7.12 have been realised. It consists in using a vacuum cleaner to draw air through the Ricardo laminar flow meter and through the PSFGL HEX measuring the volume floe in the laminar Ricardo flow meter and the pressure drop on the gas channel of PSFGL HEX. The gas output of PSFGL Hex is connected to a long pipe in which have been introduced the anemometer sensor output. A vacuum cleaner is connected to this last pipe. Air is the rejected at the vacuum cleaner output. A photo of the setup titled Figure 7.13 will be found below.

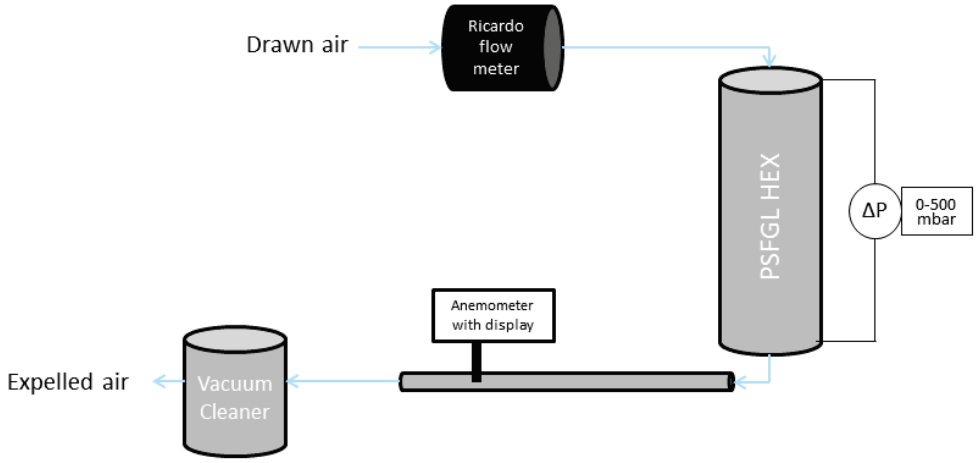

Figure 7.12: Setup of the air flow measurement comparing anemometer measurements and Ricardo measurements.

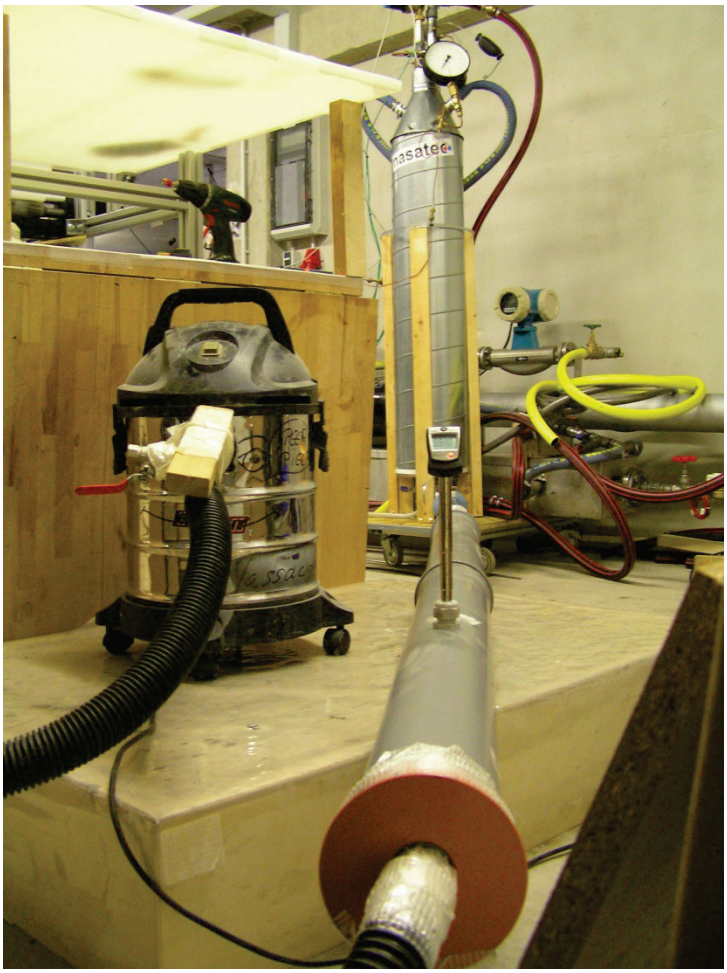

Figure 7.13: Photo representing the setup when comparing volume flow measured with an anemometer and with the laminar Ricardo flow meter

Figure 7.14 present the measurements of the volume flow using the anemometer and using the Ricardo laminar flow meter. Both measurements have been correlated with the pressure drop on the gas channel before the PSFGL HEX has been tested.

Figure 7.14 shows that both devices are measuring the same flow in the range 0 to $8m^3/h$. Divergence between the two measurements for a volume flow higher than $8m^3/h$ is explained as following. When the measurements have been done, the Ricardo flow meter haven't been cleaned and the meshes were soot up, in this sense a difference of $18m^3/h$ when the flow is maximal can be justified. As when meshes of the Ricardo flow meter are soot up, the pressure drop in the flow meter increases and the measured volume flow is higher than the real value of the flow.

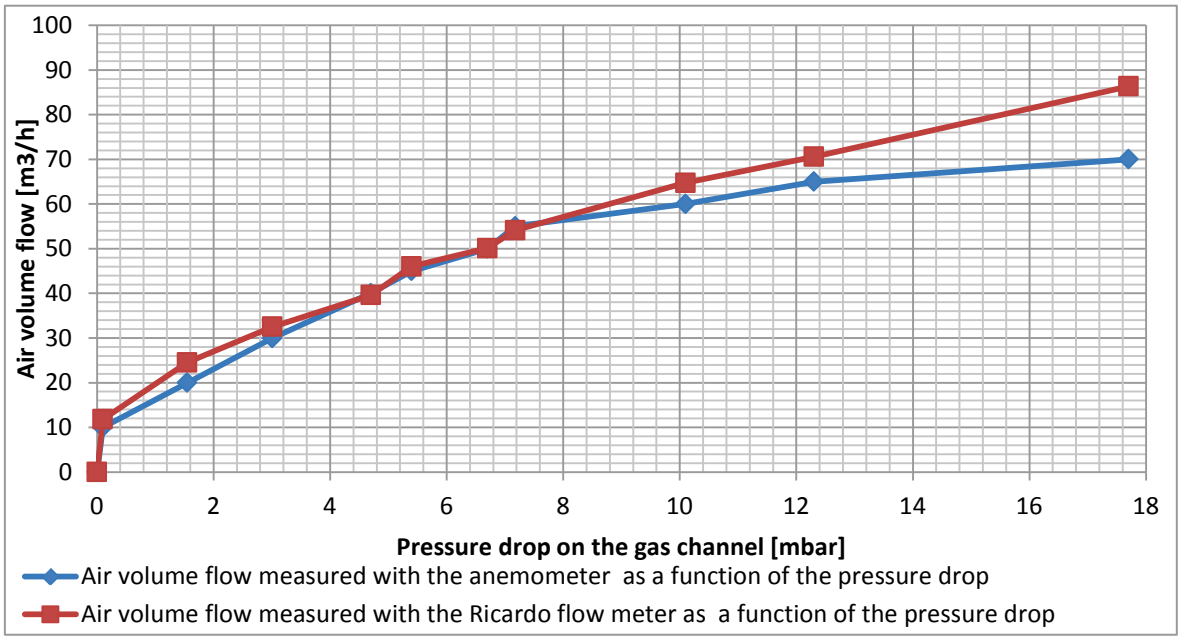

Figure 7.14: Air volume flow measured as a function of the pressure drop in the gas channel of PSFGL HEX before the tests.

Anyway this test measurement convinces us that the laminar flow meter was a good device for measuring volume flow. It is the only one to be able to resist to temperature and to give with a good accuracy volume floe and mass flow. Furthermore is can resist to the high temperature of exhaust gases. The price to pay using this device is the obligation to clean it and to empty the condensed water that remains inside.

D.4Volume flow computed with an equation depending on the gas pressure drop

This appendix presents shortly a method that has been tried for measuring the exhaust gas volume flow but didn't give good results. Bad results obtained can be justified by the fact that the pressure drop on the gas channel is not accurate enough and this method is very sensible to the measurement.

As the volume flow in PSFGL HEX have been measured as presented on Figure 7.14 above, it is possible now to make an approximation of the volume that flows in the PSFGL HEX as a function of the PSFGL pressure drop in the gas channel.

As presented in section 5.1 page 45, the pressure drop on the gas channel vary with the squared of the volume flow (or speed) following the Darcy-Weisbach law. Doing the same for the measurement of Figure 7.14, the following equation (7.24) have been approximate for the pressure drop.

$$Dp(\dot{V}) = 0.0042\,\dot{V} \ \text{[mbar]}, \ \dot{V} \ \text{in [m}^3\text{/h]} \tag{7.24}$$

By inverting equation (7.24), equation (7.25) has been computed giving the volume flow as a function of the pressure drop in the PSFGL HEX gas channel.

$$\dot{V} = \sqrt{\frac{Dp}{0.0042}} \ [\text{m}^3\text{/h}], \quad \text{Dp in [mbar]} \tag{7.25}$$

However this method require to makes measurements presented in Appendix D.3 page 80 above for each new PSFGL HEX tested, as the function of the pressure drop as a function of the volume flow will change for each PSFGL HEX. Also the gas channel is subjected to fouling as presented in Figure 5.8 on page 57 of section 5.1. As fouling occurs, the pressure drop will increase during the tests for the same volume flow and it will lead to wrong volume flow measurements.

Appendix E Labview measurement software

As the measurement software has already been partially presented in Section 4.6 page 32, this appendix will give a larger overview on its functioning and the possible improvements that can be done.

In Section 4.6 the front summary user interface panel has been presented and a screen capture of this panel figures on Figure 4.9 page 32. The front summary panel is the main part of the measurement software. Is presents all the measurements of the facility in real time during a test of the PSFGL HEX.

Before exploring the user interface, we will mention that all values measured on the facility during a test are saved in a .txt file named using the following format: Mesurements˙HX˙Year-Month-Day˙Time". This file is saved in a directory that has the following path: D:/Documents/Experimenten/Datas Measurements/2012-08-13, where 2012-08-13 corresponds to the date of the test.
All values computed in the software and that are useful for a later analysis of the PSFGL HEX performances are saved in another .txt file named Data˙summary˙HX˙Year-Month-Day˙Time and is saved in the following directory D:/Documents/Experimenten/Datas˙Summary/2012-08-13, where 2012-08-13 correspond to the date of the test. Sadly data saving paths can only be changed in the code of the software.

As the user can refer to Figure 4.9 page 32 for the list of the tabs of the user-interface, we will now present each of them. As the aim of this report is to be concise, we will present a print screen of the various tabs only when it is required for the understanding. As the majority of the tabs are dedicated to display

measurements over time using graphics displays, we will try to refer to the other parts of this report where few screen capture have already been presented.

One has to mention that pin numbers of each thermocouple on the HP measurement unit are given in the Table 7.5 page 96. Pin numbers are used in the programming of the software to get a measurement value of a specified device. Pin numbers are not required to use properly the software. They are given as it would be useful when the software would have to be modified.

Here we will present the tabs that compose the user interface.

PolyHEX: Temperature: This tab is composed of four slide time graph displays. It allows following all inputs and outputs temperature values of the PSFGL HEX in real time.

The graph *PolyHEX - Gas input temperature* displays both input gas temperature at the entrance of the casing. Displayed measurements are taken with thermocouple TK15 and TK16. An average value of both measurements is displayed in pink.

PolyHEX - Gas output temperature displays the four gas output temperatures measured with thermocouple TK22, TK23, TK24 and TK26. Those thermocouples have been placed on various spire of the PSFGL HEX. It allows evaluating how homogenous is the gas output temperature. The average value of the four thermocouples is also displayed in pink.

PolyHEX - Water input Temperature displays the two water inputs temperatures measured by thermocouple TK12 and TK13. Initially three thermocouples have been planned, but one has shown problems and has been removed (TK14). Averaged temperature is shown in red.

PolyHEX - Water output Temperature displays the three water outputs temperature measured with thermocouple TK1, TK2 and TK3. Average temperature value is also displayed in red. There is to pay attention to these three values as when water flow in the PSFGL HEX is to high water output temperature is not homogenous enough and the three measured value will diverge. The three temperatures serve as an indicator for the heat exchange in the PSFGL HEX.

On the right corner of this tab is also displayed the heat load or heat transferred on both side of the PSFGL HEX. Those values are also displayed on the summary panel.

The next tab of the user interface is called ***Pressure drop***. It shows in real time the pressure drop on both gas and liquid channel of the PSFGL HEX.

PolyHEX - Pressure drop on gas side displays the pressure drop in mbar over time this measurement is done on pin number 0418.

PolyHEX - Pressure drop on water side displays the pressure drop in the PSFGL HEX water channel in mbar over time. The displayed value is acquired through pin number 0419.

The tab called ***Mass flow*** presents the values of the mass water and gas mass flow in g/s flowing in the PSFGL HEX. Those measurements are respectively acquired through pin 0416 and 0417. For the gas mass flow, the value is computed

as presented in Appendix D.1 page 75 using the pressure drop and the temperature of TK 25.

SteelHEX: Temperature tab has already mentioned in section 4.12 page 41 and shown during the tests in Figure 4.17 page 42 and Figure 4.20 page 44. This tab presents all inputs and outputs, gas and liquid, temperature in the tubular steel heat exchanger that has been used to pre-cool the exhaust gases before entering in the PSFGL HEX. All thermocouples numbers figure on legend display and thermocouples placement are shown in a Figure 7.8 page 74 of Appendix C .

The ***Acquisition Settings*** tab is used to set values used in the software computations. A screen capture including the values set is shown in Figure 7.15.

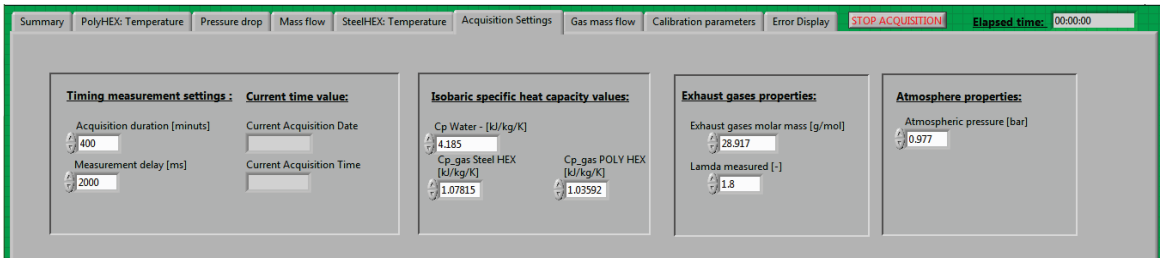

Figure 7.15: Acquisition settings of Labview user interface

The timing measurement settings define the duration of the test in *Acquisition duration*. The measurements will be automatically stopped when this period is elapsed. *Measurement delay* in milliseconds is the time elapsed between two measurement of all values measured on the facility.

The *isobaric specific heat capacity* square defines these values for the water and for the gases. As for gases this value is subject significant change with the temperature two values have to be set. The first one corresponds to the average temperature in the steel heat exchanger, the second to the average temperature in the PSFGL HEX.

Exhaust gases properties square allows to enter the molar mass of exhaust gases and the corresponding lambda value that are both saved in the txt files for later data analysis. The molar mass of exhaust gases is used for gas mass flow computation.

Atmospheric pressure must also be given to be able to compute the volume flow in the laminar Ricardo flow meter. The atmospheric pressure taken has been taken on the internet, see source [14], and actualised before each test session. One has to pay attention that the atmospheric pressure must be given in bar.

The ***gas mass flow*** tab is dedicated to exhaust gas mass flow measurements using both methods presented in appendix D.1page 75 and appendix D.2 page 78.
Considering the laminar flow meter, both volume and mas flow are displayed.
Considering the method of the heat load of the steel tubular heat exchanger, there is the need to enter the water input temperature and the water volume flow of the steel heat exchanger that is manually read on the heat-payers. One can refer to section 4.11 page 39 and subsection 4.11.2 page 41 for more details about heat-payers measurements.

The *Calibration parameters* tab is used to set to 0 the differential pressure sensors. See section 4.8, page 34 and subsection 4.11.1, page 40 for more information about conversion equations and theirs coefficients for differential pressure sensors and water flow. As differential pressure sensors are not temperature corrected, the zero of each sensor has to be set regularly during the tests. To proceed so one can adjusts the additive component of each sensor. However the multiplicative component is linked to the sensor itself and must not be changed.

Finally the *Error display* tab shows the possible error that can occur in the software. We have to mention that as our program is not very complex, we haven't encountered any errors during the test sessions.

We can now conclude this appendix on the developed software. As it was our first Labview development after taking Core 1 and Core 2 courses before the beginning of the master project, we have to recognize that many points can still be improved. Keeping in mind that many other things have been realised during in this project and time has been short to make such improvements on the code as it should be done. Also it was quite a great challenge to put together all this measurements devices that haven't been used for a long time. Also no tutorials were available for the devices used and it was necessary to find solutions by myself.

However we have to mention here that the usage of clusters would make the code much clearer grouping the flows of data. It would also be required to make the code more modular integrating a specific VI for the sensors and one for the gas flow computation. Also error handling is a critical point and could be seriously improved to make the software stronger. However this software has been good enough to make good measurement and to make the facility operating securely in a first try.

Appendix F Destructive tests with sealant in PSFGL HEX

To make sure to provide a good sealing on the liquid side of the PSFGL HEX, there was the need to study as how well various sealant can stick to the polymer film in the PSFGL HEX. Here is presented a series of destructive tests with materials used in the production process. This test was necessary to select good materials and to find the best process to obtain the best pressure resistance in the PSFGL HEX

We'll draw here the meaningful conclusions of these tests. The lecturer can go further below by reading conclusions of each test independently

Recommendations:

The use of one component rather than two components silicon is necessary to provide the best sticking resistance.

A plasma treatment on PEEK films before gluing helps to have a better sticking between PEEK and silicon. However the plasma treatment made by the manufacturer at production still provides a good sealing joint efficiency after few months.

Humidity has to be strictly avoided on all surfaces to be glued with silicon. Surfaces have to be strictly dry to allow silicon to sticking.

The silicon hardening time can be reduced by increasing the temperature of the environment.

The polymer primer base on toluene mixture provides a bad sticking.

The silicon doesn't stick to the PP mesh; even a plasma treatment of the mesh can't improve a good sticking between silicon and the PP mesh.

Pressure exerted inside the HEX compress the silicon between its stitches of the mesh lozenges leading to the shearing of the silicon. The pattern of the mesh is acting as a knife. On the other hand such mesh pattern provides a better turbulence profile when liquid or gases are flowing in the HEX and allow to heat exchange between the HEX film separating both HEX channels.

Tests analysis:

For each test two squared film samples of PEEK polymer have been cut and have been glued with acetoxy drying silicon[3] in order to form a pocket as shown on Figure 7.16.

Initially three of such pockets have been prepared testing various polymer film surface treatments.

Figure 7.16: First pocket lot that has been realised

[3] Silicon used was from brand EGO, called EGOSILICON 111

Specifications of each test will be here presented and will be followed by the conclusions on the tested gluing configuration.

Test 1: Both glued film surfaces have been coated with a special primer toluene solution suitable for PP/PE/PVC materials. Once primer dried, silicone has been applied to glue on both films.

Conclusions are the following, after 40 hours of drying time silicon doesn't stick on both film surfaces. A primer layer that remains on film surfaces and provide a bad gluing strength when pulling films with hands as shown on Figure 7.17. Observing again Figure 7.17 silicon is torn in bands and sticks alternatively better on one film or on the other. The usage of the polymer primer is not appropriate to increase gluing resistance.

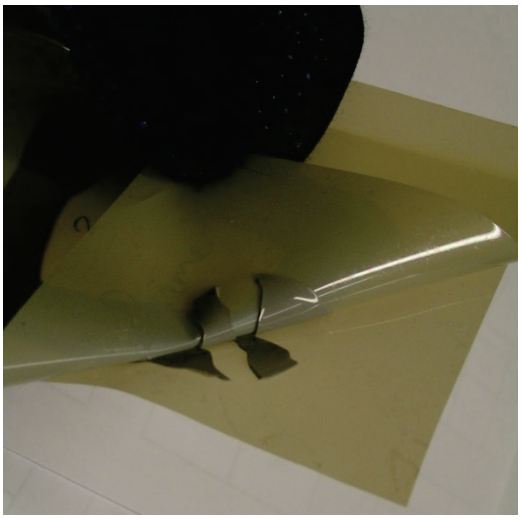

Figure 7.17: Silicon gluing resistance with primer layer

Test 2: In this test both PEEK films surfaces (as it as be the same for *Test 1)* have been previously plasma treated by the manufacturer months ago at production. Both films samples have been glued with silicone.

Conclusions are the following, after a 40 hours drying time, silicone sticks well to PEEK films and both films can hardly be separated. Silicone tends to stick more on film surfaces and is mostly torn in its thickness. With efforts pulling we can reach the point where the silicone separates itself at the surroundings of the film surface. A small quantity of silicon remains stuck on the film surface. We can conclude that the plasma treatment is a good surface treatment. But can we provide an even better sticking?

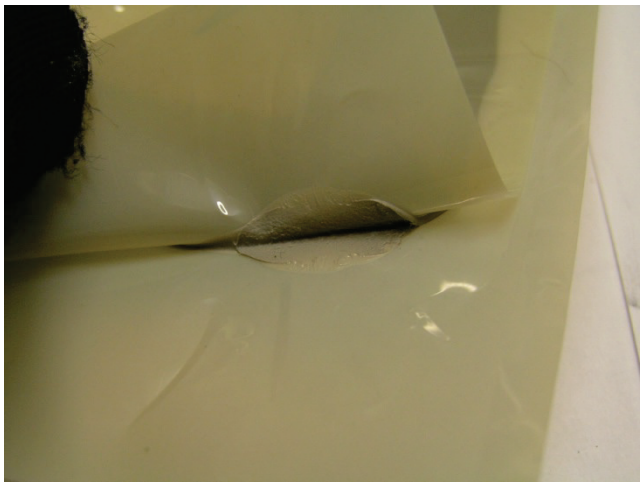

Figure 7.18: Silicon stress resistance with PEEK film plasma treated at production only.

Test 3: Here both PEEK films surfaces have been plasma retreated just before silicone application. (they have also previously treated at production)

Conclusions are the following, after 40 hours drying time, even pulling with hands and putting lots of efforts, silicone sticks to PEEK films so well that we can't separate silicone from the films. After strength test silicon returns in the initial state as show in Figure 7.19. Plasma retreatment before gluing seems to be the best preparation to provide the best gluing resistance between silicon and the polymer film.

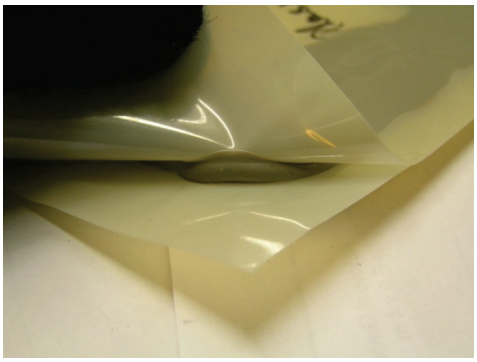

Figure 7.19: Silicon stress resistance with PEEK plasma treated before gluing

Second step consists in adding a layer of Polypropylene (PP) mesh. It is reproducing the configuration in the heat exchanger when rolled up.

Test 4: Both PEEK film and mesh have been freshly plasma treated (as in *Test 2*). We were interested knowing if we could improve silicone drying reproducing condition in PSHE at the sealing zone where the mesh ended, thus we wanted to estimate how the mesh could be a source of leakage in the HEX boundary.

Conclusions are the following, after 40 hours drying time; when pulling with hands zones stick both very well film where there remains only silicon between the films where the mesh has ended. Cutting silicone in its thickness with a knife and reaching zone where the mesh is present between films, it has been observe that the silicone doesn't stick to the PP mesh. Pulling with hands on both films silicon can

be easily torn in its thickness due to the fault created by the mesh design. Lozenge mesh design compresses the silicone when stress is applied and helps propagating fault tearing silicone in its thickness without effort.

In Red cycles on Figure 7.20, it is showed that silicon can be torn where mesh has stopped.

Yellow circles on Figure 7.20 show zones where silicon has a smooth surface. On those places where the mesh is missing it has been necessary to cut silicone with the knife in its thickness to open the sealing joint.

In the green cycle of Figure 7.20 it is shown that silicon layer is missing between the film and the mesh decreasing the gluing resistance. In these zones there are no chances to make provide a sealing joint between the films.

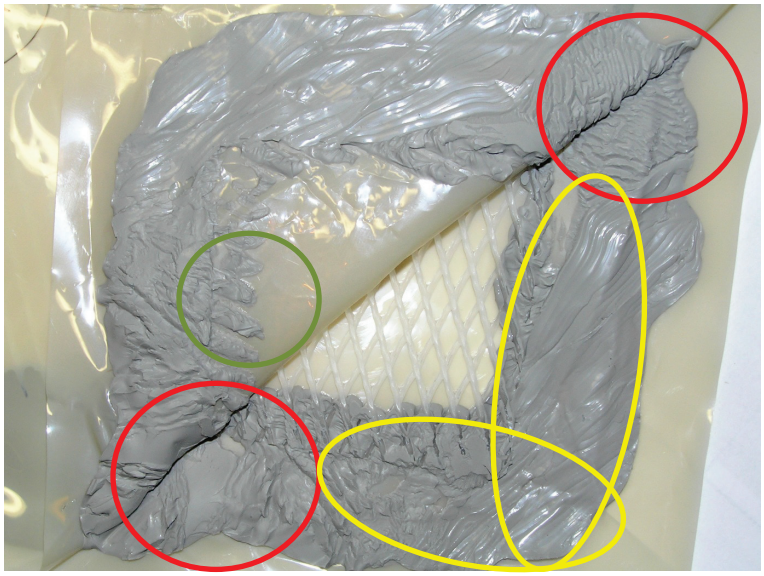

Figure 7.20: Silicon tear when a PP mesh is inserted between the PEEK films.

Test 5: In this case both films have been plasma retreated before gluing and a PP mesh has been added as previously. In addition a moist duster has been inserted before to close the pocket (Case 2). The idea was to compare if the humidity added in the duster would help setting quicker the silicon. For lecturer reminding the silicon used is hardening using chemical reaction where humidity is the activator.

As conclusion we can here make the same report as the *Test 4*. As show on Figure 7.21 it can be seen in yellow circle that the silicon didn't stick at all to the mesh and is even completely separated from the gluing area. This can be justified by the following reason the surface of the mesh was humid before silicon was applied and in this case silicon can't set to the mesh. All surfaces glued with silicon have to be as dry as possible before gluing even if the silicone needs humidity to harden. The moist duster didn't seem to help providing a better sealing joint, even less it make glued surfaces moist and prevent the silicon to stick on glued surfaces.

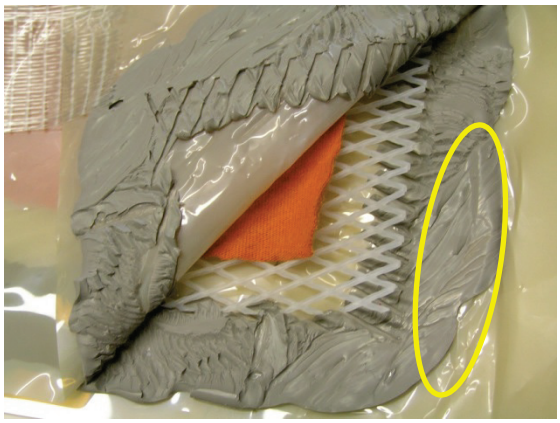

Figure 7.21: Silicon tear when a moist duster is inserted in the pocket. Otherwise identical configuration as Test 5.

Test 6: Both PEEK films have been plasma retreated and a PP non plasma threated mesh has been added. This test is similar to *Test 5*, but no moist duster has been inserted in the pocket.

Results obtained on Figure 7.22 show that sticking between mesh and silicon isn't much better, even if the mesh surfaces haven't been moist when gluing.

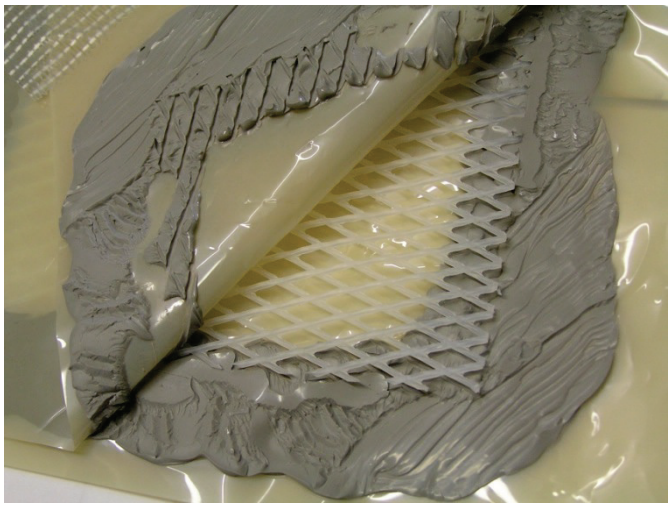

Figure 7.22: Without plasma treatment, the mesh and the silicon don't stick together.

Test 7: This test is identical as *Test 5*. But changing the drying process here the pocket has been placed in an oven during 3 hours to 80°C rather than left for 40 hours to atmospherics conditions.

Conclusions are saying that silicon hardening is operated quicker due to the heat. Letting the sealing joint hardening to atmospherics condition for some 24 more hours, we obtain the same strength resistance and behaviour as in Test 4.

As shown on Figure 7.23, the silicone hardened deepness has been measured to be about 20mm, at oven exit about 5mm on each side of the silicon profile is already dried as shown on Figure 7.23. The part that has flowed in the middle when film and joint have been cut is non-dried silicon when it exits the oven.

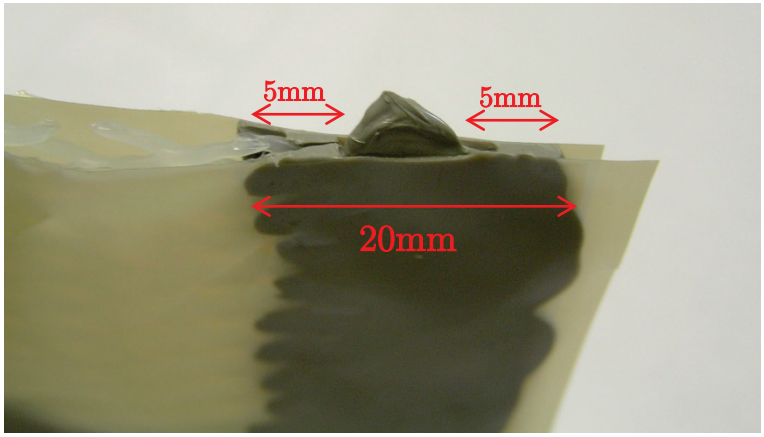

Figure 7.23: Silicon gluing section when the pocket is inserted in an oven during 3 hours at 80°C.

Test 8: It has been reproducing the same configuration as in *Test 7*. The pocket has been placed in the microwave for 6 minutes, to observe if microwave could shorten hardening duration. After 6 minutes in the microwave half of a millimetre of silicon has hardened on the silicone joint surfaces. It also appeared after few seconds that the air inside the pocket has been inflated due to the increased of air temperature; both films have been then separated and this test could show that microwave can shorten silicon hardening time but no air should be prisoner in the sealing joint. Result is presented on Figure 7.24.

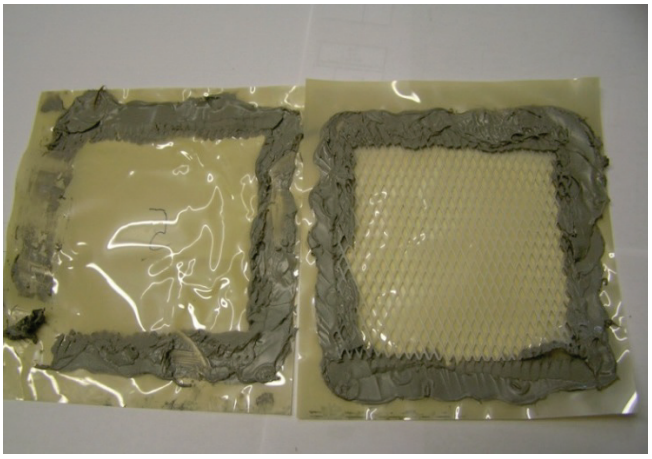

Figure 7.24: Results of Test 8, both film have been separated due to the air inflated by temperature increasing in the microwave.

Test 9 : Here both PEEK films have been plasma treated and their surfaces have been humidified before silicon application trying to reproduce the same moist glued surface we had in Test 5 on the mesh.

Conclusions shown in Figure 7.25 are the following, when booth films are humid sticking between PEEK and silicon can't be operated. It appears some clearer zones in the yellow circle of the Figure 7.25 where the water layer on the film inhibits gluing between silicon and film. Figure 7.25 shows both appearances with and without water with the ban on the upper part

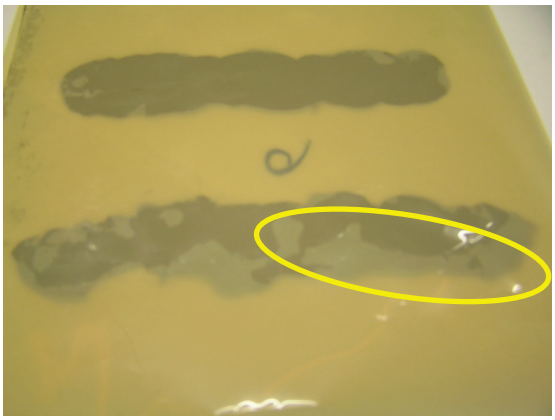

Figure 7.25: Results of *Test 9*. Bottom silicon line: PEEK films have been humidified before silicon application. Humidity created clear grey zones that inhibit sticking between silicon and PEEK films. Upper silicon line: Without humidity the silicone stick to the PEEK films, sticking is well operated.

Test 10: Here two components (2 Comp.) silicon has been tested. This type of silicon allows a much quicker hardening and both PEEK films have been plasma treated.

After 20 hours the silicon is completely set but it can be easily torn pulling with hands. The sticking with this silicon and PEEK films are quite good but the 2 Comp. silicon possess a quite lower shear resistance as the 1 Comp. silicon that have used previously for all other tests.

Figure 7.26: Results of *Test 10*. Two components silicon sticks well to PEEK film but has a lower shear resistance. Separation can be done by pulling with hands and is operated in the silicon thickness confirming silicon lower shear resistance.

Appendix G Sensors calibration

G.1 Differential pressure sensor

Here is given the conversion measurement equation for the four differential pressure sensors PD-11 that have been calibrated. One has to note that the sensors are quite sensible to temperature and the zero of the conversion equation has to be

set if the temperature is different of the calibration ambient temperature. The slope of the calibration equation should always remain the same. Calibration measurement has been done at approximately 22°C.

Setting the zero when no pressure difference is exerted on the sensor means to add or subtract the pressure measured by the sensor in mbar at sensor rest state. By example if the Keller PD-11, 0-100mbar sensor measures 54,19 mbar when no differential pressure is exerted, then the conversion equation should be modified as follow:

$$\mathrm{Dp} = 2000.9 + (64.197 - 54{,}19) = \mathbf{2000.9 + 10.007}\ [\mathrm{mbar}] \tag{7.26}$$

Also a numerical differential pressure sensor branded Rikenda for the range 0.25mbar has been used for the Ricardo gas flow meter. The corresponding conversion for this sensor is equation (7.27) below:

$$\mathrm{Dp} = 2.5095 + 0.0308\ [\mathrm{mbar}] \tag{7.27}$$

Figure 7.27 to Figure 7.30 present the calibration measurement points and the corresponding computed conversion equation for the four sensors that have been calibrated.

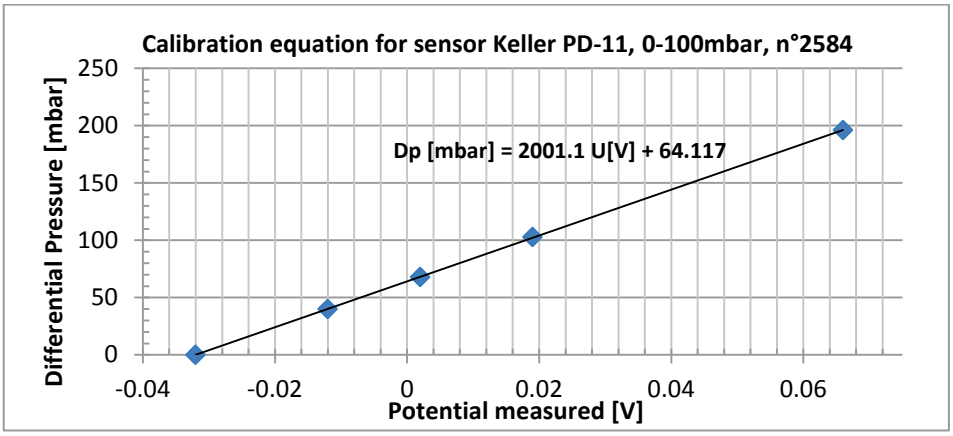

Figure 7.27: Calibration equation for sensor Keller PD-11, 0-100mbar, no.2584

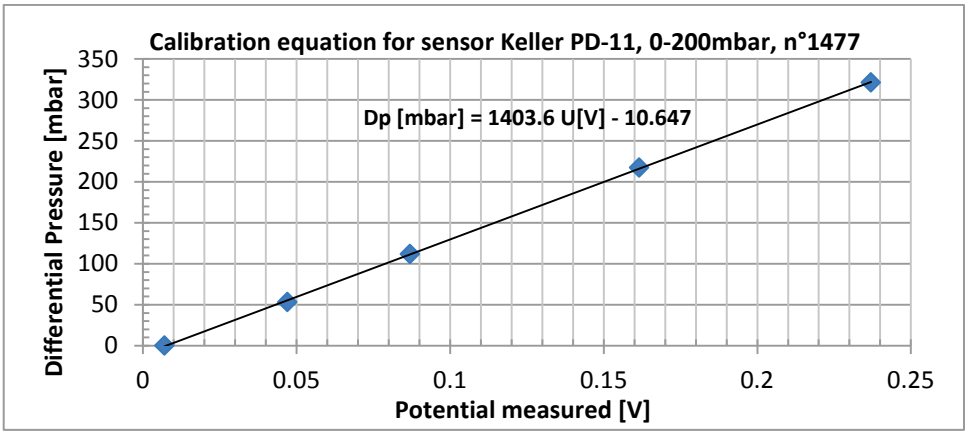

Figure 7.28: Calibration equation for sensor Keller PD-11, 0-200mbar, no.1477

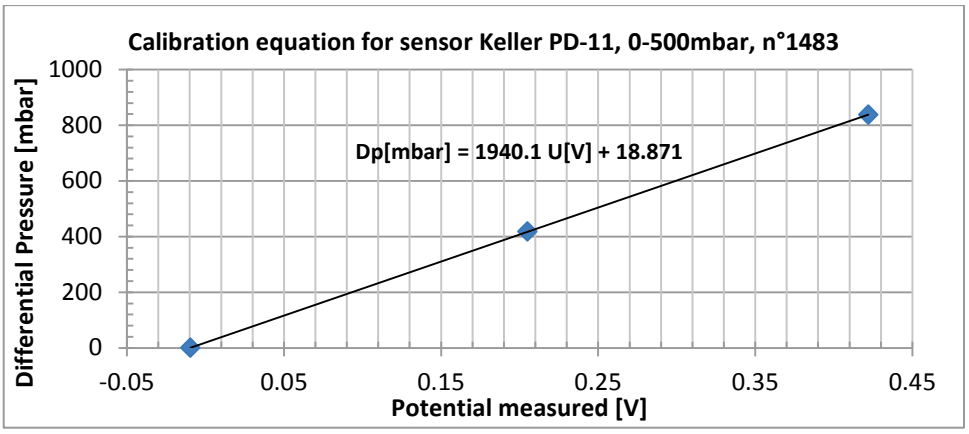

Figure 7.29: Calibration equation for sensor Keller PD-11, 0-500mbar, no.1483

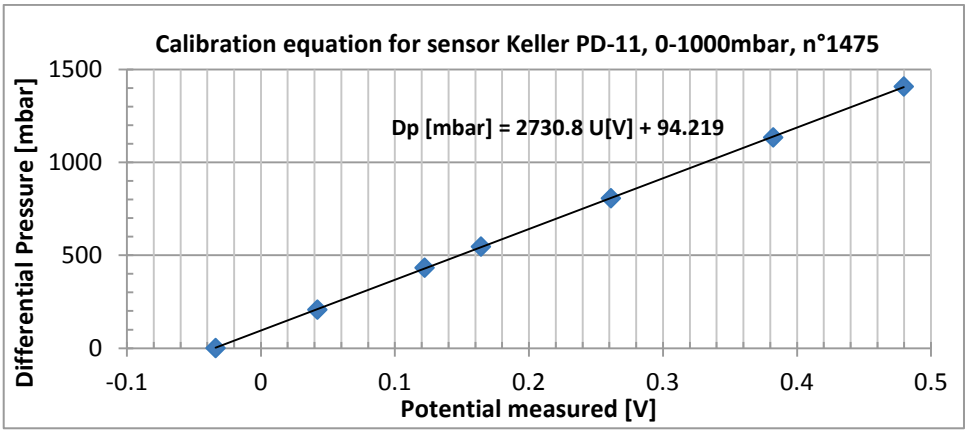

Figure 7.30: Calibration equation for sensor Keller PD-11, 0-1000mbar, n°1475

G.2 Thermocouple calibration

Table 7.5: Thermocouples placement and calibration values, with pin number on the HP measurement unit.

Number	Placement	Pin number on HP unit	Multiplicative component	Additive component
TK1	PSFGL HEX Water out 1	0300	1.0031	0.2482
TK2	PSFGL HEX Water out 3	0301	0.9999	0.3528
TK3	PSFGL HEX Water out 2	0302	0.9995	0.3385
TK4	Not used	0303	0.9968	0.4009
TK5	Steel HEX gas out 1	0304	1.0069	-0.1612
TK6	Steel HEX gas out 2	0305	0.9951	0.3885
TK7	Steel HEX gas in	0306	0.9993	0.4675
TK8	Steel HEX water in 1	0307	1.0017	-0.0433
TK9	Steel HEX water in 2	0308	0.9987	0.323
TK10	Steel HEX water out 1	0309	1.0074	0.2059
TK11	Steel HEX water out 2	0310	0.997	0.3437
TK12	PSFGL HEX Water in 1	0311	1.0032	0.2748
TK13	PSFGL HEX Water in 2	0312	1.0002	0.3235
TK14	Broken	-	-	-
TK15	PSFGL HEX gas in 1	0314	0.9944	0.4167
TK16	PSFGL HEX gas in 2	0315	0.9959	0.3583
TK17	Not used, thin thermocouple 1	0316	1.015	-0.0862
TK18	Not used, thin thermocouple 2	0317	1.0278	-0.3892
TK19	Not used, thin thermocouple 3	0318	1.0083	-0.0238
TK20	Not used, thin thermocouple 4	0319	1.0143	-0.1836
TK21	Broken	-	-	-
TK22	PSFGL HEX gas out 1, centre ring	0401	1.0001	0.053
TK23	PSFGL HEX gas out 2, middle ring	0402	0.9999	0.0556
TK24	PSFGL HEX gas out 3, middle ring	0403	0.9995	0.0577
TK25	Ricardo mass flow meter	0404	1.0001	0.0359
TK26	PSFGL HEX gas out 4, outer ring	0405	0.9999	0.0382
TK27	Broken	-	-	-

Chapter 8 Nomenclature - list of figures – list of tables

8.1 Nomenclature

Subscripts:

Symbol	Unit	Description
atm	-	Atmospheric
Gc	-	Combustion gases
F	-	Fuel
i	-	Substance I, indices
j	-	indices

Latin:

Symbol	Unit	Description
A/F Ratio	[Kg air/Kg Fuel]	Air Fuel Ration of the Diesel engine
A	[m^2]	Heat exchanger surface
a	[-]	Multiplicative component of conversion equation
b	[-]	Additive component of conversion equation
$C_{cylinder\ capacity}$	litres	Cylinder capacity of the engine
c_i^F	[kg i/kg Fuel]	Mass concentration of component i in the fuel
c_i^{Gc}	[kg i/kg Gc]	Mass concentration of component i in the Combustion Gases
$\tilde{c}_i$	[kmol i/kmol]	Molar concentration of component i in the mixture
$\tilde{c}_i^{Gc}$	[kmol i/kmol Gc]	Molar concentration of component i in combustion gases
Cp	[kJ/(kg K)]	Specific heat load coefficient
ΔT_{LMTD}	[degree Celsius]	Logarithmic meat temperature difference
D	[m]	Diameter of the pipe
Dp	[mbar]	Pressure drop
f_D	[-]	Darcy friction factor
HHV	[kJ/kg]	High heating value of the Diesel
K	[Kg/m^3]	Simplified coefficient for Darcy-Weisbach law
K'	[Kg/m^7]	Simplified coefficient for Darcy-Weisbach law with volume flow
$\widetilde{m}_i$	[kg/kmol]	Molar mass of component i
$C_{p\,Gc}$	[J/(kg K)]	Specific heat load of the combustion gases

K	[W/m K]	Thermal conductivity
L	[m]	Length of the channel
LHV	[kJ/kg]	Low Heating Value of the Diesel
$\widetilde{m}_i^{Gc}$	[kg i/kmol	Mass of component i in one kilomole of combustion gases
$\widetilde{m}_{Gc}$	[kg Gc/kmol Gc]	Molar mass of the combustion gases
$\dot{m}$	[g/s]	Mass flow
$\dot{m}_{Gc}$	[g Gc/s]	Mass flow rate of the combustion gases
$\dot{m}_F$	[g F/s]	Mass flow rate of the Fuel consumed by the engine at full load
M_F	[kg]	Mass of fuel
N_i	[mol]	Quantity of mole of substance i
$N\dot{V}$	[Nl/s]	Normal volume flow rate
P	[mbar]	Pressure
Q	[kW]	Heat exchanger heat load
T	[degree Celsius]	Temperature
$\hat{T}$	[degree Celsius]	Temperature in Celsius degree
TK	-	Thermocouple measurement device
U	[W/(m^2 K)]	Overall heat transfer coefficient
U	[volt]	Potential difference
V	[volt]	Volt unit
V	[m/s]	Flow speed
$\dot{V}$ or V˙dot	[m^3/h]	Flow rate

Greek:

Symbol	**Unit**	**Description**
Δ	[-]	Difference
ρ	[Kg/m^3]	Fluid density
λ	[-]	Ratio air/stoichiometric air of the engine
ω_{engine}	$[rpm]$	Rotation speed of the engine
$\varnothing$	[mm]	diameter

8.2 List of figures

8.3 List of tables

Chapter 9 Bibliography

[1] Cuse/Alto, Werkstatt-Handbuch FOCS Motorenreihe cod. 1.5302.353˙7fl ed˙ rev. 06, Lombardini, 2008.

[2] "Thermocouple Tables," National Instruments, [Online]. Available: http://zone.ni.com/devzone/cda/ph/p/id/273. [Accessed 29 07 2012].

[3] Wkikpaedia, "Darcy–Weisbach equation," [Online]. Available: http://en.wikipedia.org/wiki/Darcy%E2%80%93Weisbach˙equation. [Accessed 11 08 2012].

[4] J. H. L. I. /. J. H. V, A Heat Tramsfer Textbook, Third Edition, Cambridge, Massachussets, USA: Phlogiston Press, 2008.

[5] A. E. B. A. B.-C. P. R. Juan Gabriel Cevallos, "Polymer Heat Exchangers—History, Opportunities, and," *Heat Transfer Engineering,* no. http://dx.doi.org/10.1080/01457632.2012.663654, pp. 1075-1093, 2012.

[6] K. Automotive, "Exhaust Gas Mass Flow Sensor for Applications in Commercial Diesel engines," [Online]. Available: http://www.kspg-ag.de/pdfdoc/kspg˙produktbroschueren/2010/pb˙ags˙e.pdf. [Accessed 11 08 2012].

[7] D. F. Lucien Borel, Thermodynamique et Energétique 1, De l'énergie à l'exergie, Lausanne: Presses polytechniques et universitaires romandes, 2005.

[8] D. F. Lucien Borel, Thermodynamique et énergétique 2, Problèmes résolus et exercices, Lausanne: Presses polytechniques et universitaires romandes, 2008.

[9] www.schweizer-fn.de, «Stoffdaten - Abgas fur Dieselmotor in Abhangigkeit der Temperatur, Abgasgegendruck und des Luftverhaltnis,¸ [Online]. Available: http://www.schweizer-fn.de/stoff/abgas/abgas˙stoff.php. [Zugriff am 11 08 2012].

[10] I. Gafner, "Chapter 8: Engine Modeling by a 2 Zones model," Course Slides for Engine&Fuel Cell, Lausanne, 2011.

[11] "Air Properties," The Engineering ToolBox , [Online]. Available: http://www.engineeringtoolbox.com/air-properties-d˙156.html. [Accessed 29 07 2012].

[12] F. B. P. D. F. Malick Kane, «SPS: Projet d'une minicentrale pilote éléctro-thermo-solaire de 10 kWe, Partie A: Centrale solaire hybride,¸ EPFL-DGM-LENI, Lausanne, 1999.

[13] S. Buehler, «Groupe de cogeneration Diesel, Projet de semestre,¸ EPFL-SGM-LENI, Lausanne, 2000.

[14] M. prog, "Rottenburg," [Online]. Available: http://www.meteoprog.de/en/weather/Rottenburg/. [Accessed 01 08 2012].

[15] "Polycarbonate," Wikipaedia, [Online]. Available: http://fr.wikipedia.org/wiki/Polycarbonate. [Accessed 28 07 2012].

[16] "Plastic Properties of Polycarbonate (PC)," DynaLab Corp , [Online]. Available: http://www.dynalabcorp.com/technical˙info˙polycarbonate.asp. [Accessed 03 05 2012].

[17] J. Guibet, Carburants et moteurs, tome 2, Paris: Editions Technip, publication de l'institut français du pétrole, 1987.

[18] J. Guibet, Carburants et moteurs, tome 1, Paris: Editions Technip, publication de l'institut français du pétrole, 1987.

[19] LMGRRR, A.remy, Materiaux, Neuchatel: Federation des Ecoles de mecaniques et d'electricite de suisse FEMES.

[20] HORIBA, Instruction Manual, AFR Analyser MEXA-110 Lambda, Kyoto, Japan, 1993.

[21] N. Instruments, LabVIEW Core 1, Course manual, Austin, Texas, 2011.

[22] N. Instruments, LabVIEW Core 1, Exercices, Austin, Texas, 2011.

[23] N. Instruments, LabVIEW Core 2, Course manual, Austin, Texas, 2011.

[24] N. Instruments, LabVIEW Core 2, Exercises, Austin, Texas, 2011.

[25] "PEEK," Wikipedia, [Online]. Available: http://en.wikipedia.org/wiki/PEEK. [Accessed 03 08 2012].

[26] FIP, "General characteristics PP-H," [Online]. Available: http://www.fipnet.it/EN/Prodotti/File/-832869176.pdf. [Accessed 08 08 2012].

[27] K. Raumgefühle, "Kunststoffe / Eigenschafte," [Online]. Available: http://www.karrer-works.ch/DownloadDateien/MaterialEigenschaftKunststoff.pdf. [Accessed 08 08 2012].

[28] Wikipaedia, "Reynolds number," [Online]. Available: http://en.wikipedia.org/wiki/Reynolds˙number. [Accessed 11 08 2012].

[29] T. e. toolbox, "Water - Dynamic and Kinematic Viscosity," [Online]. Available: http://www.engineeringtoolbox.com/water-dynamic-kinematic-viscosity-d˙596.html. [Accessed 11 08 2012].

[30] Wikipedia, "Compressed air energy storage," [Online]. Available: http://en.wikipedia.org/wiki/Compressed˙air˙energy˙storage. [Accessed 11 08 2012].

[31] ThermExcel, "linear pressure losses," [Online]. Available: http://www.thermexcel.com/english/ressourc/pdcline.htm. [Accessed 11 08 2012].

[32] T. e. toolbox, "Types of Air Compressors," [Online]. Available: http://www.engineeringtoolbox.com/air-compressor-types-d˙441.html. [Accessed 11 08 2012].

[33] T. e. toolbox, "Pump Power Calculator," [Online]. Available: http://www.engineeringtoolbox.com/pumps-power-d˙505.html. [Accessed 11 08 2012].

[34] T. e. toolbox, "Specific Work of Turbo Machines - Pumps, Compressors and Fans," [Online]. Available: http://www.engineeringtoolbox.com/specific-work-turbo-machines-d˙629.html. [Accessed 11 08 2012].

[35] H. L. M. K. B. M. KANCHAN CHOWDHURY, "Analytical Studies on the Temperature Distribution in Spiral Plate Heat Exchangers: Strightforward Design Formulae for efficiency and Mean Temperature Difference," Institut fiir Thermische Verfahrenstechnik der Universitat Karlsruhe, Karlsruhe, 1984.

[36] R. J. L. Zaheed, "Review of polymer compact heat exchangers,with special emphasis on a polymer film unit," *Applied Thermal Engineering,* vol. 24, p. 2323–2358, 2004.

[37] T. M. a. C. W. Bullard, "Suitability of Polymer Heat Exchangers for Air Conditioning Applications," University of Illinois at Urbana-Champaign, ACRC, Urbana, 2005.